Performance of UHPC in Shear-Key Connections

by

Chalachew Teshager Asmamaw

A Thesis

Submitted to the Faculty of Graduate and Postdoctoral Studies of

The University of Manitoba

in partial fulfillment of the requirements for the degree of

MASTER OF SCIENCE

Department of Civil Engineering

University of Manitoba

Winnipeg, Manitoba

ABSTRACT

Ultra-high-performance concrete (UHPC) is a promising material for shear-key connections in adjacent box beam girder bridges because of its high strength, bond capacity, and durability. However, the long-term performance of UHPC cast against hardened high-strength concrete (HSC), and the effects of surface condition and transverse reinforcement on shear-key behaviour, require further investigation. This thesis addressed these issues through two independent experimental studies. This thesis used specimens cast by Tan (2021) and Erfani (2023). The strengths found in these studies were compared with the strength values obtained in this experimental program.

One study Tan (2021) provided a durability-related assessment of material and interface specimens that were exposed to outdoors environment for approximately 7 years. Temperatures in Winnipeg, MB ranged from −40°C to +37°C. Compression, indirect tension, pull-off, slant-shear, and bi-shear tests were conducted to evaluate retained mechanical and bond-related performance. The HSC specimens had average compressive and indirect tensile strengths of 101.6 and 6.25 MPa, respectively. Pull-off specimens developed an average resistance of 3.96 MPa and failed within the HSC substrate. Slant-shear specimens also failed within the HSC rather than through complete interface separation, while bi-shear specimens developed an average shear strength of 9.42 MPa. All average strength results exceeded the average strength values obtained 7 years ago. These results demonstrate that the materials and UHPC–HSC systems retained measurable mechanical and interface resistance after long-term outdoor exposure.

The second study investigated shear-key specimens representative of shear keys in adjacent box beam girders. The specimens that were tested in shear were cast by Erfani (2023) and the test parameters investigated included interface surface preparation and presence/absence of transverse reinforcement. Surface roughness increased the peak load by 38.7%, while the presence of reinforcement in addition to the roughness increased peak load by 61.5%. Load–displacement measurements, Digital Image Correlation, and strain instrumentation showed that the smooth, unrestrained specimen experienced localized damage and an abrupt post-peak reduction in resistance. In contrast, the rough, reinforced specimens exhibited delayed crack initiation, greater deformation capacity, and higher residual load-carrying capacity. These observations indicate that surface roughness and transverse reinforcement improved shear resistance, ductility, crack control, and residual strength of the shear key specimens. Overall, the results emphasize the importance of interface preparation, and reinforcement detailing in UHPC–HSC shear-key performance.

Acknowledgment

First and foremost, I thank God for His guidance, strength, and protection throughout my academic journey, and St. Mary for her blessings and intercession.

I would like to express my sincere gratitude to my supervisor, Dr. Dagmar Švecová, for her invaluable guidance, encouragement, and support throughout this research. Her knowledge, patience, and thoughtful feedback were essential to the completion of this thesis.

I gratefully acknowledge the technical assistance provided by Chad Klowak, Daniel Szara, and Samuel Abraha at the W. R. McQuade Structures Laboratory at the University of Manitoba. Their practical support and contributions during the experimental program were greatly appreciated.

I would also like to thank my advisory committee members, Dr. Graziano Fiorillo, Dr. Ali Semendary, and Dr. Emile Shehata, for their valuable time, advice, and constructive feedback.

I gratefully acknowledge the Natural Sciences and Engineering Research Council of Canada (NSERC) for providing financial support for this research.

My heartfelt appreciation goes to my family and friends for their continuous encouragement, patience, and support throughout this journey. Special thanks are extended to Mr. Efrem Teklemariam and Dr. Daniel Asrat for their encouragement and support. Finally, I am deeply grateful to my father, Alemayehu Gizaw, and my beloved mother, Rose, for their unconditional love, sacrifices, prayers, and unwavering belief in me.

Table of Contents

Lists of Figures

Lists of Tables

1. INTRODUCTION

1.1 Background

Precast concrete bridge systems are widely used because they allow faster construction, reduce field formwork, and improve quality control compared with cast-in-place construction. In adjacent box-beam and box-girder bridges, individual box beam units are placed side by side and connected along their length through longitudinal shear keys. These shear keys allow the adjacent members to transfer loads between one another and help the bridge act as a unified load-sharing system.

Although adjacent box beam t bridge systems provide important construction advantages, the shear-key region has often been associated with long-term performance problems. Conventional grouted shear keys may experience cracking, leakage, corrosion of reinforcement or prestressing steel, and loss of load-transfer capacity. These problems are important because the shear key is not only a filling material between adjacent members; it is a crucial structural connection that must resist load transfer, environmental effects, shrinkage, temperature changes, and interface movement over time.

Ultra-high-performance concrete (UHPC) has been introduced as a promising material for bridge connections because of its high compressive strength, tensile resistance, fiber-bridging capacity, bond strength, low permeability, and improved durability (Di Bella and Graybeal 2014). These characteristics make UHPC attractive for shear-key applications where crack control, watertightness, and long-term maintenance are major concerns. However, the behavior of a UHPC-filled shear key cannot be explained by UHPC material properties alone. The performance of the connection also depends on the hardened high-strength concrete (HSC) substrate, the UHPC-HSC interface, the interface surface preparation and reinforcement crossing the interface (Hussein et al. 2017a; Al Rikabi et al. 2019).

The UHPC-HSC interface is especially important because the UHPC shear key is cast against hardened HSC. This creates a cold joint between the two materials placed at different times. If the interface is weak, cracking, slip, or debonding may occur before the UHPC reaches its full capacity, or later during service life of the structure. For this reason, understanding the bond and shear-transfer behavior of the UHPC-HSC interface is essential for evaluating the overall performance of UHPC-HSC shear-key systems.

This thesis is part of the broader Little Morris Bridge UHPC shear-key research program. Previous work by Tan (2021) investigated early-age and durability behavior of the UHPC-HSC interface using small-scale bond tests, including direct tension, pull-off, slant shear, and bi-shear tests. Erfani (2025) continued the research program by studying early age shrinkage behavior of UHPC, the effect of curing environment, the effect of presence/absence of joint reinforcement, and shear key performance under bending.

The present study extends this earlier work by evaluating the direct shear behavior of UHPC-HSC shear-key specimens and by examining how surface preparation and transverse reinforcement affect shear capacity, load-displacement response, crack development, strain localization, and failure mode. Furthermore, the effect of 7 years of environmental exposure on the interface between UHPC and HSC will be studied as well using specimens that were originally cast with the Little Morris Bridge Project (Tan 2021).

1.2 Problem Statement

Although UHPC has strong potential as a shear-key fill material, important questions remain regarding the direct shear behavior of UHPC-HSC shear-key connections. Existing design provisions for interface shear are largely based on conventional concrete-to-concrete or grout-to-concrete behavior. These provisions may not fully represent UHPC-HSC interfaces because UHPC has higher tensile strength, a dense matrix, fiber-bridging capacity, and strong bond characteristics with both hardened concrete and reinforcing bars.

Existing material and interface-level tests provide information about specific properties of UHPC and HSC systems. Compressive strength and indirect tensile tests evaluate material strength and tensile cracking resistance, while pull-off, slant shear, and bi-shear tests assess different interface stress conditions. Several specimens used for these tests were retained from the earlier experimental program and exposed to the natural outdoor environment for approximately seven years. During this period, the specimens experienced seasonal temperatures ranging from approximately -40°C to +37.0°C. Evaluating these specimens provides information about the retained material and interface performance following long-term exposure to both low and high temperatures. However, these tests are independent of the shear-key specimens because they involve different materials, casting histories, geometries, exposure conditions, and loading configurations. Their results therefore cannot be used to predict the structural response of the shear-key connection.

Structural shear-key testing is required to evaluate the complete UHPC–HSC connection under representative direct shear loading. Unlike the material- and interface-level tests, the shear-key test incorporates the connection geometry, interface surface condition, transverse reinforcement, boundary conditions, and load-transfer mechanism. It also allows the effects of surface roughness and transverse reinforcement to be evaluated through the load–displacement response, crack initiation and propagation, strain development, and failure mode.

Surface roughness and transverse reinforcement are two key variables in this behavior. A smooth/as-cast interface may rely more heavily on adhesion and may be more likely to experience localized slip or separation after bond is overcome. A roughened interface can improve mechanical interlock, frictional resistance, and shear transfer. Transverse reinforcement crossing the interface can restrain interface opening, contribute to dowel action, and improve post-cracking load resistance. However, the combined influence of these variables on UHPC-HSC shear-key behavior still requires further experimental investigation.

Long-term exposure is also an important concern. Bridge shear keys are exposed to environmental conditions such as moisture, temperature changes, and freeze-thaw cycles. These conditions can affect material properties and interface behavior over time. Therefore, this study considers not only short-term shear capacity but also the retained mechanical and bond-related response of specimens after long-term outdoor exposure.

1.3 Research Objectives

The main objective of this thesis is to evaluate the shear behavior of UHPC-HSC shear-key specimens under direct shear loading and to understand the influence of surface condition and transverse reinforcement on load transfer, cracking, deformation, and failure mode. To determine the effect of 5-year outdoor exposure on the strength of the UHPC-HSC interface.

The specific objectives of this research are:

1. To assess the direct shear response of UHPC-HSC shear-key specimens with different surface and reinforcement conditions.
2. To compare the behavior of smooth/as-cast and roughened UHPC-HSC interfaces under direct shear loading.
3. To evaluate the contribution of transverse reinforcement crossing the UHPC-HSC interface.
4. To interpret shear-key behavior using peak load, load-displacement response, nominal shear stress, crack initiation, crack propagation, DIC observations where applicable, reinforcement strain response, and failure mode.
5. To provide durability-related interpretation of material and interface performance after long-term outdoor exposure.

1.4 Scope of the Study

This thesis focuses on the experimental evaluation of shear capacity of UHPC-HSC shear-key specimens. The study is limited to one type of UHPC, one type of HSC, and one shear-key shape. Only monotonic testing was carried out in this thesis.

This thesis does not develop a final design equation for UHPC-HSC shear-key capacity. Instead, it provides experimental evidence and interpretation related to material behavior, interface response, direct shear capacity, crack development, reinforcement contribution, and failure mechanisms.

1.5 Thesis Organization

This thesis is organized into five sections.

Section 1 introduces the research background, problem statement, research objectives, scope, and organization of the thesis.

Section 2 presents the literature review. It discusses shear keys in precast concrete bridges; conventional shear-key materials and their limitations; UHPC in bridge connections; UHPC-HSC interface behavior; interface shear-transfer mechanisms; surface roughness; transverse reinforcement; experimental testing methods; instrumentation; DIC; and research gaps.

Section 3 describes the experimental program. It presents specimen groups and casting history, material characterization tests, interface characterization tests, bi-shear tests, main shear-key test matrix, specimen design, test setup, instrumentation, DIC procedure, and data collection parameters. The experimental program links material and interface behavior with structural shear-key response.

Section 4 presents and discusses the experimental results. The results include material characterization, interface characterization, bi-shear response, and main shear-key behavior. The main shear-key response is interpreted using peak load, load-displacement response, nominal shear stress, crack development, DIC observations where applicable, reinforcement strain response, and observed failure mode.

Section 5 summarizes the main findings, presents conclusions, and provides recommendations for future research.

2. LITERATURE REVIEW

2.1 Shear Key in Precast Concrete Bridge

Precast concrete bridge super structures are widely used because they allow faster construction, reduce field formwork, and improve the quality control compared with cast-in-place methods(H. G. Russell et al. 2009; Henry G. Russell 2011), Many types of precast systems rely heavily on shear keys: precast segmental box-girder bridges, which are built from short segments joined by post- tensioning, and adjacent precast prestressed box-beam or box- girder bridges, where beams are placed side by side and connected along their length (Ahmed and Aziz 2019a; Henry G. Russell 2011). In both systems, the shear key is a longitudinal or transverse keyway filled with grout, concrete, or, more recently, ultra-high-performance concrete (UHPC). This key ties the precast pieces together, making them act as a single load-sharing structure (Buyukozturk et al. 1990; Hussein et al. 2017b).

These keyways can be partial- or full-depth, and the ties can range from a few non-tensioned rods to multi-stage post-tensioned tendons (Henry G. Russell 2011). Russell pointed out that many shear- key designs are based on local standards of unclear origin rather than on a unified design approach (Henry G. Russell 2011). The shear key transfers wheel loads sideways between beams, allowing the deck to work as a single load-sharing system. For this reason, the long-term performance of the shear key is important for distributing live loads across the bridge.

2.1.1 Historical Development of Segmental Bridge Joints

Since segmental bridges became popular worldwide in the late twentieth century, the joint between precast segments has been considered one of the most important details of the system (Ahmed and Aziz 2019a) Early segmental bridges in the United States used several types of joints, including flat joints, single large keys, and multi-key joints, sometimes with an epoxy layer between the two adjacent connecting surfaces. However, there was limited experimental data on how these joints performed (Koseki and Breen 1983).

The first systematic tests began in the 1980s. Koseki and Breen (1983) tested the main joint types and found major differences in shear slip behavior among different dry joints. They also showed that almost all epoxied joints reached strengths close to those of solid, monolithic joints (Koseki and Breen 1983). In 1990, Buyukozturk et al. expanded on this work by testing flat and keyed joints, both dry and epoxied, at different prestress levels and epoxy thicknesses. They confirmed that epoxied joints were always stronger than dry ones but failed suddenly and in a brittle way. Their work also led to proposed shear-strength formulas for use with ACI and AASHTO guidelines for diagonal- shear design (Buyukozturk et al. 1990).

In the early 2000s, researchers began testing larger specimens and focused more on how key geometric features affect performance. Zhou et al. (2005) tested full-scale flat single-keyed and multi-keyed joints, both dry and epoxied, under different confining pressures. They found that shear capacity increases with confining pressures; epoxied joints are stronger but more brittle than dry ones; and dry multi-key joints have lower average shear strength per key than single -key joints due to fit-up imperfections. Epoxy helps reduce this problem (Zhou et al. 2005). They also found that AASHTO design rules underestimate the strength of epoxied joints by up to 40% but overestimate the capacity of dry multi-key joints. Therefore, they recommended reducing the strength values for the latter case (Zhou et al. 2005). Issa and Abdalla,2007 studied full-depth match- cast single-key male-female specimens under static, fatigue, and water- tightness tests. In every test, the failure was a concrete fracture along the joint, with shearing of the key, and fatigue had little effect on the post-tensioning bars (Issa and Abdalla 2007).

Recent studies have added more detail and looked at new key materials. Ahmed and Azizi (2007), tested Single-cell box-shaped specimens with web and flange keys, both dry and epoxide. They found that epoxy reduces joint imperfections and spreads shear stress more evenly. Epoxied joints carried 25-28 % more shear than dry ones and adding four flange shear keys increased joints shear capacity by about 14% and stiffness by about 73%. They also found that AASHTO predictions are conservative for epoxied and flat dry joints but greatly overestimate the strength of multi-key dry joints (Ahmed and Aziz 2019b). Yuan et el. tested 25 full-depth match-cast epoxy-resin joints with castellated keys, changing key geometry, spacing, number, angle, tendon layout, and reinforcement. They showed that these factors affect not only shear strength, but also failure mode and ductility. They proposed an improved formula for the shear strength of epoxy-resin joints with reinforced keys (A. Yuan et al. 2019a). Research on grout-filled joints has largely focused on keyed connections between precast bridge components rather than conventional match-cast box-girder segments. Annamalai et al. (1990) conducted push-off tests on post-tensioned grout-filled keyed connections and found that shear strength increased with both grout strength and compressive prestress across the joint; they consequently proposed an empirical shear-strength equation incorporating these variables. Gulyas et al. (1995) compared non-shrink grout and magnesium-ammonium-phosphate mortar in composite keyway specimens and demonstrated that grout selection substantially affected vertical shear, longitudinal shear, and tensile performance. Issa et al. (2003) subsequently tested 36 full-scale grouted joints for precast bridge-deck panels and found marked differences in strength, bond, and failure mode among four grout products, with polymer concrete providing the best overall performance. More recently, Fasching et al. Fasching et al. (2021) investigated post-tensioned mortar-filled joints for a semi-precast segmental bridge system using push-off tests on plain, grooved, keyed, and dry interfaces. Their results showed that joint geometry, grout properties, and lateral compressive force govern shear transfer and deformation, indicating that properly detailed grouted-filled joints can accommodate erection tolerances while developing effective shear continuity between adjacent box beam segments. Zou and Xu introduced a steel- shear-key joint and tested 12 full -scale specimens against concrete -key and inserted- reinforcement-key joints. The steel -key joints had higher stiffness and capacity than concrete keys, very small shear slips of 0.02-0.03mm, about 47% more capacity when moving from single to a double key, and a further 70-120% increase when the steel -key joint was epoxied instead of dry (Zou and Xu 2022). Despite 60 years of research, Ahmed and Aziz (2019) found that the research in this field remains incomplete. Prediction formulas for joint shear strength remain widely varied, and current equations are insufficiently accurate to address new design trends in segmental construction (Ahmed and Aziz 2019b). Overall, the history of segmental joints shows a gradual improvement in geometry and materials, from flat to keyed dry to epoxied, from single-to multi-key, and now to steel-key and UHPC-filled joints.

2.1.2 Reported Performance Problems

While adjacent box-beam bridges have generally performed well over the years, a common reported issue is cracking in the longitudinal grouted joints between beams. This can lead to reflective cracks in the wearing surface, water leakage through the joint, corrosion of reinforcing and prestressing steel, and in severe cases, loss of load transfer across the joint (H. G. Russell et al. 2009). Hanna et al. linked this cracking and leakage mainly to poor design and detailing of the transverse connections, which allow excessive movement and rotation between beams and create a path for early deterioration leading to corrosion (Hanna et al. 2009). An Indiana DOT study by (Frosch et al. 2020) found similar results on a larger scale: leaking joints allow chloride -laden water to move through the bridge, start corrosion, and eventually cause spalling, broken prestressing strands, and loss of strength. The researchers reported that the exterior beams and beams under wheel loads showed the most damage (Frosch et al. 2020).

Full-scale tests have shown that much of this cracking is caused by combination of applied loads and environmental factors rather than by traffic loads alone. Miller et al. (1999) tested full-scale adjacent box-girder specimens with standard non-shrink grouted shear keys and found that the keys cracked soon after casting, even before any simulated traffic loads were applied. Later, truck loading did not create new cracks but worsened the existing cracks. Measurements showed that temperature differences across the section induced strains in the keyway that are large enough to crack the grout (Miller et al. 1999). Using epoxy grout in the same keyway stopped cracking during both curing and later testing. Moving the keyway to the girder's neutral axis limited thermal cracking to minor issues at the ends and prevented further cracking under 1 million load cycles (Miller et al.,1998). Huckelbridge Jr and El-Esnawi (1997) found similar conclusions using computer models and laboratory tests. They reported that tensile stresses from negative moments in the top flange, caused by partial-depth top-flange shear keys, are behind many failures. Placing the key at the neutral axis greatly improves load capacity (Huckelbridge Jr and El-Esnawi 1997). New York state DOT had a similar experience. Before 1992, partial-depth grouted shear keys with transverse post-tensioning were used, but frequent deck cracking led to a switch to full-depth keys with more transverse tendons, which reduced cracking (Lall et al. 1998).

2.1.3 UHPC- Filled Shear Keys

Because grouted shear keys remain prone to cracking and leakage, there has been a shift toward using improved filling materials. J. Yuan and Graybeal (2016) tested four types of shear-key details, including full-depth details with either high-strength non-shrink grout plus transverse post-tensioning or UHPC, under both traffic and temperature loading. They found that UHPC connections can address connection degradation problems that limit the performance of adjacent box-beam bridges (A. Yuan et al. 2019a; J. Yuan and Graybeal 2016). Hussein et al. (2017) confirmed this trend with lab tests, showing that UHPC's higher strength and durability reduce cracking and improve load transfer compared to conventional grout. Adding transverse shear reinforcement across the key also increases capacity (Hussein et al. 2017b). Semendary et al. (2017) studied a real bridge with UHPC shear keys and transverse dowels, reporting on the early age performance of UHPC shear keys and providing field evidence to support lab results (Semendary et al. 2017). More recently, Ni et al. (2022) used static and cyclic bi- shear tests and computer models to show that adding reinforcement across the joint between block and overlay increases the shear keys' bearing capacity. They also proposed formulas linking shear transfer to relative movement across the key, a measure authors had used earlier as a sign of cracking (Ni et al. 2022).

The Little Morris Bridge project in Manitoba is a direct example of the move toward UHPC-filled shear keys. Tan (2021) studied the bond behavior between UHPC and high–strength concrete (HSC) using the Little Morris Bridge as the main field reference. The bridge is on Provincial Road No. 422 over the Little Morris River near Morris, Manitoba, and has eight adjacent precast box beams connected with UHPC shear keys and dowel bars. In this bridge, the UHPC shear keys and dowel bars are the main structural elements used to transfer load between adjacent beams and provide continuity in the transverse direction. Tan's work is important because it links laboratory testing to a real bridge and focuses on the UHPC-HSC interface, where shear transfer and bond behavior are expected to control joint performance. All specimens tested in that research were cast together with the bridge and therefore allowed direct comparison with the bridge performance.

Erfani (2025) continued this work by studying early -age shrinkage and bond performance of UHPC in shear keys using the same shear key geometry as Little Morris Bridge. Her study used materials and mix designs that matched those of Tan's project and examined how surface preparation, transverse reinforcement, and curing conditions affect UHPC shear keys confined by HSC beams. The UHPC shear key was tested in flexural test setup. Together, Tan's and Erfani's studies provide the direct background for this thesis by linking the broader literature on UHPC -filled shear keys to a specific UHPC-HSC bridge connection (Tan 2021; Erfani 2025).

Hussein et al. (2018) further investigated UHPC shear keys for adjacent box-girder bridges. Using calibrated finite-element models, they optimized the key geometry to transfer shear more effectively while maintaining the same UHPC cross-sectional area as the FHWA reference key. Experimental testing showed that the optimized Type OPT key carried 32% more load, demonstrating that the distribution and geometry of the UHPC within the joint not simply its cross-sectional area strongly influence load transfer and joint capacity.

2.2 Conventional Joint Fill Materials

Before the recent trend of specifying UHPC as a shear – key fill material, conventional grouts and concrete were used to fill joints between precast bridge beams. Materials have included non- shrink cementitious grout, magnesium-phosphate grout, epoxy grout, polymer-or latex-modified cementitious mixes, engineered cementitious composite (ECC), fiber reinforced high strength concrete, and conventional concrete. Researchers have used each of these materials at some point because they are easy to place, familiar to contractors, and provide sufficient strength for most bridge applications. However, the studies discussed in this thesis show that while each material addressed certain problems with shear keys, no conventional material prevented cracking, debonding, leakage, corrosion, and loss of load transfer entirely (Gulyas et al. 1995; Ozyildirim and Moruza 2016; Miller et al. 1999).

2.2.1 Non- Shrink Cementitious Grout

Non-shrink cementitious grout has been and still is one of the most used materials for casting shear keys between precast box beams. It is inexpensive to purchase, widely available from concrete suppliers and easy to place into any shear-key geometry. Non- shrink grout can also typically achieve the compressive strengths required for bridge applications. As a result, non- shrink grout became widely accepted as a standard material for shear keys in many bridge applications. However, field investigations and laboratory testing have shown that having high compressive strength does not necessarily mean that the grout will perform well in bridge joints.

Gulyas et al. (1995) reviewed field investigations of non – shrink grouts used in precast bridge keyways and experimentally studied keyway testing methods. They found that testing only the grout material does not accurately represent overall joint behavior. They also noted that current specifications need to limit shrinkage or require minimum bond strength of the filling material. This point is critical because overall performance is affected by many factors, including grout material properties (its tensile, compressive and bond strengths), the condition of the existing precast concrete surface, shear key geometry, and the amount of restraint provided by the adjacent beams. Many components affect performance, which is why (Gulyas et al. 1995) advocated testing a full keyway assembly rather than individual grout samples.

The non- shrink grout is known to still develop shrinkage and thermal cracking. Miller et al. (1998) conducted laboratory testing on full scale prestressed beams with non- shrink grout used in the shear keys. Visible cracking occurred soon after casting, well before any traffic loads were applied. When truck loading was applied later in testing, no new cracking occurred, but existing cracks have enlarged due to temperature effects. This research indicated that damage could occur before a bridge opens to traffic. Di Bella and Graybeal (2014) also showed that grouts marketed as non-shrink can experience both early-age and long-term shrinkage.

Once cracks form, water and deciding salts can infiltrate the joint. This can allow corrosion of prestressing strands, corrosion of reinforcement near the joint, and deterioration of the grout. The corrosion products then expand, further damaging the surrounding concrete and reducing the shear key's ability to transfer load from one beam to the next. H. G. Russell et al. (2009) found that longitudinal cracking, reflective cracking, leakage, corrosion, and loss of load were common in adjacent box- beam bridges. Hanna et al. (2009) attributed these problems to transverse connection details that allow excessive beam movement and rotation. Overall, the literature indicates that problems associated with non-shrink cementitious grout stem from both material properties and joint design flaws (Hanna et al. 2009; H. G. Russell et al. 2009; Ozyildirim and Moruza 2016).

2.2.2 Magnesium - Phosphate Grout

Magnesium phosphate grout has been used in bridge connections because it can gain strength quickly. Magnesium - phosphate grout has high early strength and usually sets in about 20 minutes.

It is advantageous when fast construction speed or repair work is needed. Gulyas et al. (1995) tested non shrink grout and magnesium ammonium phosphate mortar in full- scale shear key tests. Magnesium phosphate mortar performed better than none shrink grout in some respects. For example, magnesium phosphate retained bond strength and capacity better over time. Magnesium phosphate grout can provide advantages when early strength gain and rapid placement speeds are essential.

Huckelbridge Jr and El-Esnawi (1997) also tested magnesium - phosphate grout to help develop improved shear - key details. They compared magnesium - phosphate, non - shrink, and epoxy grouts placed in similar shear - key geometries and loaded under both static and fatigue loading. Their testing concluded that grout performance was heavily dependent on shear - key geometry and location. This means that the material could not be evaluated without considering the details of the connection.

Magnesium - phosphate grout has advantages over other conventional grouts, but it is not widely used for shear -key connections. Limitations of magnesium phosphate include cost, compatibility with existing concrete, and challenges with filed placement. Magnesium- phosphate grout also lacks the ductility and fiber – bridging capabilities of UHPC. Like another conventional grout, it becomes brittle once cracked. For these reasons, magnesium phosphate may improve certain performance aspects, but it does not solve major durability concerns such as cracking and leakage Gulyas et al. 1995; Huckelbridge Jr and El-Esnawi (1997).

2.2.3 Epoxy Grout

Epoxy grout is specified when watertight joints, greater bond strength, and early strength gain is desired. Miller et al. (1999) conducted full-scale laboratory testing on epoxy - grouted shear key. They reported no cracking during grouting or during testing. Epoxy grout performed noticeably better than non-shrink grout when both were placed in the same shear key geometry. Lopez de Murphy et al. (2010) reported that cracking potential was reduced when using a full - depth epoxy - grouted shear key along with proper transverse post-tensioning and bearing -pad details. Epoxy grout does have drawbacks, however. Researchers have shown that epoxied segmental bridge joints may fail in a brittle manner, even when the epoxy improves the peak strength. Buyukozturk et al. (1990) found that dry joints failed at about 50% of the peak load of epoxy joints. While the epoxy improved strength, failure occurred suddenly and in a brittle mode. Zhou et al. (2005) and Issa and Abdalla (2007) reported similar behavior with joints of varying shapes. In both studies, failure occurred through shearing of concreate near the joint interface. These studies show that epoxy improves strength and watertightness but may leave little capacity after cracking initiates.

Epoxy grout can also be sensitive to field conditions. Surface preparation, moisture condition of the existing concrete, placement temperature, mixing method, and long-term environmental exposure can all negatively affect the properties of epoxy grout. A. Yuan et al. (2019a) stated that epoxy mortars and polymer concrete mixtures had low permeability and high bond strength, but were sensitive to moisture conditions, difficult to mix and clean up, inconsistent in bonding to cementitious substrates. and difficult to place under varying temperature and loading conditions. Overall, epoxy grout can limit cracking for certain applications, but does not overcome issues with brittle failure, sensitivity to placement and environmental conditions, and uncertain long- term durability (Buyukozturk et al. 1990; Zhou et al. 2005; Issa and Abdalla 2007; A. Yuan et al. 2019a).

2.2.4 Polymer - and Latex - Modified Cementitious Materials

Polymer - and latex - modified cementitious materials are specified when a middle ground between workability and strength is desired. These mixes were created to increase bond strength, decrease permeability, and improve durability over ordinary non-shrink grout while maintaining ease of placement of traditional cement -based materials. Application of polymer-or latex -based grout is typically easier than that of epoxy, and it is more compatible with concrete substrates. These materials are usually designed to have lower water-cement ratios, high flow, slight expansion, and low bleed rates (Alhassan and Issa 2010).

Chang (Cheng et al. 2016) experimentally tested a high-performance cementitious grout capable of filling shear keys between adjacent concrete box-beam bridges. They described the grout as highly fluid, with a low water -cement ratio, slight expansion, and low bleed. Testing performed on a full scale three beam specimen showed that the repaired shear key not only exceeded design requirements but also performed better than conventional grout. These results indicate that modified cementitious grouts can improve mechanical performance when compared to traditional grout. Despite these promising results, polymer-and latex-based materials still require high-quality construction and connection details. Surface cleaning, moisture condition, curing, and profiling of s all affect the final performance of these materials. Cheng et al. (2016) emphasized that brushes and high – pressure water should be used to clean shear key before they are grouted, showing the final performance depends on both material properties and joint preparation. Polymer- and latex-based grouts improve certain aspects of conventional grouts but have not completely solved cracking, debonding, and leakage in shear key connections (Cheng et al. 2016; A. Yuan et al. 2019b).

2.2.5 Engineered Cementitious Composites and Fiber-Reinforced High - Strength Concrete

Engineered cementitious composites (ECC) and fiber -reinforced high-strength concretes bridge the gap between conventional grout and UHPC. While both materials are cement-based, adding fibers helps improve crack control and post cracking performance. Fiber-reinforced cementitious materials have been used experimentally to improve serviceability, control leakage, and enhance ductility when compared to traditional non-shrink grout.

Ozyildirim and Moruza (2016) compared non-shrink grout, ECC with polyvinyl alcohol fibers, and UHPC with steel fibers in shear keys between adjacent voided- slab bridges. Testing showed that all three materials had good bonds, but ECC performed better with respect to leakage over the monitoring period. Although this is just one study, the results indicate that fiber -reinforced cementitious materials can improve cracking control and leakage compared to traditional non - shrink grout in certain applications. Halbe (2014) and Halbe et al. (2017) experimentally showed that certain alternative connection details using fiber reinforced high strength concrete can behave well when paired with proper joint detailing. One experimental joint detail used a blackout filled with fiber reinforced high strength concrete and short-bar lapping of stirrups between adjacent beams. This connection withstood 1 million HL-93 load cycles with minimal or no visible cracking and no leakage (K. R. Halbe 2014; K. Halbe et al. 2017).

Despite having good results in experimental studies, neither material has replaced UHPC as the primary material for high – performance shear-key testing. Their tensile strength and fiber-bridging capabilities are typically lower than those of UHPC. The performance of engineered cementitious composites can vary depending on mix design, fiber distribution, curing method, and placement quality. While these materials show improvements over conventional grout, they require specialized joint detailing and, on their own, have not solved broader durability challenges in concrete infrastructure (Ozyildirim and Moruza 2016; K. Halbe et al. 2017).

2.2.7 Limitations of Conventional Materials that Apply to Multiple Materials

After analyzing each conventional material individually, some general drawbacks apply to all materials. First, conventional materials have low tensile strength and exhibit brittle behavior once cracked. Magnesium-phosphate grouts lack crack-bridging capability. Epoxy grout can achieve higher tensile strength but may still exhibit brittle failure if the concrete substrate or joint interface cracks. Normal concrete has low tensile strength and very little ductility past initial cracking.

Another general drawback of conventional materials is their susceptibility to shrinkage and temperature induced stresses. Cementitious grouts shrink during hydration, and temperature gradients across the bridge cause stress to develop within the joint. If the joint is restrained by existing precast concrete, shrinkage and thermal stress can cause cracking or debonding to occur before the bridge experiences any service loads. Miller et al. (1999) observed this occurrence during full-scale testing when non-shrink grout cracked under environmental conditions with no traffic loading applied to the joint. J. Yuan and Graybeal (2016) discussed this and showed that early dimensional stability is important because small amounts of grout shrinkage can lead to joint cracking or debonding. Joint performance has also been shown to rely heavily on interface shear strength between grout and concrete. For a shear key to function, it must develop sufficient bond with the existing precast concrete member to resist interface shear stresses. If the precast surface is too smooth, contaminated, dry, or otherwise poorly prepared, failure can occur at the interface before the grout itself reaches failure. Oz Yildirim and Moruza (2016) showed that joint performance was mainly affected by the condition of the existing precast member, rather than by the grout used to fill the blackout. Yuan and Graybeal (2016) emphasized proper surface preparation and joint curing, including pre-wetting the existing surface and carefully curing the joint. Experimental results have shown that the interface is often the weak link of a shear -key connection (Ozyildirim and Moruza 2016; J. Yuan and Graybeal 2016).

As with normal-strength concrete, cracking will reduce watertightness when conventional material is used. Water and deciding chemicals can enter the joint and begin corroding the reinforcing steel, damaging nearby grout and concrete, causing leakage, and reducing load transfer between beams. Crack-to-leakage progression has been shown through both field investigations and laboratory testing, which is one reason conventional shear keys have had long-term durability issues (H. G. Russell et al. 2009; Hanna et al. 2009; Frosch et al. 2020; Ozyildirim and Moruza 2016).

Lastly, as mentioned in the previous individual sections, connection details matter just as much as the material used to fill the joint. Lopez de Murphy et al. (2010) showed that grout type was not the only factor affecting whether shear keys cracked. Transverse posttensioning, shear-key shape, and bearing -pad details also affect shear-key performance. Huckelbridge Jr and El-Esnawi (1997) showed that shifting the shear key location reduced stress levels and improved performance, regardless of the grout type used. K. Halbe et al. (2017) found that the best results were achieved with the optimal combination of fill material, lockout geometry, and transverse reinforcement spacing. These studies have shown that no single conventional material can address all issues associated with shear-key connections.

Researchers should know that UHPC is not without its limitations. Flores et al. (2020) found that when tested in similar full-scale channel girder specimens, UHPC grout and non- shrink grout exhibited similar performance and that non-shrink grout surpassed UHPC in certain deflection criteria. However, the authors noted that this may not be conclusive and that UHPC may still be a better material choice for shear-key repair applications due to its durability benefits and comparable cost to some conventional materials. This example shows the importance of choosing a shear-key material that aligns with the project’s overall goals, including strength, bond, crack control, durability, construction quality, and future maintenance costs, rather than seeking a single material to satisfy every demand (Flores et al. 2021).

2.3 UHPC in Bridge Connections

Ultra-high -performance concrete (UHPC) is increasingly used in bridge construction connection regions in difficult to reach areas to construct because they are often located in tight spaces, subjected to high stress, and exposed to environmental conditions. These regions can experience distress or detailing challenges, such as cracking or congested reinforcement. UHPC has been shown to address several of these issues. Instead of bulky sections, UHPC provide secure connections between adjacent parts, transfer loads, and remain durable for decades (Henry G. Russell and Graybeal 2013; B. Graybeal 2014).

In bridges, UHPC has been used for closure pours, deck joints, deck-to girder pockets, and shear keys between adjacent box beams. These applications demonstrate that the benefits of UHPC extend beyond strength. Its primary advantages are connecting separate structural parts, resisting water and chloride ingress and improving crack control. UHPC is engineered to create a strong, durable connection between different structural members (B. Graybeal 2014; Seibert et al. 2019).

UHPC differs from conventional concrete and grout because of its composition and proportioning. UHPC uses a low water-to-binder ratio, little to no coarse aggregate, small practices, and added fibers. These properties allow UHPC to attain high compression and tensile strengths, enabling it to resist crack opening after cracking begins. This property is important for bridge joint applications because joints are often subjected to repeated and variable stress from traffic loads, temperature fluctuations, and thermal expansion and contraction (B. A. Graybeal 2006; B. Graybeal 2014).

One key component of UHPC is the addition of small fibers. If cracking begins, these fibers help bridge the crack and maintain tensile resistance, keeping the joint serviceable. Conventional concrete has limited tensile resistance after cracking, but UHPC's added fibers allow it to remain more dependable in structural applications. Since cracking is less likely to develop into larger structural issues, UHPC is well-suited for bridge joints. Joints can last longer and require less maintenance as a result (B. A. Graybeal 2006; Yoo et al. 2020). Joint regions of bridges are often where distress begins. Water enters the joint and begins corroding the reinforcing steel. Due to UHPC's dense matrix, very little water and chlorides enter the joint, reducing damage to the reinforcement and prolonging the bridge's life by limiting common forms of deterioration (Henry G. Russell and Graybeal 2013; B. Graybeal 2014).

In addition, UHPC bonds very well to reinforcing bars and hardened concrete. This allows shorter reinforcing bar lengths to develop a strong connection. As a result, UHPC can create shorter, cleaner joints with less reinforcement congestion. Detailing still plays an important role, including embedment depth and reinforcement configuration, but overall, UHPC enables more efficient bridge joints (J. Yuan and Graybeal 2016; B. Graybeal 2014).

2.3.1 UHPC Shear Keys in Adjacent Box – Beam and Box- Grider Bridges

Yuan and Graybeal (2016) tested different UHPC connection details in full-scale adjacent box-beam specimens. Their research included partial depth and full- depth UHPC connection details and incorporated both structural loading and temperature change effects. The results of their study showed that UHPC connections can improve connection behavior compared with conventional grouted shear keys. This study is significant because it demonstrated that the UHPC can serve as a primary material for shear keys rather than merely an option for their repair (J. Yuan and Graybeal 2016; A. Yuan et al. 2019a).

Hussein et al. (2017b) tested UHPC shear keys using direct shear, direct tension, and flexure tests. They concluded that UHPC shear keys had higher capacity than grout materials and joint details previously studied. They also concluded that adding transverse shear reinforcement increased the shear capacity of UHPC shear keys. This finding is significant to the present thesis because transverse reinforcement effects on shear transfer, the restraint against interface opening, dowel action, and post-cracking behavior will be studied.

Researchers have also analyzed how shear key geometry and reinforcement details affect bridge performance. Hussein et al. (2018) examined the optimized UHPC shear-key geometry and demonstrated that it affects load transfer and the shear key's failure behavior. Semendary et al. (2017) compared UHPC shear-key connection details from the United States and Canada and found the shear – key shape and reinforcement details differ by region. UHPC shear-key performance depends not only on material properties but also on geometry, reinforcement, surface condition, and bridge environment (Semendary et al., 2017; Hussien et al., 2018).

Field reports have also helped justify the use of UHPC as a shear-key filling material. Semendary et al. (2019) monitored the early -age behavior of a bridge that implemented UHPC shear keys. During their monitoring, no cracks were observed in the UHPC shear key. Neirinck et al. (2023) studied the long-term behavior of UHPC shear keys under temperature effects and found that after two years of filed monitoring, UHPC shear keys showed satisfactory performance. Their finite element results also showed that damage and debonding can start near the top of the shear key under cold-temperature effects. This shows that UHPC shear keys require proper evaluation under real-world environmental conditions (Semendary et al., 2019; Neirinck et al., 2023).

2.3.2 UHPC -HSC Interface and Bond Considerations

When using UHPC as a shear key fill material, the interface between UHPC and the adjacent high - strength concrete (HSC) surface is one of the most critical areas of the connection. While UHPC can have high strength, the weakest link in the joint may still be bond between UHPC and the hardened concrete surface. Weak interfaces can lead to cracking, slip, or debonding before the UHPC material itself reaches its strength. Therefore, studying the behavior of the UHPC -HSC interface is crucial for understanding shear -key behavior (Hussein et al., 2016; Tan,2021; Erfani, 2025).

Surface preparation can significantly affect the bond strength between UHPC and HSC. Smooth surface can reduce mechanical interlock, while roughened or exposed aggregate surfaces can improve adhesion, friction, and shear transfer. Hussein et al. (2016) demonstrated that UHPC can achieve a strong bond with HSC across various surface -roughness conditions. However, the level of roughness changed the bond response. Tan (2021) conducted research on the behavior of the UHPC-HSC interface using direct tension, pull-off, slant shear, and bi- shear tests. She demonstrated that surface condition and loading types significantly affect bond strength and failure mode (Hussien et al., 2016; Tan, 2021).

The interface matters because a shear key can be under many different types of loads. Under service and ultimate loading, the UHPC-HSC interface may be subjected to shear, tension, sliding, and dilation. Transverse reinforcement crossing the interface can help resist these actions by providing clamping resistance and dowel action. This interaction among bond strength, surface roughness, friction, and transverse reinforcement explains why UHPC shear key behavior cannot be defined solely by material strength (Mattock,2001; Yuan and Graybeal, 2016; (Hussein et al. 2017b).

This information relates directly to this thesis. The specimens used in this research were UHPC cast against hardened HSC with varying surface preparation and transverse reinforcement. Therefore, the research on UHPC-HCS bond strength provides a background for understanding how changes in roughness and transverse reinforcement affect shear capacity, crack development, and failure mode.

2.3.3 Remaining Design Questions

Although UHPC has proven highly useful in bridge connections, outstanding design questions remain. Most current bridge design codes were developed using conventional concrete and conventional shear – friction behavior. These codes do not account for UHPC-specific interface behavior, fiber bridging, high tensile strength, or the ways in which UHPC alters the roles of cohesion, aggregate interlock, friction, and dowel action. This leaves uncertainty when designing UHPC -filled shear keys or UHPC -HSC interfaces in accordance with existing code guidelines (CSA Group, 2019; AAHTO, 2020).

Another concern when using UHPC is that it is not a fully standardized material. There can be many proprietary and non-proprietary UHPC mixtures with varying strengths, flowability, fiber distributions, shrinkage, bond behavior, and curing sensitivity. Research conducted on non-proprietary UHPC and comparing different commercial UHPC class materials has shown that current bond related design assumptions do not directly apply to all UHPC mixes. This indicates that mixture – specific testing and detailed construction control remain critical for UHPC bridge connections (Swenty and Graybeal 2017; Haber et al. 2018; Shokrgozar et al. 2024).

Experimental data remain limited regarding the direct-shear behaviour of UHPC shear keys cast against hardened HSC substrates. Much of the existing research has focused on UHPC material properties, field-cast bridge-deck connections, large-scale bridge joints, or overall structural performance (Graybeal, 2012, 2014). Although several studies have examined the shear behaviour of UHPC–concrete interfaces, relatively few have investigated crack initiation and propagation in UHPC–HSC shear-key specimens under direct shear while varying both surface roughness and transverse reinforcement (Semendary et al., 2020; Sharma et al., 2021; Feng et al., 2022). These parameters are important because substrate roughness and reinforcement crossing the interface can significantly influence interface shear capacity, load transfer, crack localization, and failure mode (Sharma et al., 2021; Muzenski et al., 2022).

Consequently, UHPC should not be treated simply as a direct replacement for conventional connection grout. Although UHPC is a high-performance material, the behaviour of a UHPC connection depends on the complete structural system, including the UHPC properties, condition and preparation of the HSC substrate, shear-key geometry, reinforcement details, mixing and placement procedures, curing conditions, and loading history (Graybeal, 2012, 2014). Therefore, the design and construction requirements of each UHPC shear-key application should be evaluated based on its specific materials, geometry, detailing, and exposure conditions. This thesis addresses part of this research need by testing UHPC–HSC shear-key specimens under direct shear and examining how surface roughness and transverse reinforcement affect crack development, load transfer, and shear behaviour.

2.4 Research Gaps

Research has shown that UHPC can serve as a shear-key fill material in precast bridge connections. More specifically, studies have shown that UHPC exhibits higher strength, bond capacity, durability, and post-cracking behavior than conventional grout and concrete materials. However, factors that affect UHPC-HSC shear key behavior include interface bond strength, surface roughness, mechanical interlock, transverse reinforcement, dowel action, shear-key geometry, and adjacent HSC strength.

Because multiple failure mechanisms contribute to load transfer during loading, the UHPC-HSC key response cannot be interpreted solely from material properties or current code equations. To gain insight into shear-key behavior, shear keys must be tested experimentally, and observations must document how load is transferred along the interface, where cracking initiates, how slip evolves, and how the final failure mode develops. This forms the research motivation for the present thesis.

The first knowledge gap is that current interface shear provisions are not developed with UHPC interface behavior in mind. Instead, provisions from AASHTO and CSA are based primarily on conventional concrete-to concrete, conventional grout HSC, or normal- strength concrete HSC interface behavior. Both standards provide guidance on the factors affecting interface shear transfer, surface roughness criteria, the relative contributions of cohesion and friction, and the calculation of the shear friction resistance provided by reinforcement crossing a potential shear plane. Due to this limitation, it is possible that existing equations and design provisions either underestimate or overestimate shear capacity or inaccurately predict what failure mode should be expected for UHPC-HSC shear keys.

A second gap in the literature is the limited amount of direct shear data available for realistic UHPC-HSC shear-key specimens. Many researchers have studied the material properties of UHPC, pull-off bond tests, the behavior of the bridge deck connection details, field-cast bridge joints, or full-scale bridge performance. Other researchers have studied the behavior of full-scale UHPC keyed joints, but used smaller specimens or highly simplified test geometries that do not accurately represent adjacent bridge connections. Very few researchers have investigated UHPC shear keys cast against hardened HSC substrates with geometries directly taken from adjacent box-beam or box-girder bridge connections. Specimen geometry is an important variable because realistic shear-key geometry can affect the load path, stress distribution, crack initiation locations, and the mechanical interaction between the UHPC shear key and the surrounding HSC.

A third knowledge gap is determining how surface roughness and transverse reinforcement interact. Numerous studies have shown that increasing surface roughness can enhance bond strength, friction resistance, dilation capacity, and mechanical interlock. Other studies have shown that transverse reinforcement can increase clamping force between the connected parts, provide additional shear-friction resistance, and add dowel action after cracking initiates or slip occurs. However, these variables are often studied independently or tested under varying load conditions. There is still a need to study how roughness and reinforcement interact when both are altered within the same UHPC-HSC shear -key system under direct shear loading.

A fourth knowledge gap exists in fully understanding crack development and the final failure mode. Measurements of load versus displacement, LVDT's, and strain gauges can provide the researcher with valuable insights into overall specimen behavior, but they may not directly reveal where or how cracking initiates and propagates across the UHPC-HSC interface. This is especially true for UHPC shear keys, as final failure can occur at the interface, within the surrounding HSC, or due to a combination of slip, cracking, and reinforcement. Additional full field observational techniques, such as DIC, can be used to better understand how measured load responses correlate with the specimen's actual physical behavior.

Each gap described above indicates the need to conduct an experimental testing program to evaluate UHPC-HSC shear keys using direct shear tests, while varying interface surface preparation and transverse reinforcement. The testing program for this thesis addresses that need by evaluating the shear capacity, load-displacement response, interface slip behavior, strain behavior, crack development, and final failure mode of UHPC-HSC keys. Furthermore, by applying DIC to tested specimens alongside traditional instrumentation, this study will visualize how the connection behaves physically during cracking and slips development, rather than simply observing how much load it can support.

2.5 Section Summary

This section provided an overview of important topics that help to understand the behavior of UHPC-HSC shear-key connections. Bridge shear keys have been used to transfer loads between adjacent box beam members and to improve overall bridge performance by allowing the bridge to behave more monolithically. However, researchers have found that conventional shear-key materials, such as normal-strength concrete or mortar grout, can experience cracking, leakage, corrosion, bond loss, and brittle failure. These deficiencies are often attributed to shrinkage and temperature effects during placement, low tensile strength, low post-cracking toughness, and sensitivity to surface preparation, detailing, or construction techniques.

To improve precast connection performance, researchers have begun using UHPC as an alternative shear-key material due to its superior compressive strength, higher tensile performance, micro steel fiber bridging, high bond strength, low permeability, and increased durability. Because of these advantages, researchers and bridge owners have successfully used UHPC as a filling material in field-cast bridge connections. Applications include bridge deck connections, closure pours, repair rehabilitation details, and shear keys between adjacent box beam or box -girder bridges. While literature indicates that using UHPC improves the overall behavior of precast connections, it does not eliminate the need to understand the behavior of the surrounding interface. Details regarding surface preparation, transverse reinforcement placement, shrinkage and temperature effects, and compressive strength of surrounding concrete can all affect the performance of a UHPC shear key.

Shear transfer across the interface between UHPC and HSC is controlled by multiple interacting transfer mechanisms. Before cracking initiates or gross slip occurs, cohesion and adhesion resist shear transfer. However, after cracking initiates or gross slip occurs, friction, mechanical interlock strength, dilation capacity, transverse reinforcement, and dowel action begin to control the response. Understanding how these variables influence response can help explain why some shear keys may initially appear stiff and linear but then suddenly exhibit sliding or debonding as shear loading continues. After cracking or slip initiation, sudden changes in failure mode are often due to another mechanism taking over the response.

Surface roughness is one of the main factors influencing this change in mechanism. Smooth interface can provide high strength while the initial adhesive bond remains intact but will suddenly slip after that bond is broken. Roughened interfaces can increase bond strength, mechanical interlock, frication resistance, and dilation capacity. However, caution should be exercised when increasing surface roughness, as excessive increases can damage aggregate particles, weaken the surrounding concrete, or reduce overall bond strength. Therefore, surface preparation should ensure a clean, sound, and textured interface rather than a uniformly rough one.

Transverse reinforcement is another major factor that can affect UHPC-HSC shear -key behavior. Bars crossing a potential shear plane an increasing clamping force on the joint, provide shear-friction resistance, and act as a dowel after cracking initiates or slip occurs. Transverse reinforcement helps to restrict joint opening and provide additional load-transfer capacity after cracks initiate or slip occur. Literature also shows that reinforcement contribution is dependent on the condition of the interface (rough bonded versus smooth sliding, the amount of slip that occurs, the development length of bars in the loaded concrete member, the bond strength between bars and concrete, and whether bars are physically able to develop stress under load.

Shear-key geometry can also influence response by altering load path, mechanical interlock strength, stress distribution, and crack initiation location. variables such as shape, depth, width, face angle, and the number of shear keys all affect shear capacity and the observed failure mode. However, car should be taken when optimizing shear-key geometry, as simply increasing its size is not always the best solution. If the surrounding HSC fails before the UHPC shear key reaches its material capacity, the connection will control the load response rather than the UHPC material properties.

Finally, this section reviewed common testing methods for studying interface behavior and or shear response. Push -off tests, direct shear tests, bond tests, full-scale beam tests, field monitoring, strain gauges, LVDT's crack mapping, and DIC techniques can be used together to understand the behavior of UHPC -HSC shear keys. No single technique can completely characterize shear-key response. For the purpose of this thesis work, direct shear testing of UHPC-HSC shear keys combined with displacement measurement, strain gauging, crack observation, and DIC provide a suitable method of testing because variables can be studied beyond ultimate shear capacity. Overall strength is an important design parameter, but it is equally important to understand how the connection behaves throughout testing.

In conclusion, prior research supports the use of UHPC as a shear key in precast bridge connections. There are still knowledge gaps that can be addressed through additional experimental testing. More specifically, there is a need to study the behavior of realistic UHPC-HSC shear -key specimens in which surface roughness and transverse reinforcement are altered simultaneously, and in which crack development can be monitored throughout loading. This thesis addresses that need by completing direct shear tests to determine how these two variables affect shear capacity, load-displacement behavior, interface slip behavior, crack initiation location, crack propagation path, and failure mode.

3. Experimental Program

3.1 Experimental Program Overview

The experimental program was developed to evaluate the shear behavior of UHPC-HSC shear key connections and to evaluate the durability of the interface between the two materials using specimens cast in previous studies. This approach was used because the performance of a UHPC-HSC shear key depends on several interacting mechanisms. These mechanisms include UHPC and HSC material strength and interface bond which is directly proportionate to surface roughness, and the presence of transverse reinforcement. Durability studies observing the changes in strength and failure modes of UHPC-HSC specimens subjected to outdoor environment are scarce in literature.

The experimental work continued from the Little Morris Bridge research program and used the specimens that were cast in earlier studies by Tan (2021) and Erfani (2025). Tan (2021) focused on the UHPC-HSC interface using small-scale bond tests, including direct tension, pull-off, slant shear, and bi-shear tests. Erfani (2025) focused on UHPC shear-key shrinkage behavior, curing environment, reinforcement and bridge-connection details.

The UHPC material used in the Little Morris Bridge research program was a commercially available material known under the trade name Ductal. Tan (2021) identified the bridge shear-key material as Ductal JS 1000, consisting of Lafarge Ductal premix, water, CHRYSO Fluid Premia 150 superplasticizer, and 0.2 mm × 14 mm micro steel fibers. The material was mixed on site under supplier supervision and used to cast the Little Morris Bridge shear keys.

Erfani (2025) used Ductal, identified as JS1000 Grey Premix Design, prepared at the University of Manitoba Concrete Laboratory. The mix contained premix, water, Premia 150 superplasticizers, and 2% steel fibers.

The experimental program in this thesis therefore consisted of two main test groups. The first group was a durability test group that included material and interface tests. Table 3.1 lists the materials and number of specimens that were tested in this program. These tests included compressive strength, indirect tension, pull-off, slant shear, and bi-shear tests. These tests helped establish the change in the material strength, tensile cracking resistance, bond strength, combined compression- shear interface behavior, and shear-dominated interface response because of 5-year outdoor exposure. The average daily temperatures during the 5-year period can be found in Figure 3.1.

The second group included structural shear-key tests on 5 shear key specimens. These tests were conducted on UHPC-HSC shear -key specimens designed to evaluate the effect of interface surface preparation and transverse reinforcement on shear performance of the keys. The shear-key series

Table 3.1: Summary of material and interface tests conducted in the present study

Test type	Material	Pour site and date	Specimen origin	Number tested
Compressive strength	HSC	Lafarge Precast plant, 2019	Tan (2021)	13
Indirect tensile strength	HSC	Lafarge Precast plant, 2019	Tan (2021)	10
Compressive strength	Ductal	Little Morris Bridge construction, 2019	Tan (2021)	2
Compressive strength	Ductal	W.R. McQuade Structures Laboratory, 2023	Erfani (2025)	3
Pull-off	Ductal-HSC composite	HSC: Lafarge Precast plant, 2019; UHPC: Little Morris Bridge construction site, 2019	Tan (2021)	11
Slant shear	Ductal-HSC composite	HSC: Lafarge Precast plant, 2019; UHPC: Little Morris Bridge construction site, 2019	Tan (2021)	5
Bi shear	Ductal-HSC composite	HSC: Lafarge Precast plant, 2019; UHPC: Little Morris Bridge construction site, 2019	Tan (2021)	8
Total				**52**

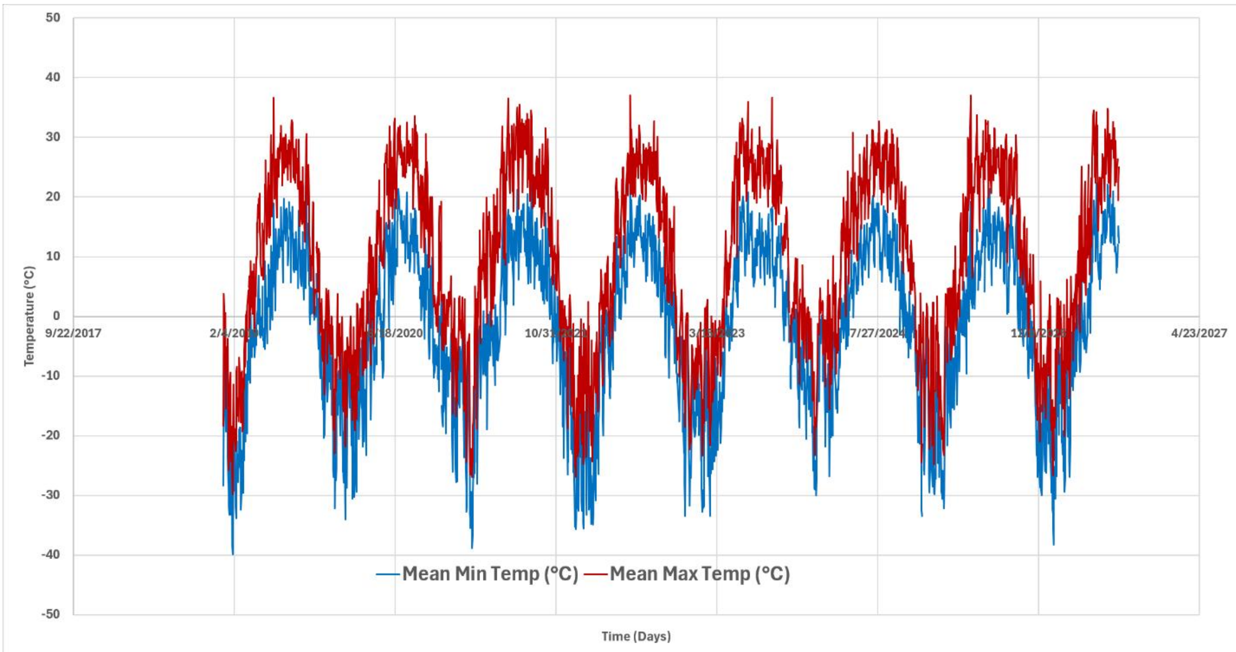

Figure 3.1: Mean minimum and mean maximum temperature fluctuation in Winnipeg between 2019-2026

included a smooth unrestrained specimen, a roughened unrestrained specimen, and a roughened restrained specimen. These four specimens were tested using direct shear setup, which allowed the effects of surface roughness and reinforcement to be compared under consistent loading and boundary conditions.

A smooth, restrained specimen was also tested in this research program. However, this specimen was tested using test setup that introduced both shear and moment in the key. Because of the loading arrangement and boundary conditions that were different compared to the rest of the shear keys, the results for this specimen will be discussed separately.

3.2 Material Characterization Tests

The material characterization tests were conducted to determine the baseline material properties required to understand the shear-key response and included compressive strength testing and indirect tension testing. The list of test types and specimen origin is listed in Table 3.2. Compressive strength tests helped define the baseline compressive capacity of the HSC and UHPC materials. Indirect tension tests helped quantify tensile cracking resistance. Cracking is an important consideration because it can develop under shear loading, even when the overall loading condition is not pure tension. The material tests will compare the present remaining strength of specimens cast in the Little Morris Bridge experimental program and will be compared to the strengths obtained in 2019.

Table 3.2: HSC and UHPC specimens tested in this program

<table>
<tr><th>Test type</th><th>Material</th><th>Pour Site and date</th><th>Specimen origin</th><th>Number of specimens</th></tr>
<tr><td>Compression</td><td rowspan="2">HSC</td><td rowspan="2">Lafarge Precast plant, 2019</td><td rowspan="3">Tan (2021)</td><td>13</td></tr>
<tr><td>Tension</td><td>10</td></tr>
<tr><td>Compression</td><td>Ductal</td><td>Little Morris Bridge, 2019</td><td>2</td></tr>
<tr><td>Compression</td><td>Ductal</td><td>W.R. McQuade Structures Laboratory, 2023</td><td>Erfani (2025)</td><td>3</td></tr>
</table>

3.2.1 Compressive Strength Tests

Compressive strength tests were conducted to evaluate the retained compressive capacity of the UHPC and HSC specimens obtained from the earlier experimental programs. Several of these specimens had been stored outdoors for approximately seven years and had experienced natural temperature variations ranging from approximately -40°C to +37.0°C. The results were compared with previously reported values, where available, to identify changes in compressive strength over time.

UHPC compressive strength tests were performed on 3 in. by 6 in. cylinders, corresponding to approximately 76.2 mm by 152.4mm. HSC compressive strength tests were performed on 6 in. by 12 in. cylinders, corresponding to approximately 152.4 mm by 304.8 mm. Both UHPC and HSC compressive strength tests were performed in accordance with ASTM C39/C39M. For UHPC testing, ASTM C1856/C1856M was also considered where UHPC-specific requirements were applicable.

The ends of each cylinder were ground flat to provide flat and uniform loading surfaces. The dimensions of each specimen were recorded to determine its cross-sectional area. Because the 3 in. by 6 in. cylinders have a standard length to diameter ratio of 2.0, no length to diameter correction was applied when the specimens remained at their standard dimensions.

Before the compressive strength tests, specimens were prepared for Digital Image Correlation (DIC) by applying a speckle pattern to the specimen surface. A digital camera was positioned to capture the deformation throughout the test, while two Linear Variable Differential Transformers (LVDTs) were installed to measure the axial displacement of the specimen. The DIC system and LVDTs were used to monitor deformation and crack development during loading as shown in Figure 3.2

Figure 3.2: HSC specimen under compressive test

Compressive strength was calculated by dividing the maximum applied compressive load by the cylinder cross-sectional area:

Equation 3.1

$$f_c = \frac{P_{max}}{A}$$

Where (f_c) is the compressive strength, (P_{max}) is the maximum compressive load, and (A) is the cross-sectional area of the cylinder.

3.2.2 Indirect Tension Tests

Indirect tension tests were completed on cylinders to characterize the tensile cracking resistance of the concrete system, casting details are provided in Table 3.2. Indirect tension tests were completed using the split-cylinder method outlined in ASTM C496/ C496M and CSA A23.2. These tests were completed on 6in. by 12 in. cylinders, corresponding to approximately 152.4mm by 304.8 mm. In this test method, compressive load is applied along two diametrically opposite lines that are parallel to the longitudinal axis of the cylinder. This loading condition induces tensile stresses along the vertical diameter of the specimen. Failure generally occurs through splitting of the specimen along the loaded diameter, as shown in Figure 3.3. The specimens used in this test were cast at the Lafarge Precast plant in Winnipeg, Manitoba, between May 15 and June 7, 2019, as part of Tan's (2021) experimental program.

The indirect tensile strength was calculated using:

Equation 3.2

$$f_t = \frac{2P_{max}}{\pi LD}$$

Where (f_t) is the indirect tensile strength, (P_{max}) is the maximum applied load, (L) is the cylinder length, and (D) is the cylinder diameter.

Failure mode during indirect tension testing was recorded at the end of each test. Splitting failure indicated that the specimen behavior was consistent with the intended test method. Observing this failure mode provided additional confidence that the measured indirect tensile strength values could be used as material-level context when evaluating crack formation in the shear key specimen.

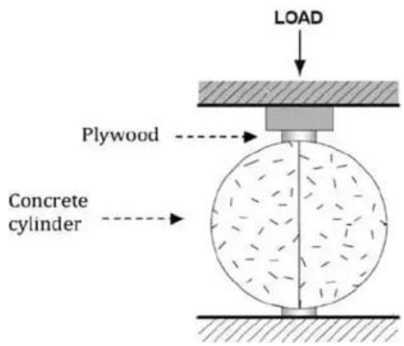

a

b

Figure 3.3: Indirect tension/ split cylinder test, (a) test setup; (b) test in progress

3.2.3 Interface Characterization Tests

The UHPC-HSC interface is critical regions in the composite concrete system. Even when the UHPC has sufficient compressive and tensile strength, slip, or debonding along the interface can influence the ultimate capacity and failure mode of the bonded system. The list of test types and specimen origins is listed in Table 3.3.

Table 3.3: Interface characterization tested specimens

Test type	Material	Pour Site and date	Specimen origin	Number of specimens
Pull-off	Ductal-HSC composite	HSC: Lafarge Precast plant, 2019; UHPC: Little Morris Bridge construction site, 2019	Tan (2021)	11
Bi-shear		HSC: Lafarge Precast plant, 2019; UHPC: Little Morris Bridge construction site, 2019		8
Slant shear		HSC: Lafarge Precast plant, 2019; UHPC: Little Morris Bridge construction site, 2019		5

Two types of interface characterization tests were considered: pull-off tests, bi-shear and slant shear tests. These tests were selected because they describe different stresses of the interface. Pull-off testing provides information about tensile bond strength normal to the interface. In contrast, slant shear testing provides information on how the interface behaves under combined normal and shear stresses. The bi-shear test represents a condition of pure shear stresses.

Tan (2021) studied the behavior of the UHPC-HSC interface using small-scale bond tests, including direct tension, pull-off, slant shear, and bi-shear configurations. Results from Tan (2021) are used to study the effect of 7 years outdoor exposure on the specimen strength.

3.2.4 Pull-off Tests

Pull-off tests were conducted to determine the tensile bond strength between the UHPC overlay and the hardened HSC substrate. The pull-off test was included in this study because the UHPC-HSC interface may experience localized opening and tensile stresses during shear loading. Even though the shear-key specimens were not loaded in pure tension, tensile stresses will be present in the interface region due to the shear key shape. For these reasons, the pull-off test provided useful interface -level data regarding the tensile bond resistance of the UHPC-HSC interface.

Pull-off specimens consisted of a 330 mm long by 178 mm wide by 152 mm thick HSC slab with a 51 mm thick UHPC overlay. The UHPC surface was partially cored using 51mm diameter cores drilled to a depth of 76 mm into the substrate. Each pre-cut core was prepared by cleaning the top surface before bonding a 51 mm diameter steel disc to the core surface using epoxy. The epoxy was allowed to be cured before testing commenced.

Pull-off testing was performed following the procedure outlined in ASTM C1583/C1583M. Tensile load was applied perpendicular to the bonded surface and directly to the steel disc until failure occurred. The maximum tensile load achieved during testing was recorded and used to calculate the pull-off tensile bond strength. Because the pull-off load was applied normally to the bonded surface, the test provided a direct measurement of tensile resistance across the bonded UHPC-HSC interface.

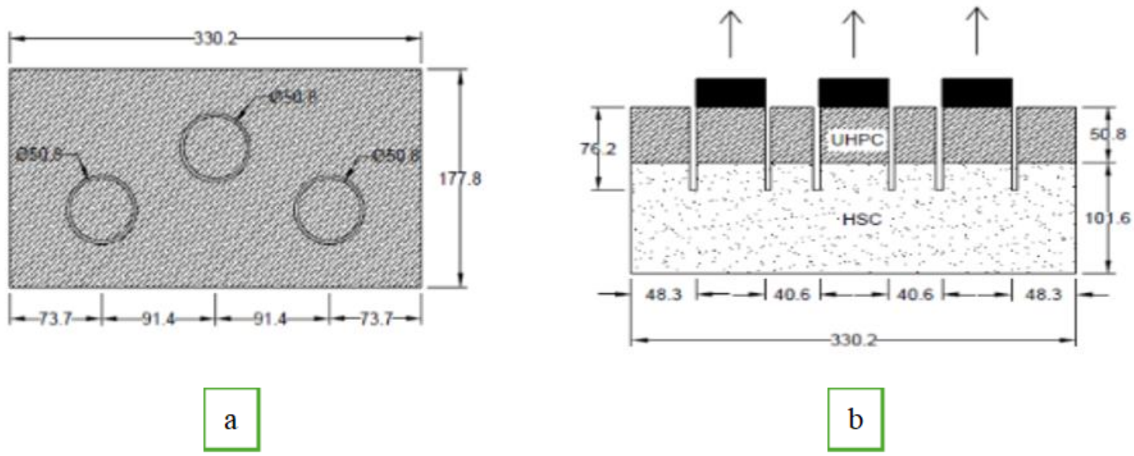

Figure 3.4: Pull off test specimens (a) position of the cores in plan view; (b) side view dimensions (Tan 2021)

Pull-off tensile bond strength was determined using Equation 3.3:

Equation 3.3
$$f_{po} = \frac{P_{max}}{A_c}$$

Where (f_{po}) is the pull-off tensile bond strength (MPa), (P_{max}) is the maximum load recorded during pull-off testing, and (A_c) is the cross-sectional area of the drilled core.

The failure mode during pull-off testing was also evaluated. Failure could occur along several different paths, including the UHPC-HSC interface, within the HSC substrate, within the UHPC overlay, through the epoxy bond, or through a combined failure path. Evaluating the failure location helped identify the weakest region within the bonded system under direct tensile loading. If failure occurred within the HSC substrate, the bonded interface was not the weakest region under pull-off loading. If failure occurred along the interface, this would suggest that the bonded interface controlled the tensile response of the pull-off specimen.

Pull-off tests results were not used directly to predict shear-key capacity. This is because the stress state across the bonded UHPC-HSC interface during pull-off testing is primarily tensile and normal to the interface. In the shear-key specimens, the response within the bonded interface region was more complex and involved shear, compression, and tension.

3.3 Bi-Shear Tests

Bi-shear tests were conducted to evaluate the shear response of the UHPC-HSC interface under a shear-dominated loading condition. Interface behavior was previously described using pull-off and slant shear testing; however, these tests do not fully represent direct shear transfer along the bonded interface.

The bi-shear specimens were molded as 152 mm by 152 mm cubes. The UHPC portion of each bi-shear specimen was cast along one edge of the cube and bonded to the adjacent HSC portion. This created a single 152 mm by 152mm UHPC-HSC interface along which shear loading was applied. The loading setup allowed the bonded interface to be subjected to pure shear loading condition. The specimen origin is shown in Table 3.3.

Bi -shear tests were completed using displacement rate of 0.2 mm/min. Steel plates were used during testing to apply load to the specimen and develop shear along the bonded interface, as shown in Figure 3,5 (b). The specimen response was assessed by examining load-displacement behavior, crack initiation and propagation, localized deformation, and failure mode.

Bi- shear strength was calculated using Eq. 3.7:

Equation 3.7

$$\tau = \frac{P_{max}}{A_i}$$

where:

- τ = average shear stress at failure (MPa)
- P_{max}= maximum applied load (N)
- A_i= area of the UHPC-HSC interface (mm²)

The maximum applied load, (P_{max}), was used to calculate the ultimate bi-shear strength of the specimen. This load represents the greatest resistance developed by the UHPC–HSC interface during testing. The first sudden drop in the load–displacement response was interpreted separately as an indication of initial cracking or damage and was not used in the calculation of the ultimate bi-shear strength.

Mode of failure was recorded during testing of each bi-shear specimen. Specimens could fail along the UHPC-HSC interface, within the HSC portion of the specimen, within the UHPC region, or along path consisting of multiple failure types. Identification of failure mode helped determine whether the response was controlled by interface bond strength, material-level cracking, localized shear failure, or a combination of these mechanisms.

a

b

Figure 3.5: Bi-shear test (a) specimen detail (Tan 2021); (b) instrumented face

During the bi-shear tests, one face of each specimen was prepared with a speckle pattern for Digital Image Correlation (DIC), while a Linear Variable Differential Transformer (LVDT) was installed on the opposite face to measure specimen displacement. DIC was used to measure full-field surface deformation and crack formation on the observed face of the specimen, while the LVDT provided displacement measurements throughout the test. DIC allowed full-field displacement and strain results to be obtained on the observed side of the specimen during testing. DIC was particularly helpful during the bi-shear tests because localized strain concentrations and cracking can occur near or along the interface before they are easily observed during testing. Therefore, DIC results supported the interpretation of where cracks initiated, how strain localized near the bonded interface, and how damage evolved with increased load.

3.2.5 Slant Shear Tests

Slant shear tests were conducted to evaluate the UHPC -HSC interface under combined normal compression and shear stresses.

The slant shear specimens consisted of 76.2 mm by 142.2 mm cylindrical specimens composed of both HSC and UHPC, with details on casting and their origin listed in Table 3.3. The UHPC-HSC interface was inclined within the cylinder so that axial compressive loading produced both normal and shear stresses along the bonded interface. The interface inclination angle was 30^0. The specimens were prepared and tested in accordance with ASTM C882/C882M. Before testing, the cylinder ends were ground to provide flat and uniform loading surface.

The slant shear tests were conducted under displacement control at a loading rate of 0.2 mm/min. A linear variable displacement transformer (LVDT) was installed across the UHPC-HSC interface to measure the relative slip that developed along the bonded interface throughout the test. The test setup is shown in Figure 3.5 (b) During testing, compressive load was applied to the ends of the cylindrical specimen until failure occurred. As axial displacement increased, stress developed across the inclined UHPC-HSC interface. Because the interface was inclined, the applied compressive stress was resolved into a normal stress component perpendicular to the interface and a shear stress component parallel to it.

These calculated stress components were used to describe the combined stress state acting along the bonded interface.

The applied compressive stress was calculated using Equation 3.4

Equation 3.4

$$\sigma_0 = \frac{P_{max}}{A}$$

where

- σ_0= applied compressive stress (MPa)
- $P_{\max}$= maximum applied compressive load (N)

- A= cross-sectional area of the cylindrical specimen (mm^2)

The normal stress acting on the inclined UHPC-HSC interface was calculated using equation 3.5:

Equation 3.5 $\sigma_n = \sigma_0 cos^2 s\theta$

where

- σ_n= normal stress on the interface (MPa)
- σ_0= applied compressive stress (MPa)
- θ= inclination angle of the interface

The shear stress acting along the inclined UHPC-HSC interface were calculated using Equation 3.6:

Equation 3.6 $\tau_n = \sigma_0 \, sin\,\theta \, cos\,\theta$

or equivalently,

$$\tau_n = \frac{\sigma_0}{2}\sin(2\theta)$$

Where: τ_n= shear stress acting along the inclined interface (MPa)

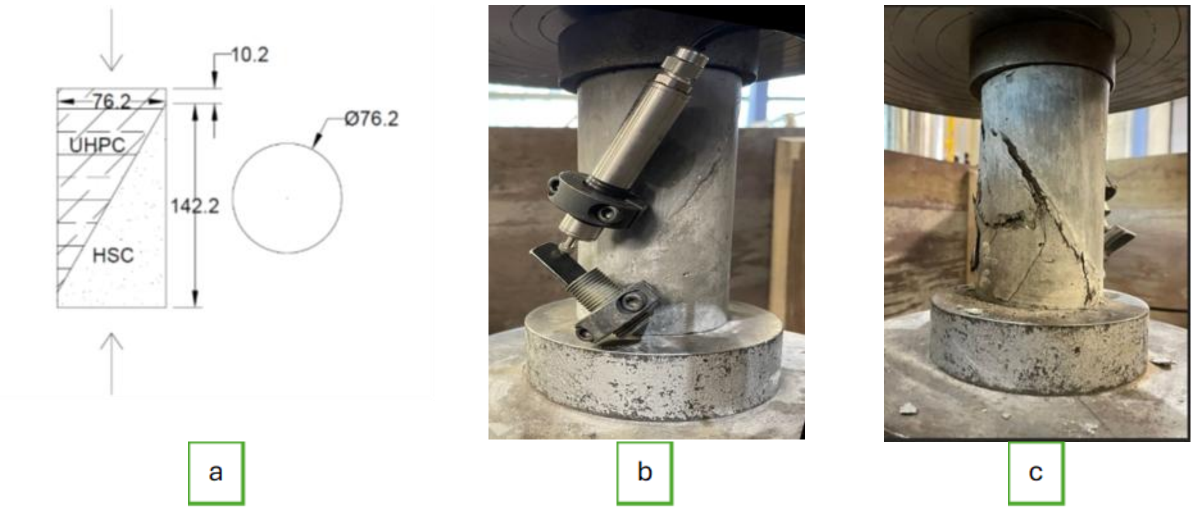

Figure 3.6: Slant Shear test (a) specimen details (Tan 2021); (b) instrumentation setup; (c) Slant shear failure

Failure mode was also evaluated during slant shear testing. Failure could occur along the UHPC-HSC interface, within the HSC portion, within the UHPC portion, or through a combined path. Observing the failure mode was important because it helped determine whether the bonded interface controlled the response under combined normal and shear loading, or whether failure occurred through one of the materials instead.

3.4 Shear -Key Tests Matrix and Variables

The variables of interest were selected, and a test matrix was organized to assess the effect of interface surface condition and transverse reinforcement on the direct shear behavior of UHPC-HSC shear-key specimens. These variables were selected because they relate directly to the expected shear-transfer mechanism at the interface. Surface roughness enhances mechanical interlock, friction, and bond behavior, whereas transverse reinforcement restrains, through dowel action, the interface opening after initiation of cracking or slip.

The directly comparable shear-key test series consisted of four specimens representing three connection configurations, all tested using the same direct-shear setup: one smooth/as-cast unrestrained specimen, one roughened unrestrained specimen, and two roughened restrained specimens. The smooth/as-cast unrestrained specimen served as the baseline. Comparison with the roughened unrestrained specimen was used to evaluate the influence of surface roughness without transverse reinforcement. The two roughened restrained specimens were used to evaluate the effect of transverse reinforcement under the roughened interface condition and to assess the consistency of the measured response.

Specimen labels were selected to describe the interface and reinforcement conditions. The first term of each label refers to the surface condition of the interface. The letter S indicates a smooth, as-cast interface, while the letter R indicates a roughened interface. The second term of each label refers to the restraint condition. NR indicates that the specimen was unrestrained, meaning that no transverse reinforcement crossed the UHPC-HSC interface. R indicates that the specimen was restrained, meaning that transverse reinforcement crossed the interface.

Following this naming convention, the primary comparable tests series consisted of specimens S-NR, R-NR and R-R. These specimens were tested under the same general loading and boundary condition of pure shear. Maintaining a consistent test setup is important because it allows differences in shear capacity, load-displacement response, crack development, and failure mode to be interpreted mainly in relation to surface roughness and transverse reinforcement, while other testing conditions are kept relatively consistent.

A smooth, restrained shear-key specimen, labeled S-R, was tested as part of the broader shear-key testing program. However, this specimen was tested using a combination of flexure and shear. Because the loading arrangement and boundary conditions were different compared to the rest of the specimens, this specimen is discussed separately from the rest of the tests. Table 3.4 summarizes the shear-key specimen configurations and their role in the experimental program.

Table 3.4: Shear-key specimen configurations

Specimen ID	Interface condition	Number of specimens	Casting Time	Transverse reinforcement	Test setup	Role in analysis
S-NR	Smooth (as-cast)	1	HSC 2022, UHPC 2023	No	Direct shear	Baseline specimen
R-NR	Roughened	1		No	Direct shear	Effect of surface roughness
R-R	Roughened	2		Yes	Direct shear	Combined effect of roughness and reinforcement
S-R	Smooth (as -cast)	1		Yes	Shear and bending test	Effect of dowel action

This test matrix was organized to separate the main variables as much as possible. The comparison between S-NR and R-NR is used to evaluate the effect of surface roughness in the absence of transverse reinforcement. The surface roughness of the shear-key specimens was quantified using Mean Texture Depth (MTD), which describes the average depth of the surface macrotexture. The MTD values measured for the rough UHPC-HSC interfaces ranged from 1.79 to 2.27 mm, while those measured for the smooth/as-cast interfaces ranged from 0.53 to 0.69 mm (Erfani 2025). Based on the fib/CEB-FIP classification, surfaces with an MTD below 1.5 mm are classified as smooth, while surfaces with an MTD of at least 1.5 mm are classified as rough. Therefore, the measured MTD values confirm that the two specimen groups represented distinctly different surface conditions.

The comparison between R-NR and R-R is used to evaluate the added influence of transverse reinforcement when the interface is roughened. The S-R specimen provides additional information on the smooth restrained condition, but because it was tested under a different setup, it is not considered a direct companion to the primary comparable series.

This distinction is important for maintaining a consistent interpretation of the results. Direct comparison between specimens is most reliable when the loading arrangement, boundary conditions, and specimen geometry are the same. For this reason, the main discussion of surface roughness and reinforcement effects focuses on S-NR, R-NR and R-R, while the S-R specimen is used as supplementary context where appropriate.

3.5 Specimen Design Geometry

3.5.1 Geometry

The shear-key specimens were designed and cast as representative segments of the connection region between adjacent box beam girders by Erfani (2025). At the time of the original material testing, the UHPC and HSC had compressive strengths of 142 MPa and 73.5 MPa, respectively, while the transverse reinforcing steel had a yield strength of 524 MPa. These material properties represent the original strengths associated with the shear-key specimens.

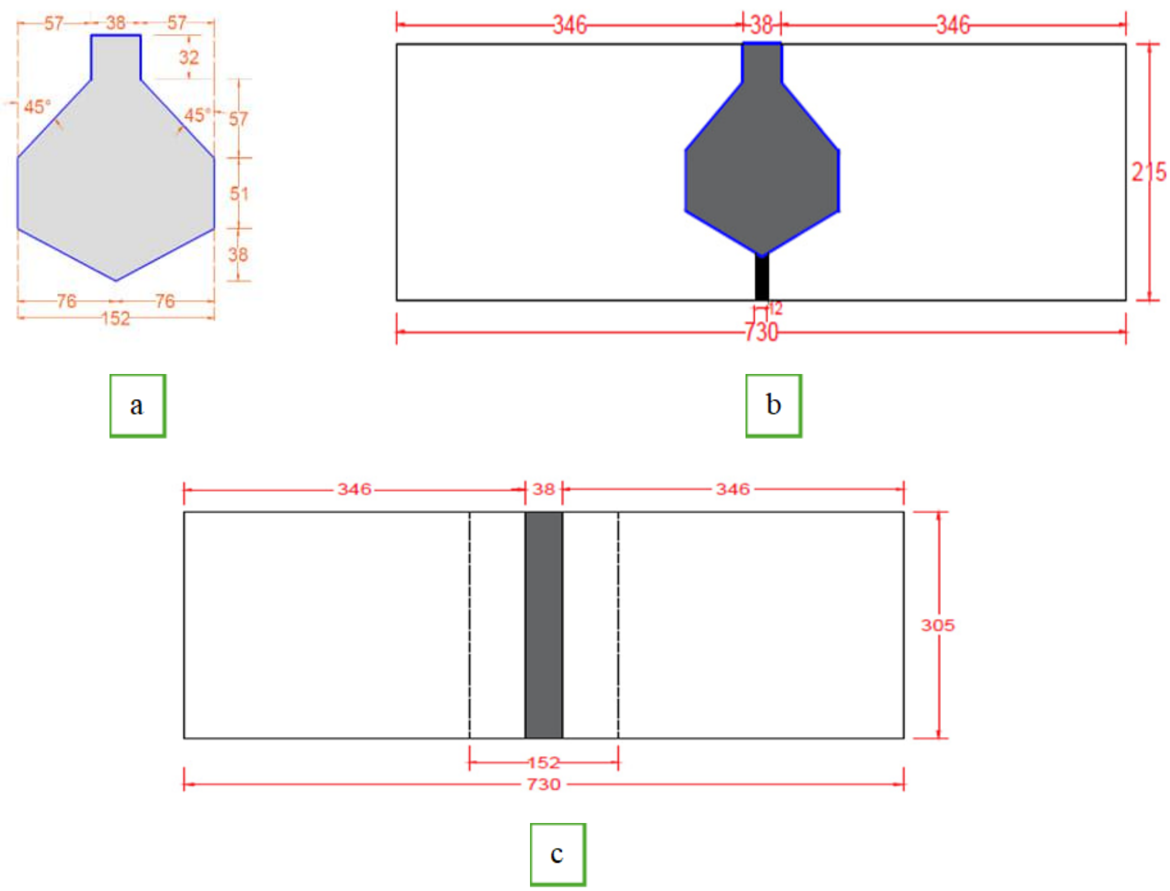

Figure 3.7: Primary shear-key specimen geometry (a) shear key detail; (b) side view; (c) top view

Figure 3.7 depicts the specimen geometry. Each specimen consisted of two exterior HSC blocks connected by concentrically placed UHPC shear key. The HSC represented the hardened precast concrete bridge member, while UHPC represented the field -cast shear -key material.

The nominal dimensions for each specimen were 730mm in length, 305 mm in width, and 215 mm in depth. The UHPC shear key was centered within the specimen and spanned fullwidth. This geometry enabled assessment of the UHPC-HSC interface under direct shear loading while maintaining a specimen shape like that of an actual bridge shear-key connection.

The goal of varying interface conditions and reinforcement details was to understand their effect on load-transfer behavior. The specimen geometry was chosen so that the load could be applied directly to the UHPC shear key. Applying load to the shear key resulted in shear stresses developing at the interfaces between the UHPC shear key and the HSC substrate on both sides. Isolating the specimen response in this manner enabled investigation of the effects of interface surface condition and transverse reinforcement on load transfer, local cracking, interface slip, and the final failure mode.

Interface surface roughness was controlled by preparing the HSC substrate surfaces in two conditions: smooth as-cast and roughened. Smooth specimens were prepared by casting against plywood formwork. The roughened interface condition was prepared by applying retardant on the surface of the plywood formwork prior to casting the HSC. The surface was then pressure washed after 24 hours. This was intended to improve mechanical interlock and frictional resistance between the UHPC shear key and the HSC substrate. Interface surface preparation was one of the primary variables investigated in this experimental program.

The transverse reinforcement condition across the UHPC-HSC interface was varied between specimens. One 10 mm steel rebar was used on each side of the shear key, as shown in Figure 3.8. Unrestrained specimens were defined as those without transverse reinforcement. Restrained specimens included steel rebar crossing the interface. In restrained specimens, this reinforcement helped resist interface opening and contributed to load transfer through dowel action after cracking or slip occurred. Therefore, the reinforcement was expected to influence both shear capacity and post-cracking behavior.

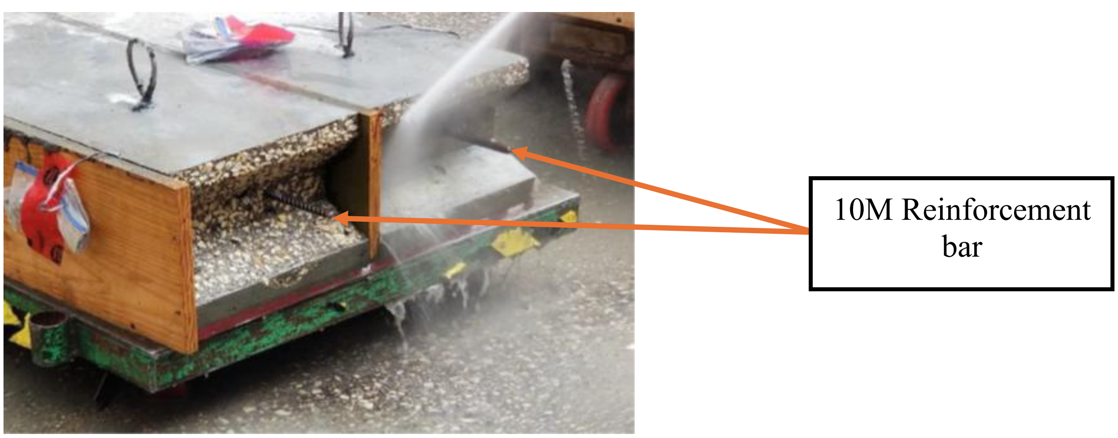

Figure 3.8: Steel rebar configuration

The specimen condition S-R represented the smooth restrained condition. This specimen condition is important because it completes the matrix of surface conditions and reinforcement conditions considered. However, this specimen was tested using a different setup than the rest of the specimens. Therefore, S-R is discussed as part of the overall experimental program where applicable, but it is kept separate from S-NR, R-NR, and R-R in direct comparisons.

3.5.2 Specimen Design

As noted above, the shear-key specimens were designed to enable the study of UHPC-HSC interface behavior under direct shear loading. The geometry of the shear key was based on the shear-key configuration used in the Little Morris Bridge, allowing the laboratory specimens to represent a practical bridge connection while maintaining a manageable specimen size for experimental testing. However, the overall geometry was still maintained to represent the connection region between adjacent box beam bridge girders.

This balance between simplicity and practical relevance was important to the experimental program. A specimen geometry that was too complex would have made it more difficult to separate the effects of surface roughness, transverse reinforcement, and boundary conditions. On the other hand, a specimen that was overly simplified would have limited the applicability of the results to actual UHPC-HSC shear-keys. Therefore, the selected specimen design enabled the study of direct shear-transfer mechanisms in controlled environment while remaining relevant to practical bridge applications.

3.6 Shear-key Test Setup and Loading Procedure

The shear-key specimens S-NR, R-NR and R-R were tested under static direct shear loading using a servo- hydraulic testing machine. The test setup was arranged so that the load was applied directly to the UHPC shear key while the adjacent HSC regions were not loaded. Loading the specimens in this manner allowed shear stresses to develop along the UHPC-HSC interfaces on both sides of the shear key. The setup enabled direct shear transfer to be investigated in relation to interface surface condition and the presence/absence of transverse reinforcement.

The load was applied concentrically at the mid-length of the specimen, directly above the shear-key region. The applied load was transferred to the top of the UHPC shear key through a rigid steel loading plate. The loading plate was 70 mm thick, had a contact width of 38 mm in the loading direction, and was extended across the full specimen width of 305 mm. The rigid loading plate distributed the applied force uniformly across the top surface of the UHPC shear key, allowing the load to be transferred through the shear key and subsequently across the UHPC-HSC interfaces into the adjacent HSC regions.

A 30 mm thick steel base plate supported the two HSC end blocks, while the central shear-key region was intentionally left unsupported to allow vertical deformation. This support arrangement minimized flexural restraint beneath the shear key and ensured that the applied load generated predominantly interface shear stresses rather than flexural stresses within the specimen. The test setup is shown in Figure 3.9.

Both specimen ends were clamped to the base of the testing frame throughout loading. Restraining the specimen ends limited global rotation and minimized unintended bending moments, allowing the measured response to be governed primarily by direct shear transfer through the UHPC shear key and the adjacent HSC interfaces. Together with the unsupported central region, this boundary condition produced a bi-shear loading configuration similar to those commonly adopted in conventional shear-friction interface studies.

Testing was carried out under displacement control at a loading rate of 0.2 mm/min. Displacement-controlled loading was selected to capture the complete structural response of the specimens, including the pre-cracking stage, crack initiation, crack propagation, peak load, post-peak softening, and final failure. Recording the full response was essential because the objective of the tests was not only to determine the ultimate shear capacity but also to evaluate load-displacement behaviour, interface slip, crack development, and failure mechanisms.

The S-NR, R-NR, and R-R specimens were tested using the same loading arrangement, support conditions, and boundary conditions. Consequently, their responses could be directly compared for evaluating the influence of interface roughness and presence/absence of transverse reinforcement on shear transfer. The S-R specimen was the first specimen to be tested. It was tested using a different loading configuration, as shown in Figure 3.10. In this setup, one end of the specimen was rigidly clamped while the opposite end was left free, creating an overhanging configuration. The loading plate was positioned on the HSC region immediately adjacent to the UHPC shear key on the free side of the specimen, rather than directly above the shear key. As a result, the applied load was applied through HSC to subject the interface to shear in the vicinity of the loading plate. The interface on the opposite end was subjected to bending in addition to the same shear stresses. Because the loading configuration introduced flexural effects and did not produce a pure bi-shear condition, this test configuration was modified for the rest of the shear key specimens.

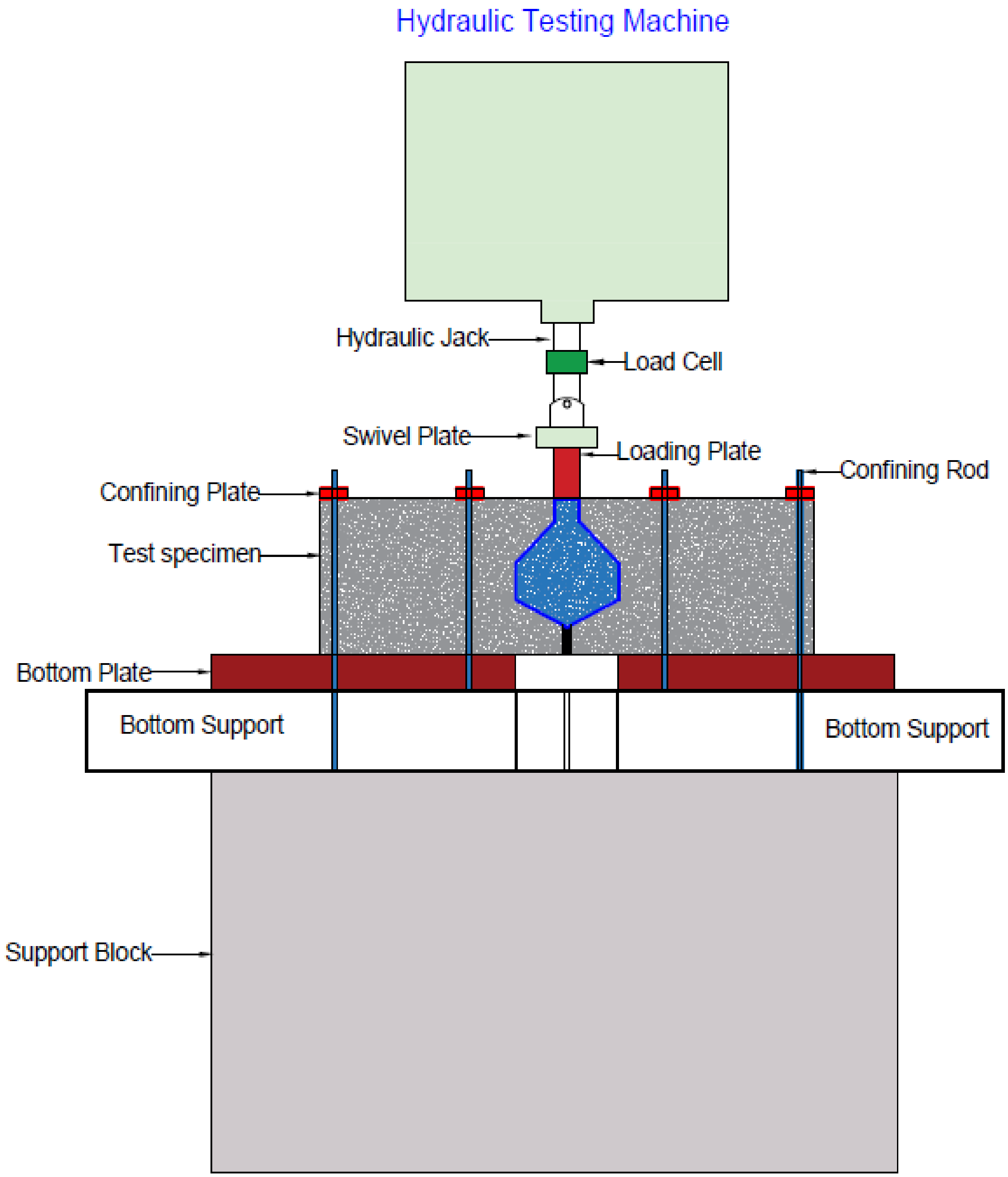

Figure 3.9: Test setup for S-NR, R-NR, and R-R specimens

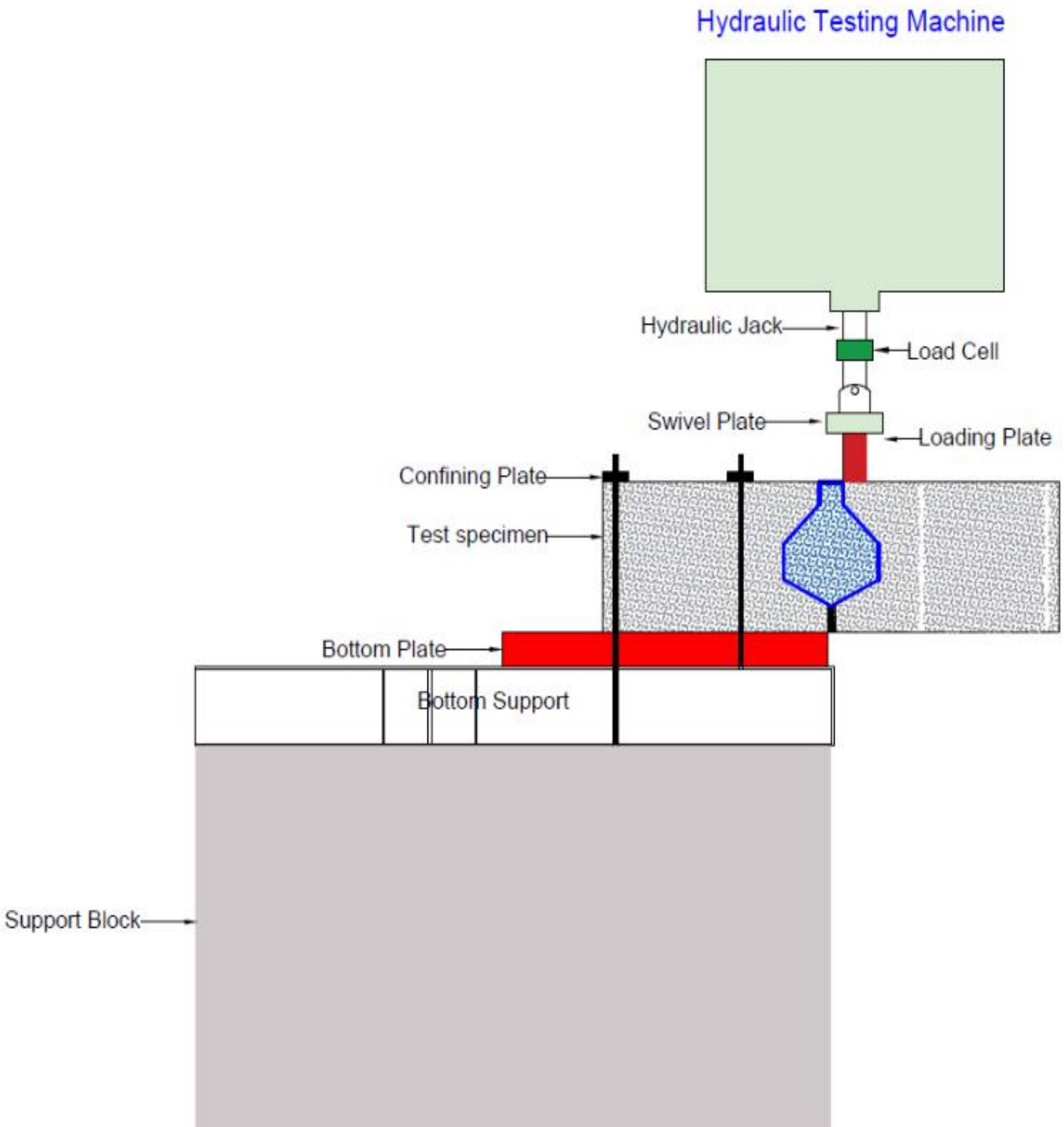

Figure 3.10: Test setup for S-R specimen

3.7 Instrumentation and Digital Image Correlation

Instrumentation was utilized to monitor both global and local responses during testing. Due to the nature of the response exhibited by UHPC-HSC shear-key specimens, characterization of peak load alone is not sufficient to fully understand its performance. Although load capacity is an important metric, cracking, slip, localized deformation, strain development, and post-peak response also play important roles in understanding load-transfer mechanisms and failure progression.

The instrumentation layout used in the present study was designed to capture localized deformation near the UHPC–HSC connection while enabling full-field surface-deformation measurements using Digital Image Correlation (DIC). One face of each specimen was prepared for DIC, whereas the opposite face was equipped with conventional instrumentation. This arrangement allowed the specimen response to be evaluated using both full-field image-based measurements and point-based measurements obtained from physical sensors.

On one of the faces of the specimen, three pi-gauges were installed to monitor localized deformation across selected regions of the shear-key connection. These gauges were used to evaluate local crack opening, relative movement, and deformation development near the UHPC-HSC interface during loading. In addition, one LVDT was positioned at the center of the shear key to record displacement response at the connection region. The LVDT measurement provided useful information on the vertical displacement of the shear-key region during loading and helped relate localized deformation to the overall load-displacement response.

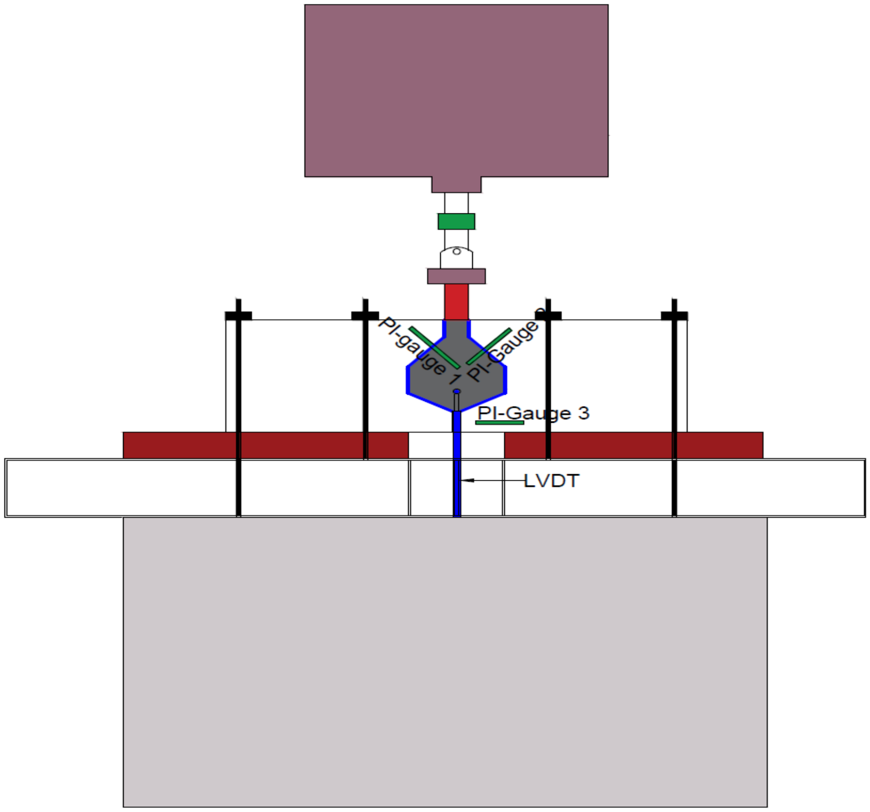

Figure 3.11: Instrumented face of S-NR, R-NR, and R-R specimens

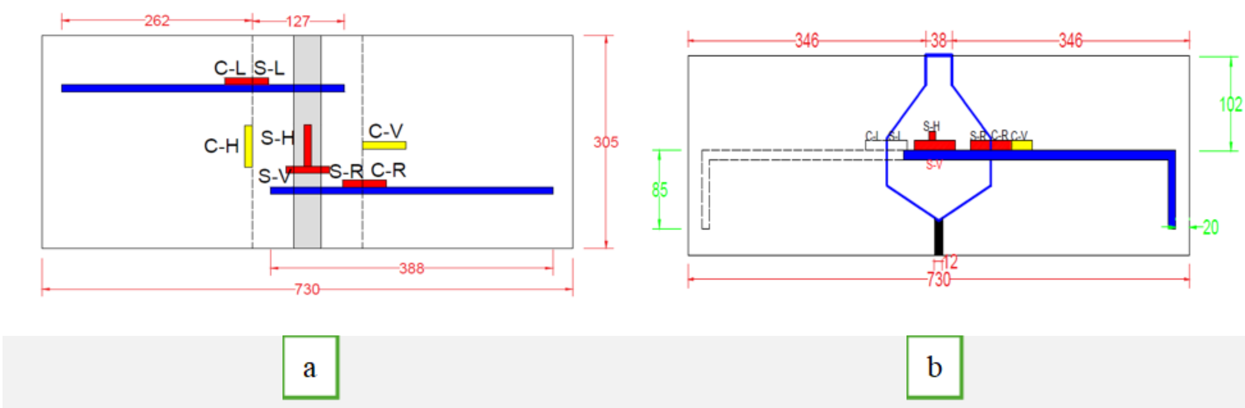

Figure 3.12: Specimen strain gauge instrumentation (a) top view; (b) side view

Strain gauges were also embedded inside the specimens to monitor strain development within the HSC and UHPC sections as shown in Figure 3.12 (a) and (b). The embedded gauges provided internal strain measurements that could not be captured from surface observations alone. These measurements helped describe how strain developed within the concrete materials as load was transferred through the UHPC shear key and surrounding HSC regions. For restrained specimens, additional strain gauges were installed on the reinforcement crossing the UHPC-HSC interface. These reinforcement gauges were used to monitor reinforcement engagement and to help interpret the contribution of the transverse reinforcement to load transfer and post-cracking response.

Digital Image Correlation was utilized to provide full-field displacement and strain measurements on the surface of the shear key opposite the instrumented face. DIC was included in this experimental program because point-based instrumentation, such as LVDTs, pi-gauges, and strain gauges, provides information only at selected locations. In contrast, DIC allows a broader deformation field to be observed and makes it possible to identify strain localization, crack initiation, crack propagation, and failure development during testing.

To use DIC, selected face of each specimen was ground flat, painted with white paint and prepared with a high-contrast random speckle pattern. As load was applied, digital images of the specimen surface were recorded at selected intervals. These images were later processed to calculate displacement and strain fields. The DIC results were then correlated with the load-displacement response and sensor measurements obtained during testing.

DIC was especially useful for characterizing crack development and progression. As load was applied, local strain concentration could be identified before any cracking was visible through visual observation. DIC allowed these local strain concentrations to be monitored as they developed and progressed with increasing load. This helped connect the mechanical response measured by the testing machine to the physical damage occurring on the specimen’s surface.

Each type of instrumentation used in the present study provided different levels of information. Global response was evaluated through load and displacement measurements. Local deformation near the connection region was evaluated using the center LVDT and pi-gauges. Internal strain development within the HSC and UHPC sections was monitored using embedded strain gauges. Reinforcement engagement was monitored using steel strain gauges where reinforcement crossed the UHPC-HSC interface. Finally, DIC provided full-field observations of deformation and cracking on the prepared specimen face.

Through the combined use of conventional instrumentation and DIC, the experimental program was able to assess not only load capacity, but also the load-transfer mechanisms, strain development, crack progression, and failure mechanisms controlling the overall response of the UHPC-HSC shear-key specimens.

The analysis of experimental results was carried out using two DIC processing workflows. ZEISS Inspect Correlate, also known as GOM Correlate, was used for compressive tests and selected bi-shear test analysis. A MATLAB-based Ncorr workflow was used for the shear-key DIC analysis. Although the software platforms differed, both approaches were used to track the movement of the surface speckle pattern during loading and to calculate displacement and strain fields from the recorded images.

Ncorr is a MATLAB-based Digital Image Correlation program that calculates displacement and strain by comparing a reference image with images that contain deformation due to applied loads. The program tracks the movement of subsets within the speckle pattern and uses this movement to calculate horizontal and vertical displacement fields. These displacement fields are then used to calculate strain fields across the monitored specimen surface. Each user needs to write a program based on the needs of their analysis to draw values of strains and deformations from Ncorr.

After the DIC analysis was completed, strain-field data from selected points or regions of interest were exported as CSV files for further analysis. MATLAB code was developed to organize the exported strain data, match the DIC strain values with the corresponding load or calculated stress values, smooth the strain response where needed, and generate strain-versus-stress plots.

The smoothing process was used to reduce local noise in the exported DIC strain data and to make the strain trend easier to interpret. These point-specific strain responses helped identify how local deformation developed during loading and how strain localization changed as the applied load increased. The DIC strain-field data were evaluated together with load-displacement response, calculated stress, visual crack observations, and conventional instrumentation.

ZEISS Inspect Correlate/GOM Correlate is commercial software that has built-in interfaces to calculate deformation and strains in the monitored area. The use of this software does not necessitate any programming skills.

3.8 Data Collection and Response Parameters

Data was collected during shear-key testing to evaluate both strength and deformation response. The primary objective of the data collection process was to document each specimen's response from initial loading through crack initiation, peak load, post-peak behavior, and final failure. Capturing response parameters beyond peak load was necessary because the behavior of a UHPC-HSC shear-key specimen is not defined by maximum load capacity alone. Understanding how the specimen deforms, cracks, slips, transfers strain, and fails provides a more complete understanding of the mechanisms controlling the overall response.

The main response parameters included peak load, load-displacement response, calculated shear stress, local displacement, strain response, crack initiation and propagation, post-peak response, and failure mode. These parameters were selected because each one describes a different aspect of the shear-key response. Peak load and calculated shear stress describe strength. Load - displacement response and local displacement describe stiffness, deformation, and slip. Strain measurement describes load transfer within the UHPC shear key and, where present, the effectiveness of transverse reinforcement. Crack propagation and failure mode describe damage development throughout testing.

Peak load was defined as the maximum load achieved during each individual test. This parameter served as the primary strength parameter for comparison among the shear-key specimens S-NR, R-NR, and R-R. Because these specimens were tested using the same general loading setup, peak load could be compared mainly in relation to surface condition and reinforcement condition. The S-R specimen was also included in testing and evaluated using the same response parameters. However, because it was tested using a different setup, its peak load is discussed separately from the primary comparable group. Calculated shear stress was used to normalize the peak load by the shear-interface area. By dividing the peak load by sheered area, specimen capacity could be described in terms of average shear stress instead of total load. The maximum applied load was divided by the vertical interface area on both sides of the UHPC shear key to determine the calculated shear stress. Calculated shear stress was used as a secondary strength parameter when comparing the behavior of the shear-key specimens.

Load -displacement response was used to describe the general deformation response of each specimen. The initial slope of the curve provided information on stiffness before major cracking or slip occurred. Changes in slope during loading helped identify stiffness reduction and possible damage development. The peak point of the curve defined the maximum load capacity. The post-peak response showed whether the specimen failed abruptly or was able to maintain load-carrying capacity after initial cracking.

Local displacement measurements were used to better understand interface movement and localized deformation. These measurements were important because global displacement may not fully describe what occurs along the interface between UHPC and HSC. Localized slip, crack opening, or deformation may occur before a noticeable change is observed in the overall load – displacement curve. LVDT and pi-gauge measurements were therefore used to support the interpretation of interface movement, localized deformation, and damage progression.

Strain response was also an important response parameter. Concrete strain gauges placed on the UHPC shear key were used to monitor strain development within the UHPC region during loading. These measurements helped show how strain varied through the depth of the shear key and how the UHPC region responded as load was transferred across the connection. In reinforced specimens, strain gauges on the dowels crossing the UHPC-HSC interface were used to evaluate reinforcement engagement. This information was useful for interpreting when the reinforcement became active and how it contributed to load transfer through dowel action after cracking or slip began.

Crack initiation and crack propagation were documented during testing. The load at first cracking was determined where possible, and the crack path was monitored as loading progressed. Crack development was evaluated using visual observation, instrumentation readings, and DIC results.

Monitoring crack development allowed the location and progression of damage to be correlated with the load-displacement response, local displacement measurement, and strain-field results.

DIC data was used to provide additional information on full-field displacement and strain development. While point -based instrumentation provided measurements at selected locations, DIC allowed strain localization and crack progression to be observed across the monitored specimen surface. This was important for identifying where damage was initiated and how it progressed during loading. DIC results were therefore used to support the interpretation of crack initiation, crack propagation, interface slip, and failure mode.

Failure mode was characterized based on the final crack pattern and location, the condition of interface, and other observed damage at the end of each test. Potential responses included cracking along the UHPC-HSC interface, cracking through the surrounding HSC, cracking near the shear-key geometry, slip along the interface, or a combined failure mode involving reinforcement action. Identifying the failure mode of each specimen was important because two specimens could achieve similar peak loads but still exhibit different responses depending on how damage progressed.

The response parameters were used collectively rather than independently. Parameters such as peak load and calculated shear stress described strength, but they did not fully explain the test behavior. The load -displacement response described stiffness and deformation characteristics, but it needed to be interpreted together with crack observations, local displacement measurements, strain-gauge data, and DIC results. Using these parameters together allowed for a more complete understanding of shear key behavior.

Collectively, the data collected and response parameters were selected to support the overall objective of this thesis. The objective was not simply to determine which specimen had the highest load capacity, but to explain why the response changed with surface condition and the inclusion of transverse reinforcement. Considering strength, deformation, strain development, cracking, slip, and failure together allowed the experimental program to assess the shear behavior of the UHPC-HSC shear-key system more comprehensively.

4. RESULTS AND DISCUSSION

4.1.Introduction

This Section presents and discusses the experimental results obtained from the material characterization tests, interface characterization tests, bi-shear tests, and main shear-key tests. The purpose of this section is to connect the measured test responses to the overall objective of the study, which was to evaluate the shear behavior of UHPC-HSC shear-key specimens and to understand the influence of surface condition and transverse reinforcement on load transfer, cracking, deformation, and failure mode.

In addition to evaluating the shear-key response, this section also considers the effect of long-term outdoor exposure on the tested materials and bonded UHPC-HSC system. Several specimens in the present study have been exposed to outdoors environment for approximately seven years. Therefore, the material and interface test results are used to provide durability-related context by comparing the present long-term exposed specimens with earlier material and interface data from the Little Morris Bridge research program.

The section begins with the results of the material characterization tests. These tests included compressive strength, and indirect tension. The purpose of presenting these results first is to establish the baseline material properties of the UHPC and HSC used in the experimental program. These properties provide important context for interpreting later interface and shear-key behavior, especially where cracking, strain development, or stiffness differences influenced the observed response.

The interface characterization results are then presented. Pull-off tests were used to evaluate tensile bond resistance across the UHPC-HSC interface, while slant shear tests were used to evaluate interface behavior under combined compression and shear. These results help explain how the UHPC-HSC interface responded under simplified bond-related loading conditions. The failure modes observed in these tests also provide useful context for determining whether the bonded interface or the surrounding HSC controlled the response after long-term exposure.

The bi-shear test results are then discussed as a shear-dominated interface response. The bi-shear test provided additional information on interface shear resistance, crack development, and strain localization near the bonded interface. Digital Image Correlation results are included where applicable to support interpretation of crack initiation and damage progression.

The main focus of this section is the response of the structural shear-key specimens. The shear-key results are interpreted using load-displacement behavior, nominal shear stress, crack initiation, crack propagation, DIC strain fields, reinforcement strain response, and observed failure mode.

The section concludes by comparing the influence of the primary variables considered in the study. The effect of surface roughening is evaluated by comparing the smooth/as-cast and roughened unrestrained specimens. The effect of transverse reinforcement is evaluated by comparing the roughened unrestrained and roughened restrained specimens. The supplementary S-R specimen is used to provide additional context for the smooth/as-cast restrained condition, while recognizing the limitations associated with differences in test setup.

4.2. Compressive Strength Results

Compressive strength results were used to describe the baseline compressive capacity of the HSC and UHPC materials and to provide durability-related context for the specimens after long-term outdoor exposure. Since the present study includes specimens that had been exposed to outdoors environment for approximately seven years, the compressive strength results were also used to evaluate whether the materials retained high compressive capacity after exposure to natural environmental conditions.

The results from all HSC tested cylinders are shown in Table 4.1. The HSC compressive strength results showed an average compressive strength of 101.6 MPa based on 13 tested specimens. Individual HSC compressive strengths ranged from 88.6 MPa to 116.3 MPa. These values indicate that the HSC substrate had high compressive capacity after long-term outdoor exposure, which is important because the HSC portion of the shear-key specimens contributed to load transfer and influenced crack development near the UHPC-HSC interface.

Table 0.1: HSC cylinder compressive strength results

Specimen label	Peak load (N)	Compressive strength (MPa)
G7-4-5	1649000.9	90.4
G7- 1-3	2013000.9	110.4
G7- A-2	2013000.5	110.4
G7-3-6	1681000.8	92.2
G7 - A-7 -T2	1894000.3	103.9
G7-1-3 - T2	1924000.6	105.5
G7-2-7 - M3	1760000	96.5
G7-4-5 -M5	1873000.1	102.7
G7-A-2 - T1	1616000.4	88.6
G7-3-6 -M4	1805000.4	99.0
G7-A-7-T2	1795000.2	98.5
G7-T3	2121000.3	116.3
G7-T4	1932000.6	105.9
AVG		**101.6**
STD		**8.02**

The UHPC compressive-strength results are summarized in Table 4.2. They were separated into two groups according to their casting source and material history. The first group (Ductal T) comprised retained UHPC specimens originally cast by Tan (2021) at the Little Morris Bridge construction site near Morris, Manitoba, in 2019. When tested in the present program, these specimens had an average compressive strength of 218.8 MPa, with individual values ranging from 217.2 to 220.4 MPa. For comparison, Tan (2021) reported average compressive strengths of up to 164.4 MPa during the original testing program.

The second group (Ductal M) comprised retained UHPC specimens cast by Erfani (2025) at the University of Manitoba's W.R. McQuade Structures Laboratory. In the present program, these specimens had an average compressive strength of 161.3 MPa, with values ranging from 157.1 to

164.1 MPa. Erfani (2025) originally reported 28-day average compressive strengths of 141.93 MPa for laboratory-cured specimens and 138.17 MPa for chamber-cured specimens.

The two UHPC groups were not combined into a single average because they differed in casting location, batch composition, curing history, storage conditions, and age at testing. As shown in Table 4.2, both groups exhibited higher compressive strengths in the present program than the values reported at their original testing ages. This increase may be associated with continued hydration and long-term development of strength.

Table 0.2: UHPC 72.6 by 152.4 mm size cylinder compressive strength results

Specimen label	**Pick Load (N)**	**Compressive strength (MPa)**
Ductal T1	1786000.6	220.4
Ductal T2	1760000.6	217.2
Ductal M1	1272809.3	157.1
Ductal M2	1319582.3	162.8
Ductal M3	1329421.6	164.1

This study continues the UHPC-HSC shear-key research program previously studied by Tan (2021) and Erfani (2025). Therefore, the compressive strength results were considered in relation to the long-term outdoor exposure. The specimens used in the present study have been exposed to the outdoor environment for approximately seven years. The high and low temperatures ranged between -40°C to +37.0°C. Therefore, the compressive strength results provide durability-related information regarding the retained compressive capacity of the HSC and UHPC materials after long-term environmental exposure.

Table 0.3: Compressive strength compression of Tan and present

Material	Present study Average (MPa)	Tan (2021) Average	Difference
HSC	101.6	76.8	+32.3%
UHPC	218.8	158.6	+38.0%

The HSC specimens in the present study had an average compressive strength of 101.6 MPa after long-term outdoor exposure, compared with 76.8 MPa reported by Tan (2021). The UHPC specimens had an average compressive strength of 218.8 MPa, compared with 158.6 MPa reported by Tan (2021). Both materials therefore showed higher average compressive strength values in the present study than the earlier reported values. This comparison suggests that the HSC and UHPC materials not only retained but increased their high compressive strength capacity after approximately seven years of outdoor exposure in the Winnipeg environment. The result is important because it provides reassurance to the engineering community that like HSC and UHPC strength does not decrease with time.

These results show that compressive strength degradation was not evident from the tested specimens.

4.2.1 DIC Interpretation for Compressive Tests

Digital Image Correlation was used during selected compressive strength tests to monitor surface strain development during axial compression loading. For these tests, ZEISS Inspect Correlate/GOM Correlate was used to process the recorded images and calculate displacement and strain fields on the monitored specimen surface. The purpose of using DIC in the compressive tests was to obtain additional strain-field information that could support the interpretation of material response beyond the peak compressive strength value.

During compression testing, the applied load was recorded by the testing machine and converted into compressive stress using the cylinder cross-sectional area. At the same time, ZEISS Inspect Correlate/GOM Correlate provided surface strain measurements on the specimen. The strain-field data were then exported from the software as CSV files for further analysis.

After the strain-field data were exported, MATLAB code was used to organize the data, match the DIC strain values with the corresponding compressive stress values, smooth the strain response where needed, and generate stress-strain plots. This process allowed stress-strain relationships to be plotted at specific points on the specimen surface. Since the specimens were loaded axially, the strain component ε_y aligned with the direction of loading was used as the primary compressive strain response. The transverse strain component was considered supplementary because it describes lateral expansion rather than the main axial compressive response.

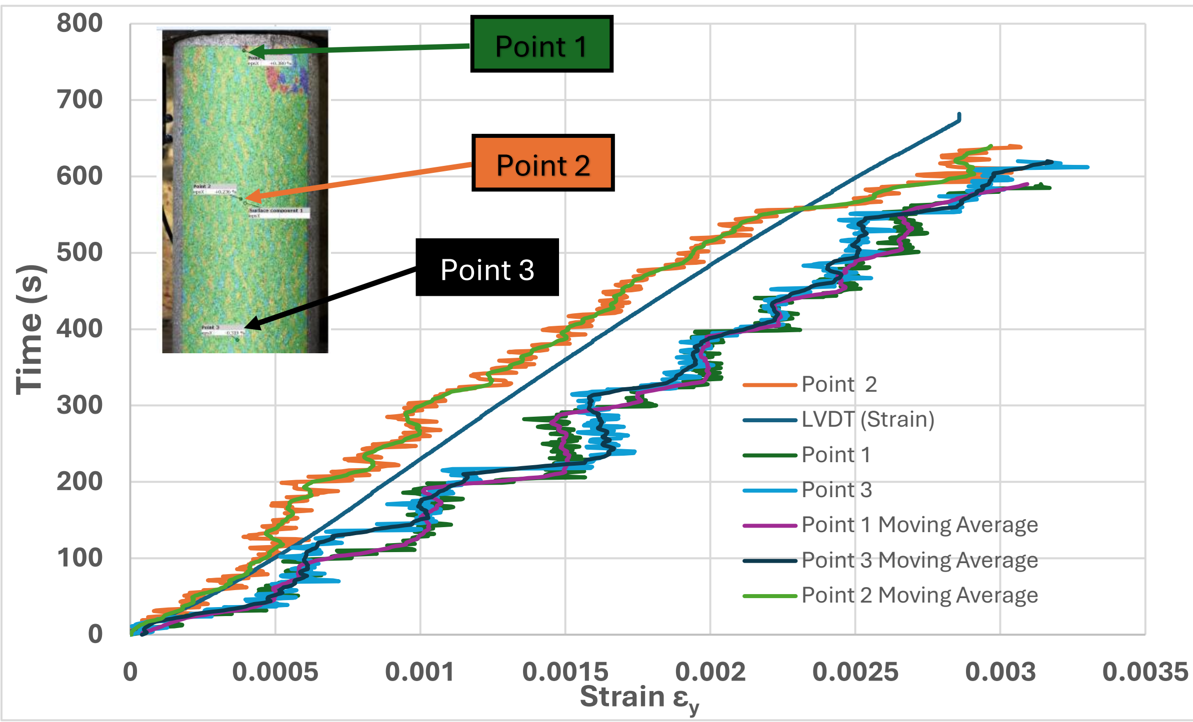

Figure 0.1: DIC strain-point locations and strain-time response for the compressive specimen G7-T4

Figure 4.1 shows the locations of the selected DIC strain points on the compressive cylinder and compares the strain response obtained from these points with the strain measured using the LVDT. Points 1, 2, and 3 were selected at different locations along the monitored surface of the cylinder so that local strain development could be evaluated during axial compression. The strain-time plot in Figure 4.1 shows that the strain measured at the selected DIC points generally increased with loading time. The response was not perfectly smooth because DIC captures local surface-level strain, which can be influenced by speckle tracking, local surface deformation, and small measurement noise. For this reason, 15 point moving-average curves were also plotted to make the overall strain trend clearer.

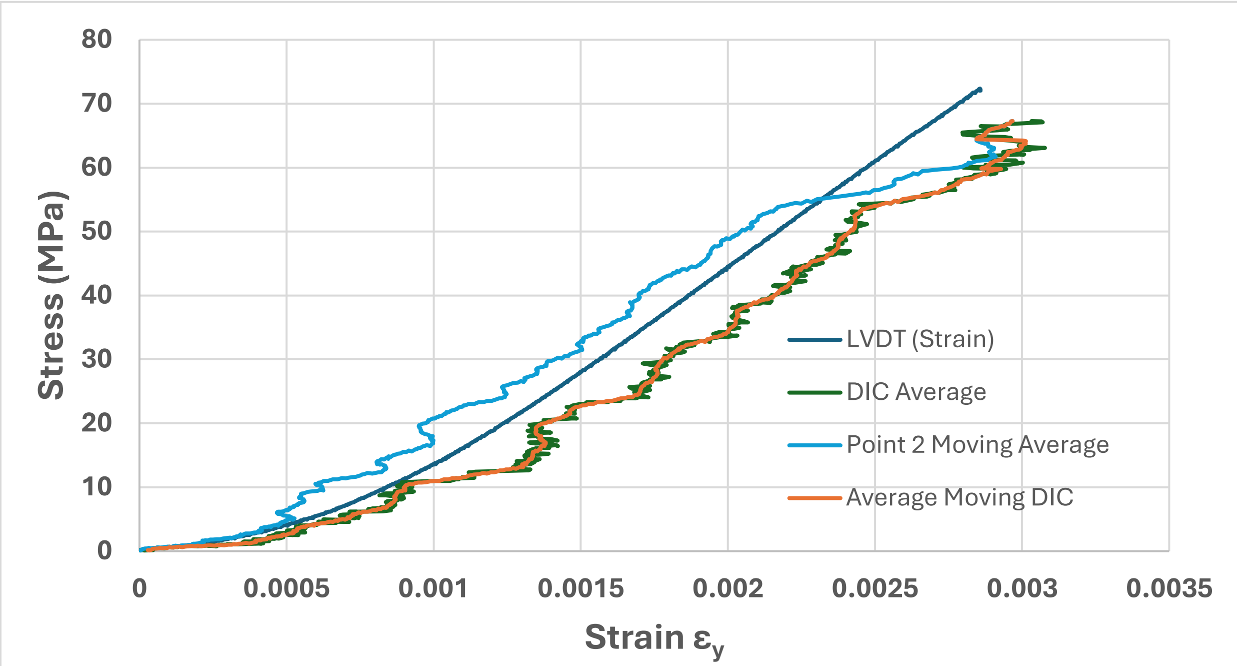

Figure 0.2: Stress-strain response for the compressive strength specimen G7-T4

Figure 4.2 presents the corresponding stress-strain response obtained from the compressive test. The stress was calculated from the applied load divided by the cross-sectional area of the cylinder, while the strain was obtained from the selected DIC points and compared with the LVDT data. The plotted curves show that the DIC strain response follows the same general increasing trend as the LVDT strain response. However, the DIC data show more local variation because they represent strain at very small-time intervals (2 seconds in this case). LVDT provides an average global measurement of deformation over the entire height of the cylinder. The data from the two measurement types shows a good comparison. It has to be noted that the LVDT was located outside of the DIC strain measurement area.

4.2. Indirect Tension Test Results

Indirect tension tests were conducted on HSC cylindrical specimens to evaluate the tensile cracking resistance of the HSC material after long-term outdoor exposure. A total of 10 HSC cylinders were tested, as shown in Table 4.4. Each specimen had a diameter of 152 mm and a height of 305 mm. The maximum applied load was recorded for each specimen and used to calculate the indirect tensile strength using the split-cylinder equation using Equation 4.1.

Table 0.4: Indirect tension test HSC 152 by 305 mm cylinder results.

Specimen ID	**Diameter (mm)**	**Height (mm)**	**P_{max} (kN)**	**f_t (MPa)**	**Failure Mode**
IDT-1	152	305	523.8	7.20	Fragmentation with localized crushing
IDT-2	152	305	453.6	6.23	Splitting failure
IDT-3	152	305	408.9	5.62	Mixed splitting fragmentation
IDT-4	152	305	483.2	6.64	Mixed splitting fragmentation
IDT-5	152	305	341.9	4.70	Splitting failure
IDT-6	152	305	448.7	6.16	Mixed splitting fragmentation failure
IDT-7	152	305	441.2	6.06	Splitting failure
IDT-8	152	305	509.7	7.00	Mixed splitting fragmentation
IDT-9	152	305	479.3	6.59	Splitting failure
IDT-10	152	305	461.6	6.34	Splitting failure
Average			**455.2**	**6.25**	
Standard deviation			**52.0**	**0.71**	

P_{max} = maximum applied load; f_t = indirect tensile strength

Equation 4.1 $$F_t = \frac{2P_{max}}{\pi LD}$$

Where (f_t) is the indirect tensile strength, (P_{max}) is the maximum applied load, (L) is the cylinder length, and (D) is the cylinder diameter.

The measured indirect tensile strengths ranged from 4.70 MPa to 7.20 MPa, with an average value of 6.25 MPa. The standard deviation was 0.71 MPa.

The observed failure modes were consistent with complete diametral splitting failure tensile behavior in HSC cylinders in other studies. Figure 4.3 shows the failure modes that were recorded in this study. Five specimens developed a complete diametral splitting failure, four specimens developed a mixed splitting fragmentation failure, and one specimen exhibited a Fragmentation failure with localized crushing pattern. These failure observations confirm that the test response was governed by tensile cracking of the HSC cylinder under split-cylinder loading.

Figure 0.3: Indirect tension tests complete diametral splitting failure

The standard deviation of the indirect tensile strength was 0.71 MPa. Relative to the average value of 6.25 MPa, this corresponds to a coefficient variation of approximately 11.4%. This level of variation indicates that the HSC cylinders produced reasonably consistent splitting tensile strength results while still reflecting the natural variability expected in concrete material testing. Although the measured values ranged from 4.70 MPa to 7.20 MPa, most specimens were grouped near the average value. Therefore, the average indirect tensile strength is considered representative of the tested HSC material condition after long-term outdoor exposure.

From an engineering perspective, the indirect tensile strength results indicate that the HSC retained strong tensile cracking resistance after long-term outdoor exposure. The average value of f_t = 6.25 MPa shows that the HSC was not a weak or deteriorated material at the time of testing. The moderate standard deviation further supports that this tensile resistance was not based on a single high-strength specimen but was generally consistent across the tested cylinders.

The indirect tension test results from the present study were compared with the HSC splitting tensile strength results reported by Tan (2021). Since the present specimens had been exposed to outdoor environment for approximately seven years average temperature range -40°C to +37.0°C, the comparison provides durability context to this study it is summarized in Table 4.5.

The indirect tensile strength was determined using the splitting tensile test. Tan (2021) reported HSC indirect tensile strengths ranging from 4.79 to 5.66 MPa, with an average of approximately 5.33 MPa. In the present study, the indirect tensile strength ranged from 4.70 to 7.20 MPa, with an average of 6.25 MPa and a standard deviation of 0.71 MPa. Thus, the average indirect tensile strength measured in the present study was approximately 17.3% higher than that reported by Tan (2021).

Table 0.5: Compares the indirect tensile results from the present study with Tan (2021).

Test	**Present study average strength (MPa)**	**Tan (2021) Average strength (MPa)**	**Difference (%)**
ITS	6.25	5.33	+17.3

ITS – Indirect Tensile Strength

The comparison indicates that the concrete specimens in the present study retained measurable tensile cracking resistance after long-term outdoor exposure. The average indirect tensile strength was higher than the average value reported by Tan (2021), suggesting that tensile strength degradation was not evident in the tested specimens.

4.3 Interface Characterization Results

Interface characterization results were used to evaluate the bond response of the UHPC-HSC interface under simplified loading conditions. The interface characterization tests included pull-off tests, bi-shear tests and slant shear tests. The value of mean profile depth was measured by close proximity scanner and further calculated for 40 specimens in the original study by Tan (2021) as 2.56 mm. This value corresponds to rough surface preparation.

4.3.1 Pull-Off Test Results

Pull-off tests were conducted to evaluate the tensile bond resistance between the UHPC overlay and the hardened HSC substrate. The failure mode was first considered because it identifies whether the response was controlled by the UHPC-HSC interface, the HSC substrate, the UHPC overlay, or the adhesive layer used to attach the loading disc.

In the present study, the pull-off specimens failed in the HSC substrate as is shown in Figure 4.4 (b). No specimen failure was identified as an interface-controlled failure between UHPC and HSC. This failure mode indicates that the UHPC-HSC bond was stronger than HSC tensile strength under direct tensile loading normal to the bonded surface. The measured pull-off resistance was governed by tensile failure of the HSC substrate. Therefore, the pull-off values reported in this section represent the tensile resistance of the bonded system up to HSC failure, rather than a direct interface strength.

A total of 11 pull-off specimens were tested the results are in Table 4.6. The measured pull-off tensile strengths ranged from 3.16 MPa to 5.31 MPa, with an average value of 3.96 MPa. The standard deviation was 0.71 MPa. These results indicate that the UHPC-HSC bonded system maintained measurable tensile resistance after long-term outdoor exposure.

a

b

Figure 0.4: pull off test (a) pull off test specimen; (b) HSC failure

Table 0.6: Pull-off tensile strength results.

Specimen	Average Tensile Strength (MPa)	Failure Mode
1	3.49	HSC failure
2	4.12	
3	3.97	
4	3.90	
5	3.38	
6	5.10	
7	3.16	
8	3.66	
9	5.31	
10	4.25	
11	3.25	
Average	**3.96**	
STD	**0.71**	

STD – Standard Deviation

The pull-off results were compared with the results reported by Tan (2021). Tan reported pull-off tensile strength values at different UHPC ages. The reported average pull-off strengths were 3.87

MPa at 5 days, 5.20 MPa at 7 days, 4.33 MPa at 14 days, 3.88 MPa at 28 days, and 3.80 MPa at 91 days. The corresponding standard deviations were relatively low for most groups, with coefficients of variation ranging from 6% to 13%, indicating consistent pull-off test performance. The present average pull-off tensile strength of 3.96 MPa is close to the later-age values reported by Tan (2021), especially the 28-day average of 3.88 MPa and the 91-day average of 3.80 MPa. Compared with Tan's 91-day average, the present value is approximately 4.2% higher. In comparison with indirect tensile strength, the increase in strength for this group of specimens is smaller compared to the indirect tensile strength.

Table 0.7: Comparison of the present pull-off results with data reported by Tan (2021).

Study / UHPC Age	**Number of Specimens**	**Average Pull-Off Tensile Strength (MPa)**	**Standard Deviation (MPa)**	**Failure Mode Context**
Present study, after long-term outdoor exposure	11	3.96	0.71	HSC failure
Tan (2021), 5 days	1	3.87	—	Early-age pull-off
Tan (2021), 7 days	6	5.20	0.30	HSC failure at early ages
Tan (2021), 14 days	6	4.33	0.57	Transition toward PIF
Tan (2021), 28 days	5	3.88	0.48	Pull-off strength at later-age level
Tan (2021), 91 days	7	3.80	0.44	Majority PIF at 91 days

This comparison suggests that the UHPC-HSC bonded system retained tensile resistance after approximately seven years of outdoor exposure in the Winnipeg environment. The result is especially important because the present specimens failed in the HSC substrate rather than along the UHPC-HSC interface. This indicates that interface debonding did not control the pull-off response in the tested specimens.

Tan (2021) also reported that pull-off failure modes included epoxy failure, HSC failure, and partial interface failure. Epoxy failures were excluded from Tan's analysis because they did not represent either bond strength or specimen tensile strength. Tan further observed that HSC failure was found primarily in specimens up to 7 days old, while later-age specimens shifted more toward partial interface failure. The average pull-off strength of specimens with HSC failure was reported as 5.03 MPa, while the average for partial interface failure specimens was 4.01 MPa.

In the present study, the HSC failure mode after long-term outdoor exposure shows that the bond between UHPC and HSC remained strong enough that failure occurred in the substrate rather than at the interface. Therefore, the pull-off test results support the interpretation that long-term outdoor exposure did not produce clear tensile debonding weakness at the UHPC-HSC interface. The pull-off test represents a direct tensile loading condition normal to the bonded surface.

4.3.2 Slant Shear Test Results

Slant shear tests were conducted to evaluate the UHPC-HSC bonded system under a combined compression and stress condition. The failure mode was first considered because it identifies whether the response was controlled by the UHPC-HSC interface or by one of the concrete materials.

In the present study, no interface failure was observed in the slant shear specimens. The failure occurred only in the HSC portion of the specimens. This failure mode indicates that the UHPC-HSC interface did not govern the response under slant shear loading. Instead, the bonded interface remained sufficiently strong, and failure developed through the HSC material. Therefore, the calculated slant shear results represent the resistance of the bonded UHPC-HSC system up to HSC failure, rather than a direct interface debonding strength.

Five slant shear specimens were tested, as shown in Table 4.8. The peak load ranged from 306.0 kN to 415.0 kN, with an average peak load of 360.4 kN. The calculated applied compressive stress ranged from 67.1 MPa to 91.0 MPa, with an average value of 79.1 MPa. The calculated normal stress on the slant interface ranged from 65.5 MPa to 88.9 MPa, with an average value of 77.2 MPa. The calculated shear stress component along the slant interface ranged from 10.2 MPa to 13.9 MPa, with an average of 12.1 MPa.

Table 0.8: Summary of the slant shear test results for all specimens.

Specimen ID	**Peak load (kN)**	**Compressive stress (MPa)**	**Normal stress on slant interface (MPa)**	**Shear stress on slant interface (MPa)**	**Failure mode**
SS 1	415.57	91.13	78.92	45.56	HSC failure
SS 2	343.56	75.34	65.24	37.67	
SS 3	374.82	82.19	71.18	41.09	
SS 4	364.16	79.85	69.15	39.93	
SS 5	306.56	67.22	58.23	33.61	
Average	**360.4**	**79.1**	**77.2**	**39.57**	
STD	**40.1**	**7.8**	**7.6**	**4.4**	

Figure 0.5: slant shear HSC Modes of failure

Because all specimens failed in the HSC and no interface failure was observed, this suggests that the interface had sufficient bond capacity to transfer the combined compression and shear stress until the HSC failure. The absence of interface failure suggests that the bond between the UHPC and the HSC remained effective after long-term outdoor exposure.

The slant shear failure mode observed in the present study was compared with the failure modes reported by Tan (2021). Tan reported two main slant shear failure modes: combined HSC and interface failure, and HSC failure with the bond interface remaining intact. Tan also observed that the failure mode shifted toward HSC failure as UHPC age increased, especially from day 14 onward. Most specimens tested at 28, and 91 days failed in the HSC, which Tan interpreted as evidence of improved bond performance as UHPC strength increased.

The present study showed only HSC failure in the slant shear specimens, with no observed interface failure. This agrees with the later-age behavior reported by Tan (2021), where HSC failure became the dominant failure mode. Since the present specimens had been exposed outdoors for approximately seven years in the -40°C to +37.0°C temperature, the HSC-only failure mode suggests that the UHPC-HSC interface retained sufficient bond performance under combined compression and shear loading.

The slant-shear results obtained in the present study are summarized in Table 4.8. The shear stress on the slant interface ranged from 33.61 to 45.56 MPa, with an average value of 39.57 MPa. Tan (2021) reported average shear stresses ranging from 17.4 to 28.4 MPa for specimens tested at UHPC ages between 1 and 91 days. The present average was approximately 39.3% higher than the highest average shear stress reported by Tan (2021).

4.4 Bi-Shear Test Results

Bi-shear tests were conducted to evaluate the shear-dominated response of the UHPC-HSC interface system. The failure mode was first considered because it helps identify whether the response was governed by interface debonding, cracking through the concrete, or a combined shear failure mechanism.

In the present study, the observed bi-shear failure modes were mainly A-shape failure and shear on both sides of the UHPC insert, see Figure 4.6 failure modes. These failure patterns indicate that the specimens did not fail through a simple, clean separation along the UHPC-HSC interface. Instead, damage developed through a shear-related cracking pattern involving both sides of the specimen. Therefore, the Bi-shear results are interpreted as the shear resistance of the UHPC-HSC system rather than as a pure interface debonding strength.

Eight bi-shear specimens were evaluated. Typical load-displacement response form bi-shear 1 of the bi-shear specimens is shown in Figure 4.7. The remaining load-displacement graphs are in Appendix A. The load used for calculating bi-shear strength was the load corresponding to the peak load in the load-displacement response, indicated in Figure 4.6. This point was selected because it represented the first major loss of resistance in the bonded system. Since each specimen had one 152 mm by 152 mm bonded UHPC-HSC interface, the interface area was 23,104 mm².

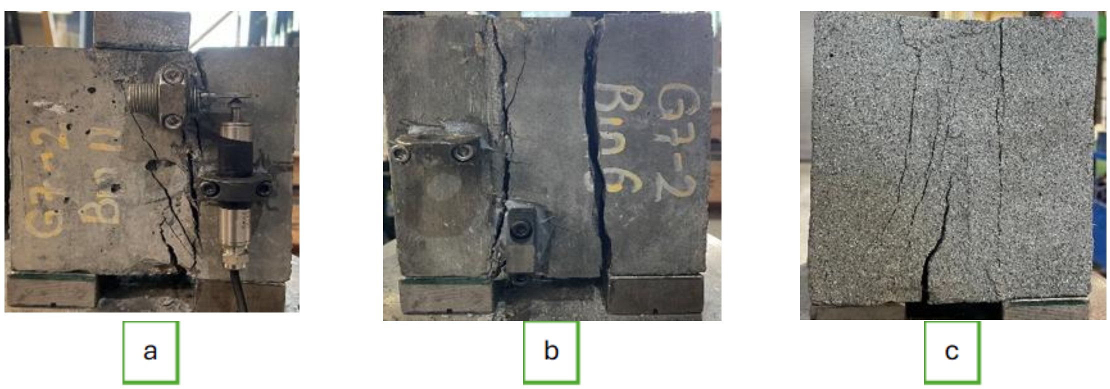

Figure 0.6: Bi-shear failure mode (a) bond interface; (b) shear on both sides; (c) A shape failure

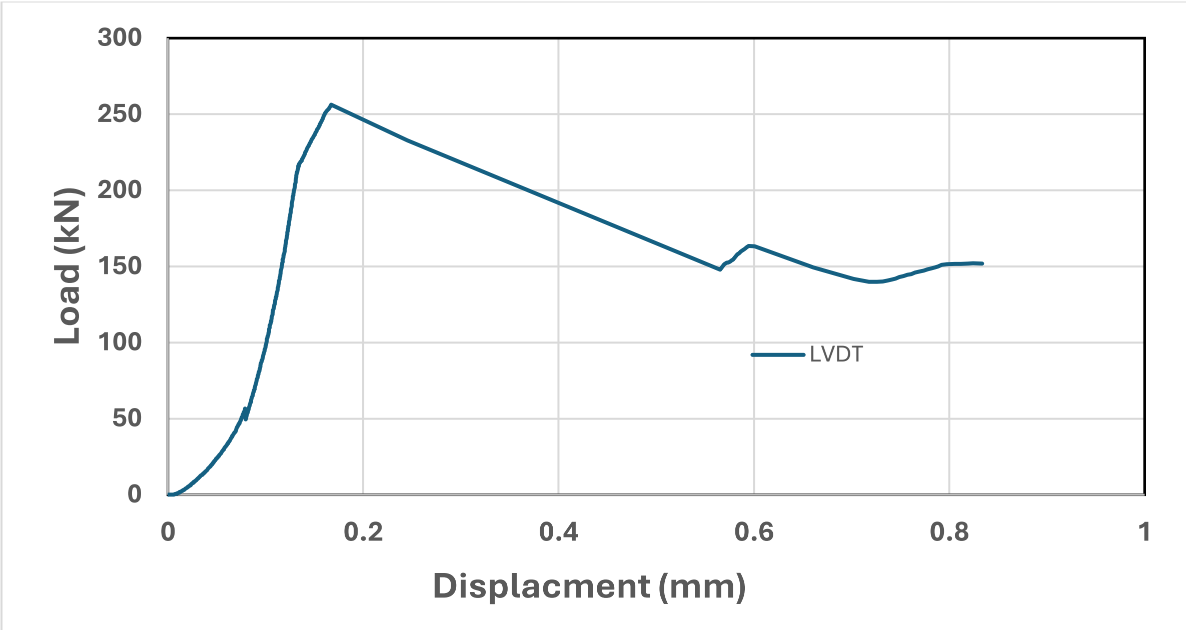

Figure 0.7: Bi-shear 1 load – displacement curve

The bi-shear strength ranged from 5.39 MPa to 11.09 MPa, with an average value of 9.42 MPa results shown on table 4.9 for all specimens tested. Most specimens developed bi-shear strengths near or above 8 MPa. The observed A-shape failure and shear-on-both-sides failure patterns suggest that the bonded system resisted shear through a broader specimen-level cracking mechanism rather than through direct interface separation alone. Results from Tan (2019) report an average shear strength of 6.6 MPa at 91 days after casting UHPC. This increase of 42% is similar magnitude increase compared to the slant shear bond stress.

The present bi-shear failure modes were compared with the failure modes reported by Tan (2021). Tan identified three bi-shear failure modes: A-shape failure, shear on both sides, and bond interface failure (2021). The research findings noted that the calculated shear stress did not necessarily represent pure bond strength because the load used in the calculation was taken from the first sudden drop in the load-stroke response. The research further stipulated that the sudden load drop was associated with a loss of load capacity related to cracking near the UHPC-HSC interface.

Table 0.9: Summarizes the bi-shear test results.

Specimen	**Peak Load** (kN)	**Bi-Shear Strength** (MPa)	**Failure Mode**
Bi-shear 1	256.3	11.09	Bond interface
Bi-shear 2	245.5	10.62	A-shape failure
Bi-shear 3	201.4	8.72	Bond interface
Bi-shear 4	195.9	8.48	Bond interface
Bi-shear 5	124.6	5.39	HSC shear
Bi-shear 6	242.2	10.48	HSC shear
Bi-shear 7	230.9	10.00	Bond interface
Bi-shear 8	245.0	10.60	A-shape failure
Average	**217.7**	**9.42**	
Standard deviation	**43.4**	**1.88**	

The present failure modes are consistent with two of the failure modes reported by Tan (2021): A-shape failure and shear on both sides. However, the present specimens did not show failure governed only by direct separation along the UHPC-HSC interface. This indicates that the bonded interface was not the only weak plane controlling the present bi-shear response.

UHPC fibers can bridge internal cracks and help transfer load after crack initiation, so specimens may not fail directly at the UHPC-HSC bond interface but instead through the weaker material region. It was further noted that bi-shear failure modes can be complex and difficult to identify during testing (Tan 2021). This explanation supports the interpretation of the present results, where the observed A-shape and shear-on-both-sides patterns reflect a combined shear cracking mechanism rather than a clean interface debonding failure.

Overall, the comparison with Tan (2021) indicates that the present bi-shear specimens followed failure patterns already observed in the earlier phase of the research program. The absence of bond-interface-only failure in the specimens after 7 years of external exposure suggests that the UHPC-HSC interface retained effective shear transfer capacity.

4.4.1 DIC Interpretation for Bi-Shear Tests

Digital Image Correlation was used for selected bi-shear specimens during shear-dominated interface loading. The bi-shear test was included in this study to provide supporting interface-level information for the UHPC-HSC bonded system. The bi-shear specimens provided useful information about how the strain was located near the UHPC-HSC interface without extending to the adjacent HSC portion of the specimen.

For selected bi-shear specimens, one face of the specimen was equipped with a random speckle pattern for DIC analysis. During testing, video recording of the speckled surface was taken as load was applied. Ncorr was used for this DIC analysis. The software tracked the movement of the speckle pattern on the specimen surface and generated displacement and strain-field results. These strain fields were used to identify regions where local deformation concentrated near the UHPC-HSC interface and where cracking began to develop during loading.

Figure 4.8 shows the load-displacement response that was captured by the testing machine in Figure (a), while the DIC strain-field contours are shown in Figure 4.8 (b) and (c) for bi-shear specimen BS-1. The load-displacement plot identifies two important stages: from the origin of the coordinate system to Point A, and from point A to Point B. The first portion of the load-deflection graph shows the initial stage of loading up to the first load drop at 56 kN (Point A). This first drop in load corresponds to the occurrence of the first crack in the specimen, however, upon visual inspection, it was not possible to see where the specimen cracked. The inspection of the ε_{xx} field in DIC analysis in Figure 4.8 (b) clearly shows a strain concentration represented by the dark red hues at the top left corner of the UHPC segment of the specimen, on the interface with HSC. This clearly indicates the initiation of cracking in that location. Further inspection of the DIC results showed that strains started to increase at that location at load of 45 kN. The strain localization at this stage provides evidence of early cracking or localized shear deformation within the monitored region.

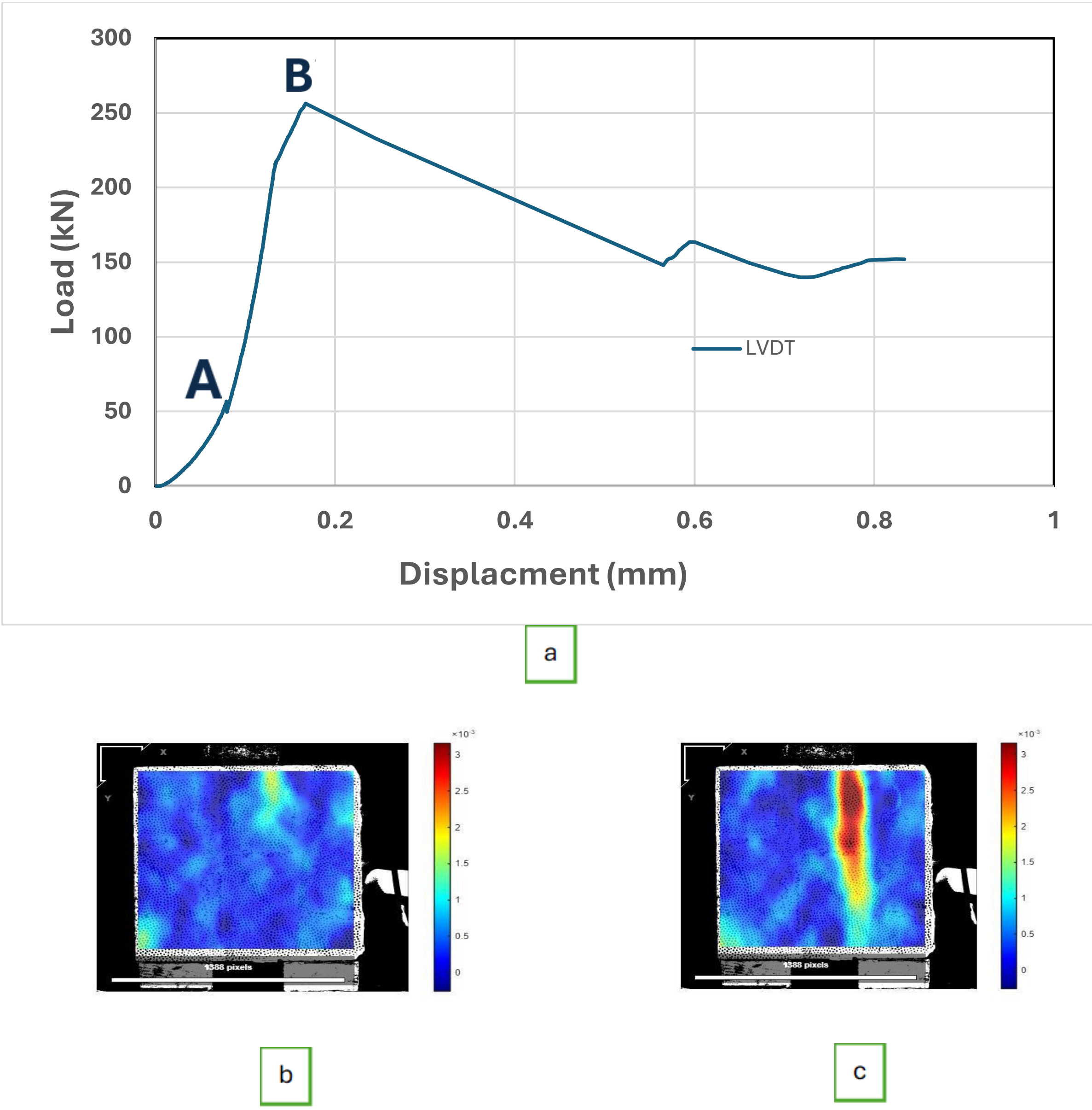

Point A (56 kN) **Point B (256.3 kN)**

Figure 0.8: Bi-shear test BS-1 specimen (a) Load-displacement response; (b) DIC strain localization at point A; (c) DIC strain localization at point B

At Point B, corresponding to the peak/failure stage, the DIC strain field shows a much stronger and more continuous localized strain band along the UHPC-HSC interface. This indicates that the local deformation had intensified and developed into a dominant cracking or shear-damage path by the time the specimen reached failure. The transition from the more limited strain localization at Point A to the stronger localization at Point B shows that the bi-shear specimen experienced progressive damage development before reaching the peak response. Furthermoe, the specimen did not fil at point B, it was capable to sustain additional load roughly equal to 60% of the peak load.

The DIC results were especially useful for the bi-shear tests because interface cracking and localized shear deformation may begin before the final failure mode is fully visible. In some cases, strain concentration can develop near the interface or within the adjacent HSC before a clear crack is observed on the specimen surface. By using DIC, the progression of localized strain could be evaluated throughout loading and compared with the load-displacement response.

The observed bi-shear failure modes were mainly A-shape failure and shear on both sides. DIC provided additional context for interpreting these failure modes by showing how strain localization developed before and during visible cracking. Therefore, the DIC results support the interpretation that the bi-shear response was not governed by simple clean separation along the UHPC-HSC interface alone. Instead, the response involved localized shear deformation, cracking near the interface, and interaction between the bonded interface and surrounding HSC.

4.5 Shear-Key Test Results

The shear-key tests were conducted to evaluate the structural response of UHPC-HSC shear-key specimens under shear loading. However, the shear-key specimens were used to evaluate the combined behavior of the full connection system.

The results in this section are interpreted using peak load, load-displacement response, nominal shear stress, crack development, DIC strain fields, reinforcement strain response, and observed failure mode. The main variables considered were surface condition and transverse reinforcement. Surface condition was represented by smooth/as-cast and roughened UHPC-HSC interfaces. Restraint condition was represented by specimens with and without transverse reinforcement crossing the UHPC-HSC interface.

The primary comparable specimens were S-NR, R-NR, R-R-1, and R-R-2. These specimens were tested using the direct shear setup and were therefore used for the comparison of surface roughening and transverse reinforcement effects. Another specimen, S-R specimen, was tested using the shear-bending setup and is therefore discussed separately.

The S-NR specimen represents the smooth/as-cast unrestrained condition and serves as the baseline specimen. The R-NR specimen represents the roughened unrestrained condition and is used to evaluate the effect of surface roughening. The R-R-1 and R-R-2 specimens represent the roughened restrained condition and are used to evaluate the effect of transverse reinforcement crossing the UHPC-HSC interface. The S-R specimen represents the smooth/as-cast restrained condition, but because it was tested using a different setup, it is not included in the direct comparison with the direct shear specimens.

4.5.1 Overall Load-Displacement Response

The load-displacement response was used to evaluate the global behavior of each shear-key specimen during testing. Figure 4.9 shows the load-displacement graph of all specimens tested. The recorded load and deflection were used to identify the peak load, displacement at peak load, and general deformation response.

Table 0.10: Summary of shear-key specimen test results.

Specimen	**Surface Condition**	**Restraint Condition**	**Test Setup**	**Peak Load** (kN)	**Displacement (mm)**
S-NR	Smooth/as-cast	Unrestrained	Direct shear	219.8	0.46
R-NR	Roughened	Unrestrained		304.8	1.1
R-R-1	Roughened	Restrained		506.1	4.5
R-R-2	Roughened	Restrained		478.4	4.6
S-R	Smooth/as-cast	Restrained	Shear-bending	141.2	7.42

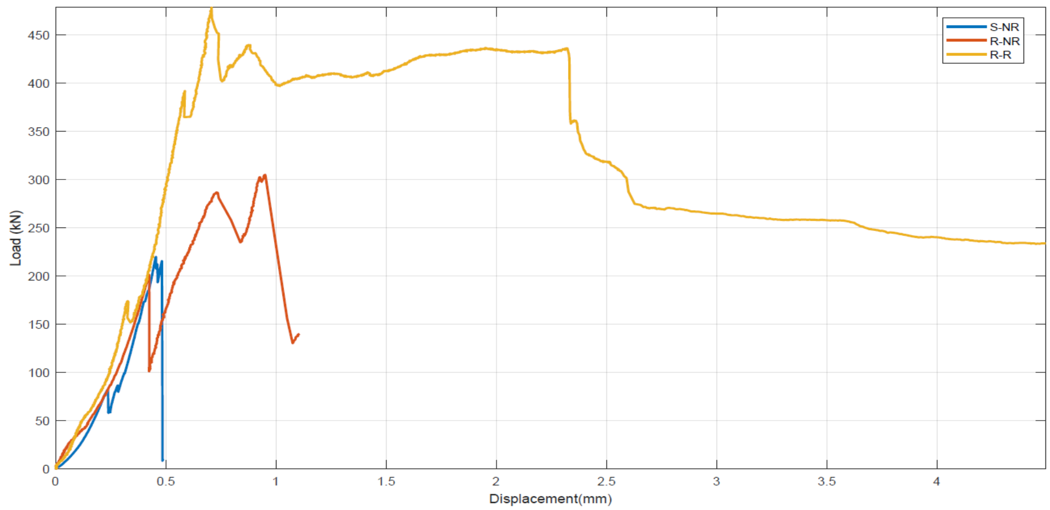

Figure 0.9: Effect of surface preparation and dowel on load deflection

The S-NR specimen reached a peak load of 219.8 kN at a displacement of 0.46 mm. Because the specimen had a smooth/as-cast interface and no transverse reinforcement crossing the UHPC–HSC interface, it was taken as the baseline specimen for the direct-shear test group. Its response represents the behaviour of the smooth/as-cast interface without additional restraint from transverse reinforcement. The R-NR specimen reached a peak load of 304.8 kN at a displacement of 1.10 mm. Relative to S-NR, its peak load was approximately 38.7% higher. Because both specimens were unrestrained and tested using the same direct-shear setup, the difference in their responses can primarily be attributed to the interface surface condition. The greater load capacity of R-NR indicates that surface roughening enhanced shear resistance by increasing mechanical interlock and frictional resistance along the UHPC–HSC interface. Photographs of the failure surfaces of S-NR and R-NR are presented in Figure 4.10. These provide a basis for qualitatively comparing the failure paths and assessing the influence of surface roughness on the interface response. The S-NR specimen exhibited a relatively clean shear-key surface after failure, as shown in Figure 4.10 (b) with no aggregates attached to the UHPC indicating that separation occurred mainly along the UHPC–HSC interface with limited removal of HSC material. In contrast, aggregate and fragments of HSC remain attached to the shear-key surface of the R-NR specimen, shown in Figure 4.10 (a). This observation indicates that surface roughness promoted stronger mechanical interlock at the interface. The contrasting failure surfaces are therefore consistent with the higher peak load measured for R-NR specimens and demonstrate the beneficial effect of surface roughness on interface resistance.

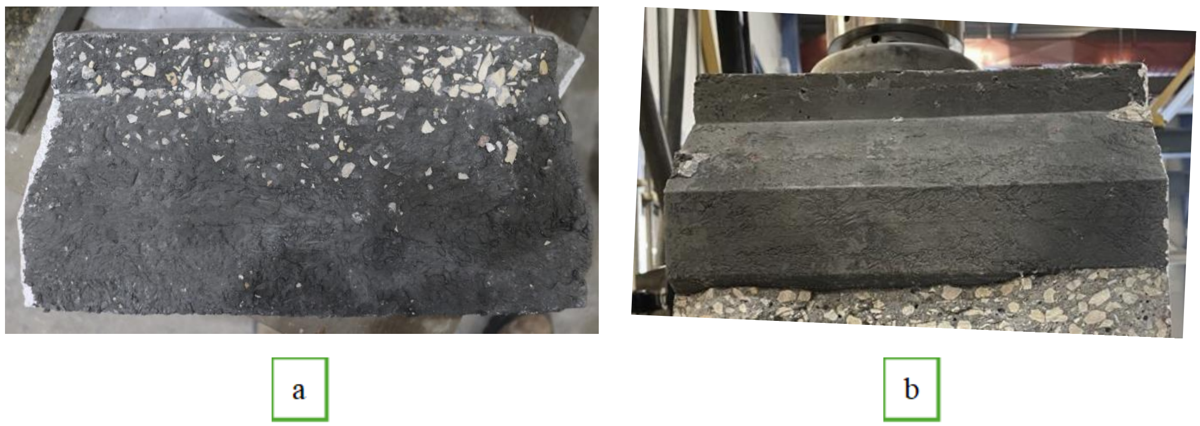

Figure 0.10: Failure surfaces of the (a) rough R-NR specimens, and (b) smooth S-NR

The rough restrained specimens developed the highest peak loads among the specimens tested. R-R-1 reached a peak load of 506.1 kN at a displacement of 4.50 mm, whereas R-R-2 reached 478.4 kN at a displacement of 4.60 mm. The two specimens had an average peak load of 492.3 kN, which was approximately 61.5% higher than that of the roughened unrestrained specimen, R-NR. Because the principal difference between R-NR and the R-R specimens was the presence of transverse reinforcement, the increase demonstrates the contribution of reinforcement crossing the UHPC–HSC interface to the shear resistance of the connection.

The comparable peak loads and displacements of R-R-1 and R-R-2 indicate that the roughened restrained condition produced a consistent response. Both specimens reached their peak loads at displacements of approximately 4.5 mm and developed substantially greater load resistance than the unrestrained specimens. This behaviour indicates that the transverse reinforcement helped maintain load transfer while cracking and localized deformation developed, thereby increasing both the resistance and deformation capacity of the connection.

The S-R specimen that is characterized by as-cast interface and steel reinforcement crossing the interface, was tested under combined flexure and shear. The load-displacement graph is shown in

Figure 4.11. The specimen reached a peak load of 141.2 kN at a deflection of about 27–31 mm. The larger deflection at peak load suggests that the test setup produced a substantial rotation. The lower measured peak load and larger displacement are therefore interpreted as part of the shear-bending response.

During loading, rotation of the specimen caused the upper portion of the unloaded side of the shear key to separate completely from the adjacent HSC as shown in figure 4.12. In contrast, the lower portion remained locked against the HSC, indicating continued contact and localized load transfer near the bottom of the interface. This asymmetric opening pattern confirms that the specimen response was governed by combined flexure and shear rather than uniform direct shear.

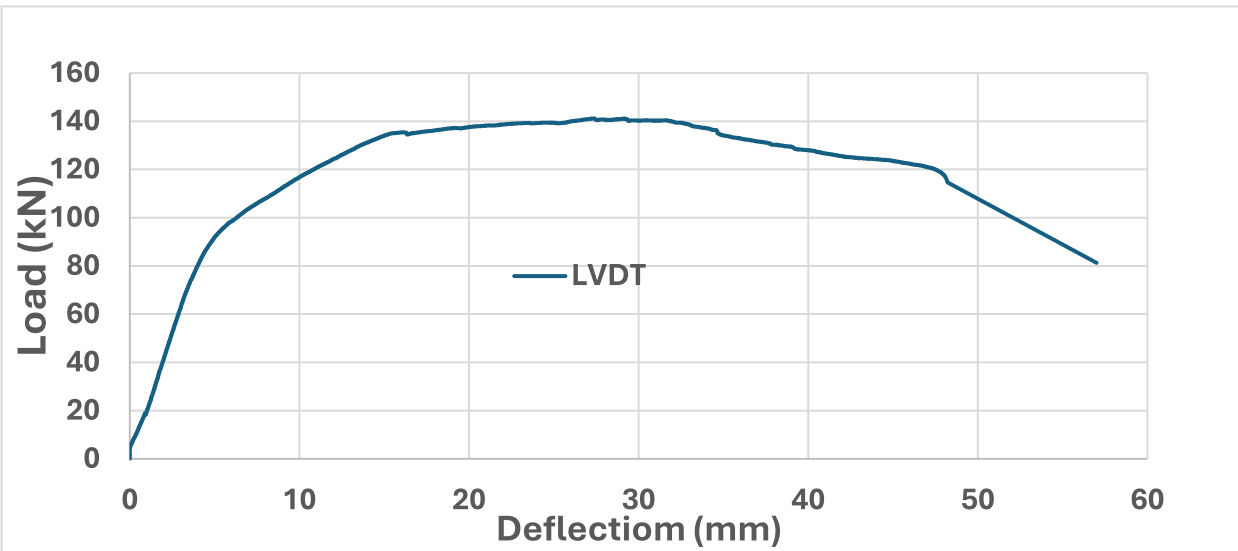

Figure 0.11: Flexural–shear response of the S-R specimen

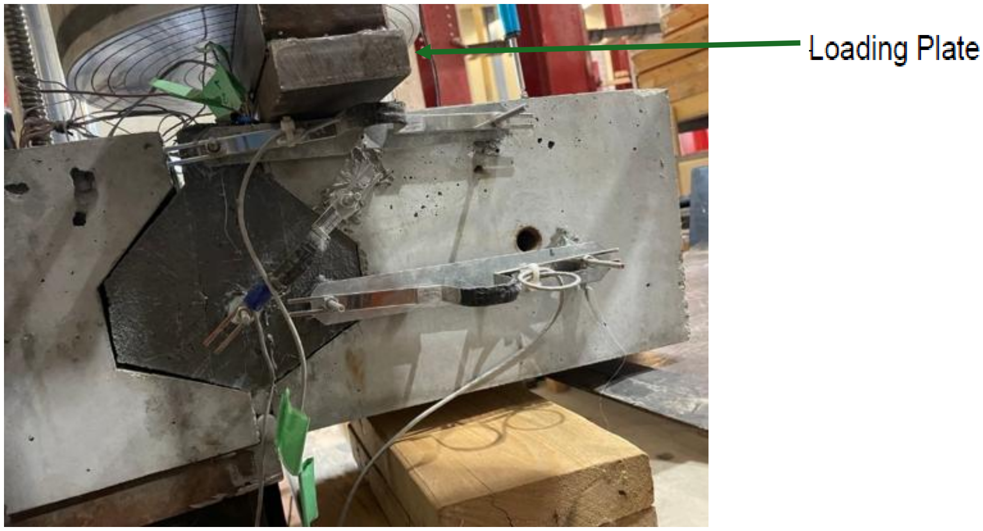

Figure 0.12: S-R specimen during test

Overall, the load-displacement results show that both surface roughening and transverse reinforcement improved the measured peak resistance of the UHPC-HSC shear-key specimens tested using the revised direct shear setup. Surface roughening increased the peak load from 219.8 kN to 304.8 kN (38.7%), while transverse reinforcement increased the average peak load from 304.8 kN to 492.3 kN (61.5%) under the roughened surface condition. These results indicate that the shear-key response was improved by the combined action of interface bond, surface roughness, mechanical interlock, localized cracking, and reinforcement action.

4.5.2 Nominal Shear Stress Capacity

Nominal shear stress capacity was calculated for the specimens tested using the direct shear setup by dividing the peak load by the total vertical UHPC-HSC interface area resisting shear, as shown in Figure 4.13 the shaded area is considered for calculation. Based on the shear-key geometry, only the vertical UHPC-HSC interface surfaces were included in this calculation. The inclined interface surfaces were not included in the nominal vertical interface area calculation, but they contribute to the resistance. This decision was supported by photographs from specimens S-NR and R-NR shown in Figure 4.13. These demonstrated that there were aggregates attached to UHPC only on the vertical surfaces of the shear key following failure.

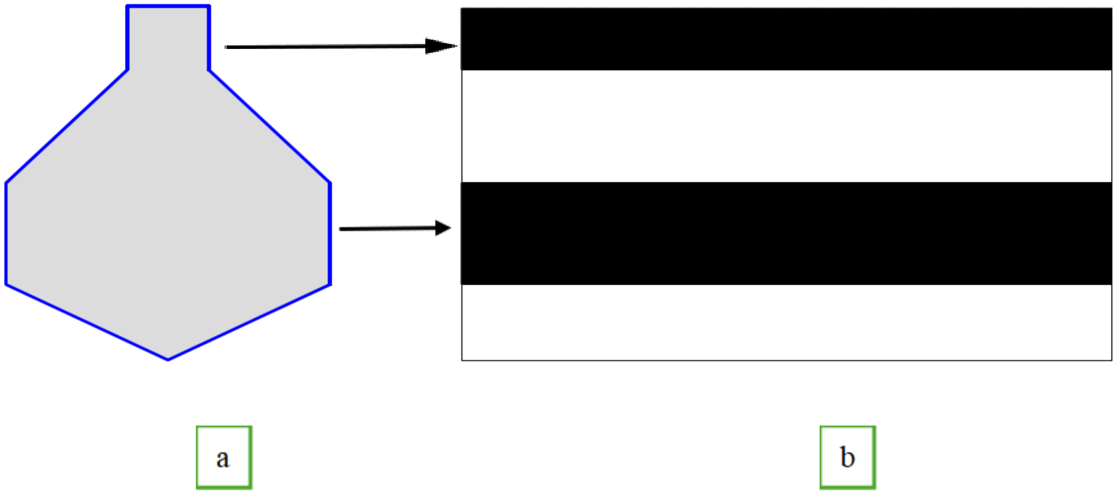

Figure 0.13: Shear key (a) shear key front view; (b) shear key side view shaded area for calculation

From the shear-key detail drawing, the vertical interface height on each side consisted of the 32 mm vertical top stem and the 51 mm vertical side segment. Therefore, the effective vertical interface height on one side was:

$$h_v = 32 + 51 = 83 \text{ mm}$$

The specimen width was 305 mm wide. Since the UHPC shear key had two vertical UHPC-HSC interface sides, the total vertical interface area was calculated as:

$$A_v = 2(305)\,(83)$$

$$A_v = 50{,}630 \text{ mm}^2$$

where (A_v) is the total vertical UHPC-HSC interface area resisting shear.

The nominal shear stress was calculated using Eq. 4.1:

Equation 5.1 $$\tau = \frac{P_{max}}{A_v}$$

where (τ) is the nominal shear stress, (P_{max}) is the peak applied load, and (A_v) is the total vertical UHPC-HSC interface area resisting shear.

Table 0.11: Summary of the nominal shear stress values

Specimen	**Peak Load** (kN)	**Total Vertical Interface Area (mm²)**	**Nominal Shear Stress (MPa)**
S-NR	219.8	50,630	4.34**
S-R*	141	25,315	5.6**
R-NR	304.8	50,630	6.02**
R-R-1	506.1	50,630	10.00**
R-R-2	478.4	50,630	9.45 **
* Tested in flexure-shear setup			
** The calculated nominal stress does not include the inclined face.			

The S-NR specimen developed a nominal shear stress of 4.34 MPa. The R-NR specimen developed a nominal shear stress of 6.02 MPa, representing an increase of approximately 38.7% compared with S-NR. Since both specimens were unrestrained and were tested using the same revised direct shear setup, this increase reflects the effect of surface roughening under the same restraint condition.

The roughened restrained specimens developed higher nominal shear stress than both unrestrained specimens in the primary comparable group. R-R-1 developed a nominal shear stress of 10.00 MPa, and R-R-2 developed a nominal shear stress of 9.45 MPa. The average nominal shear stress for the roughened restrained specimens was 9.72 MPa. Compared with R-NR, this represents an increase of approximately 61.5%. This suggests that transverse reinforcement crossing the UHPC-HSC interface improved the measured shear resistance most likely through dowel action.

The S-R specimen showed shear failure only along one side of the shear key. For reference, S-R reached a peak of 141.2 kN. Using the vertical interface area of 25,315 mm², the apparent shear stress is:

$$\tau = \frac{141.2*1000}{25{,}315}$$

$$\tau = 5.6 \text{ MPa}$$

Compared to the shear stress of S-NR, there is 29% increase in shear capacity due to presence of reinforcement in specimen S-R. The effect of surface preparation meant that specimen R-R had shear capacity that is 73% higher compared to the S-R specimen. Within the group of specimens subjected to direct shear stress, the lowest nominal shear stress occurred in the smooth/as-cast unrestrained specimens, while the highest values occurred in the roughened restrained specimens. This trend is consistent with the expected contribution of surface roughening and transverse reinforcement. Surface roughening likely improved mechanical interlock and frictional resistance, while transverse reinforcement provided additional restraint and post-cracking load-transfer capacity through development of dowel action.

Although nominal shear stress provides a useful strength comparison, it should be interpreted together with the observed failure mechanisms.

4.5.3 Crack Initiation, Crack Propagation, and DIC Strain Field Interpretation for Shear-Key Tests

Crack initiation and crack propagation were evaluated using visual observations and Digital Image Correlation (DIC) strain fields. The DIC results were especially important because they allowed strain localization and crack development to be observed before cracks were clearly visible during testing. The DIC observations were related to characteristic points on the load-deformation response, including initial cracking, crack development, ultimate load, post-peak response, and failure.

The crack development results showed that the response changed with interface condition and restraint. The smooth/as-cast unrestrained specimen, S-NR, showed localized and abrupt cracking behavior. The roughened unrestrained specimen, R-NR, showed more distributed and progressive cracking. The roughened restrained specimen, R-R, showed the most stable and controlled crack development. This trend indicates that both surface roughening and transverse reinforcement improved not only the strength of the shear-key connection, but also the way damage developed during loading.

The load-displacement response in Figure 4.15 (a) shows that the S-NR specimen reached first cracking at approximately 82 kN and about 0.24 mm displacement. At this stage, a visible crack was observed at the bottom of the shear key in the HSC region, as shown in the DIC strain field in Figure 4.15 (b). In addition to this visible crack, the DIC strain field detected localized strain concentration near the UHPC-HSC interface region that was not clearly visible during testing at that point). The localized strain band further developed from the lower portion of the shear-key region and extended upward along the interface zone, indicating that damage was beginning both in the HSC region and along the UHPC-HSC connection.

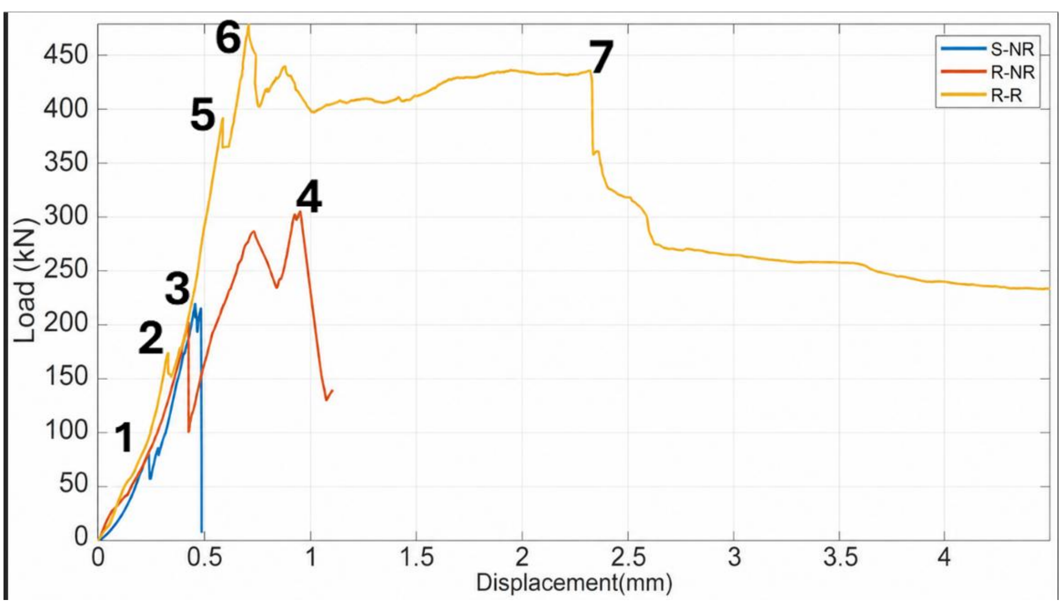

Figure 0.14: Crack development observation points

Table 0.12: Summary of crack development observations using Figure 4.14

Specimen	Point 1	Point 2	Point 3	Point 4	Point 5	Point 6	Point 7	Crack Development Interpretation
S-NR	82 kN	N/A	220 kN failure	N/A	N/A	N/A	N/A	Early strain localization and abrupt failure
R-NR	82 kN	N/A	200 kN	300 kN failure	N/A	N/A	N/A	More distributed interface cracking followed by punching through the HSC slab
R-R	82 kN	174 kN	N/A	N/A	380 kN	480 kN peak load	430 kN failure	Progressive crack development, crack branching, and sustained post-cracking resistance

The load-displacement response in Figure 4.15 (a) shows that the S-NR specimen reached first cracking at approximately 82 kN and about 0.24 mm displacement. At this stage, a visible crack was observed at the bottom of the shear key in the HSC region, as shown in the DIC strain field in Figure 4.15 (b). In addition to this visible crack, the DIC strain field detected localized strain concentration near the UHPC-HSC interface region that was not clearly visible during testing at that point). The localized strain band further developed from the lower portion of the shear-key region and extended upward along the interface zone, indicating that damage was beginning both in the HSC region and along the UHPC-HSC connection.

Following the initial cracking, the specimen continued to withstand additional load and reached a peak load of approximately 220 kN at a displacement of about 0.46 mm. The DIC strain field at

Point B, shown in Figure 4.15 (c), indicates that the initially localized strain concentration intensified and developed into a more pronounced damage zone. The damage remained concentrated near the shear-key connection rather than spreading throughout the specimen. Shortly after reaching the peak load, the specimen experienced a sudden loss of resistance, indicating an abrupt and localized failure.

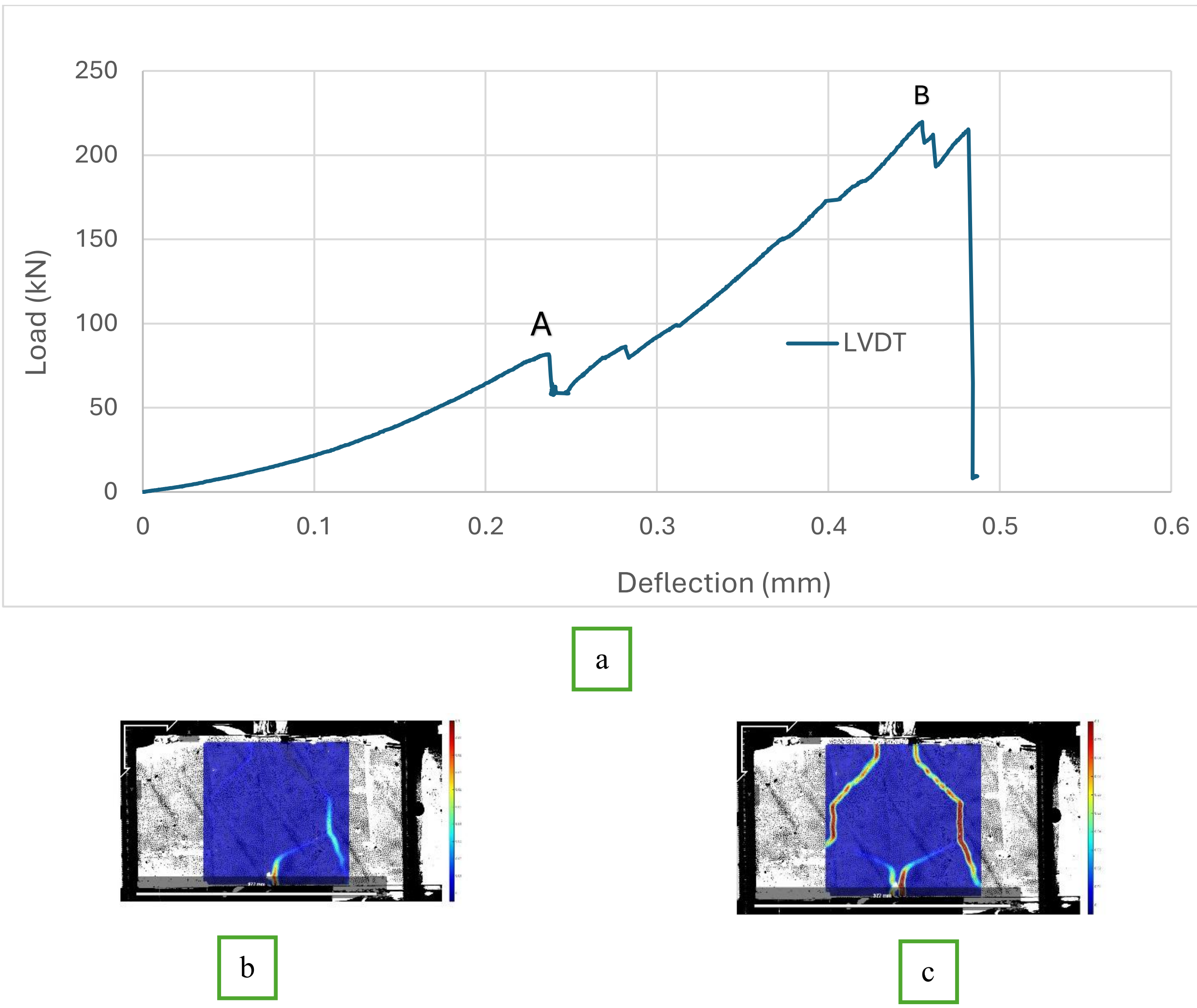

Figure 0.15: Direct shear response of the roughened, unrestrained S-NR specimen

Figure 4.14 shows the internal strain-gauge response of the S-NR specimen. Following the sensor configuration described by Erfani (2025), gauges were embedded in both the HSC and UHPC shear-key regions. The horizontal gauges were oriented parallel to the UHPC–HSC interface, corresponding to the longitudinal direction, whereas the vertical gauges were oriented perpendicular to the interface, corresponding to the transverse direction.

As shown in Figure 4.16, the concrete vertical (CV) gauge, oriented transversely to the UHPC–HSC interface, recorded compressive strain. This strain gauge was located to the right of the UHPC shear key, approximately in the middle of the cross-section, in the area where the strains started to increase as shown in DIC in Figure 4.15.(b), indicating future cracking location. Strains were increasing linearly until the interface near the location of this strain gauge cracked leading to dramatically reduced strains in CV. In contrast, the concrete horizontal (CH) gauge, oriented longitudinally along the opposite side of the shear key in HSC, recorded tensile strain. This indicates that the shear key experienced longitudinal extension. Following the cracking described in Figure 4.15 (b), the strain in CH was minimal.

The shear-key vertical (SV) and shear-key horizontal (SH) gauges, oriented transversely and longitudinally, recorded tensile strains in the UHPC shear key as shown in Figure 4.16. These localized measurements indicate that the shear key remained engaged in load transfer as the applied load increased. The differences between the HSC and UHPC strain responses demonstrate that deformation within the connection region was affected minimally in the UHPC after the cracking at the interface.

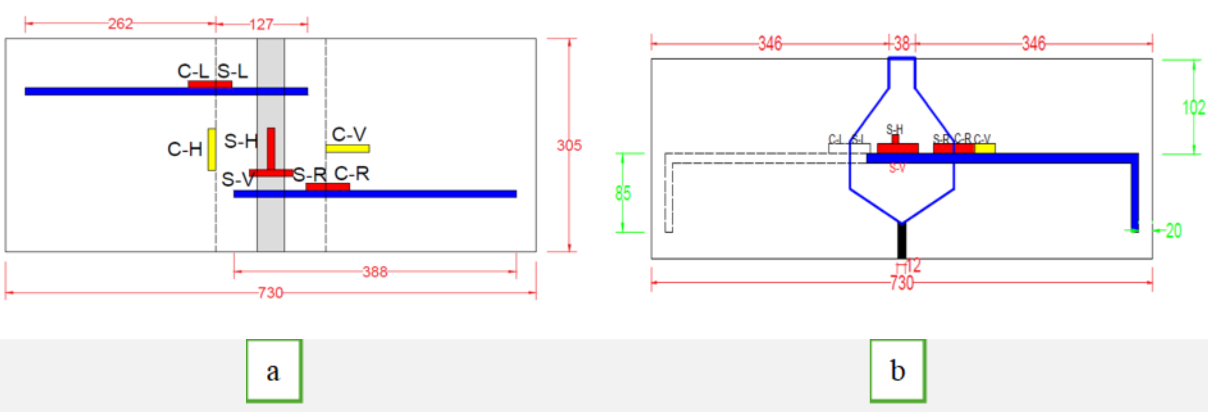

Figure 0.16: Specimen strain gauge instrumentation (a) top view; (b) side view

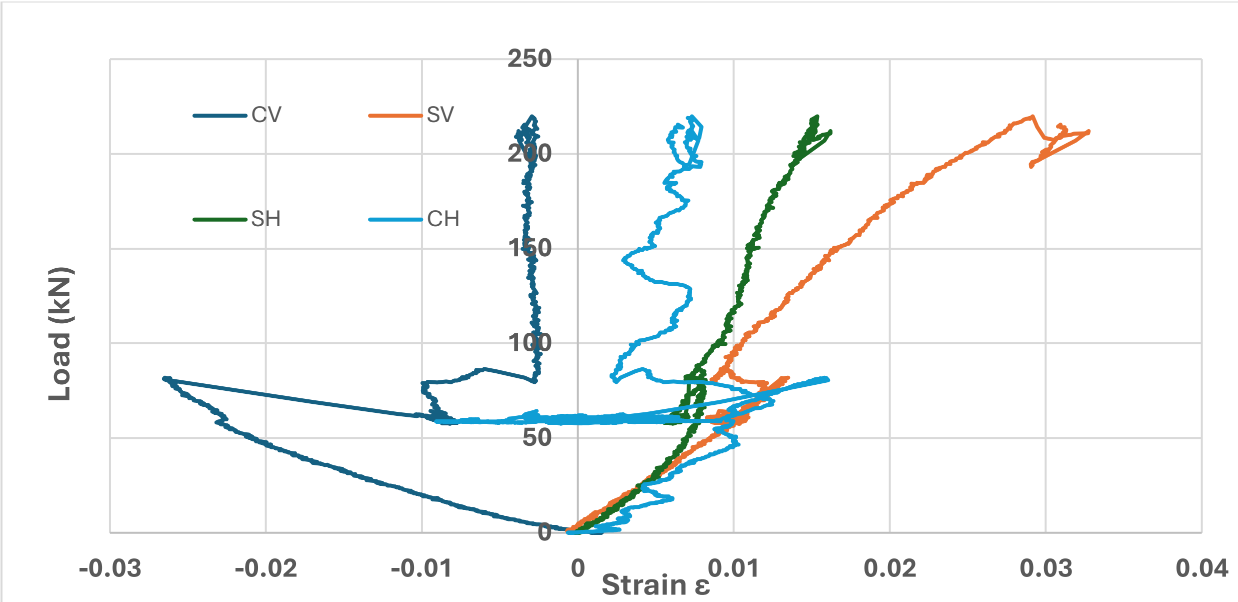

Figure 0.17: Internal concrete strain response of the S-NR specimen

The strains in specimen S-R that was subjected to combined flexure and shear load are shown in Figure 4.16. Figure 4.16 shows the load–strain responses measured by the concrete strain gauges embedded in the HSC (CV and CH) and UHPC shear-key regions (SV and SH) of the S-R specimen. The gauges measured concrete strain and were not attached to the reinforcement. The concrete vertical gauges (CV) were oriented transversely to the UHPC–HSC interface, while the concrete horizontal gauges (CH) were oriented longitudinally along the opposite interface. The HSC exhibited compressive strain in both measured directions. The concrete vertical (CV) gauge was located in the area that was subjected to no load, just beside the loading point. Therefore, the readings are nearly zero throughout the test. The Concrete horizontal (CH) gauge that was across the shear key in HSC recorded a more pronounced compressive response, indicating greater localized compression in the longitudinal direction within the HSC region during combined flexure and shear loading.

In contrast, the gauges embedded in the UHPC shear key recorded tensile strain. The SH gauge showed increasing tensile strain with increasing load, while the SV gauge developed the largest tensile strain among the concrete gauges. These responses indicate that the UHPC shear key remained engaged in load transfer and experienced tensile deformation as the combined effects of flexure and shear developed.

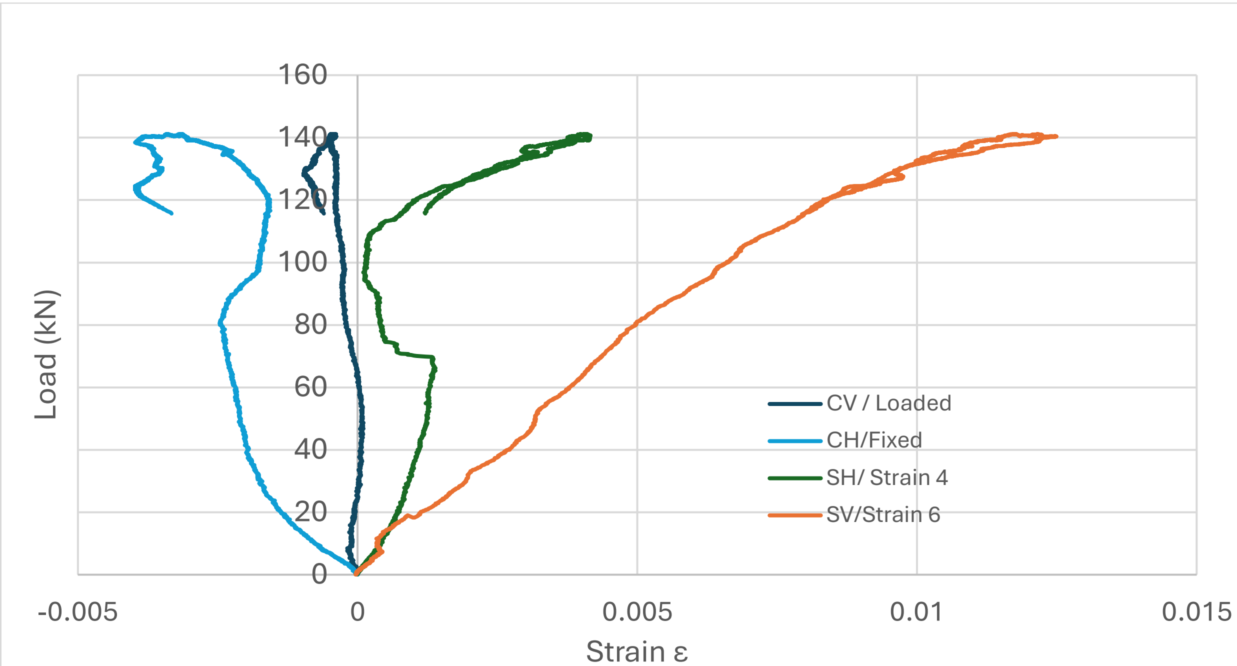

Figure 0.18: Internal concrete strain response of the S-R specimen

The specimen S-R contained reinforcement crossing the interface. Figure 4.17 shows the load–strain responses measured by the strain gauges attached to the transverse reinforcement.

Each dowel reinforcement had two strain gauges: one on the HSC side (CR and CL) and one on the UHPC side (SR and SL). The label "R" refers to the right side of the shear key, while the label "L" refers to the left side of the shear key. In the specimen S-R, the right side of the shear key was the side with the location of the applied load.

The reinforcement gauges generally recorded increasing tensile strain as the applied load increased, indicating that the transverse reinforcement became engaged in resisting crack opening near the shear-key connection. The increase in reinforcement strain during the early and intermediate loading stages suggests that the reinforcement carried a progressively greater portion of the tensile demand as cracking and localized deformation developed. Near the peak load of approximately 140 kN, the strain gauges on the loaded end recorded substantial tensile strain. After the peak load, the reinforcement strain continued to increase as the applied load gradually decreased. This response indicates that the reinforcement continued to bridge the cracked connection and provide post-cracking resistance after the specimen began to lose load-carrying capacity. The strain response varied among the reinforcement gauges, with the loaded-side and fixed-side gauges recording different strain levels. This nonuniform response is consistent with the combined flexure and shear loading mechanism, which produced different tensile demands at individual reinforcement locations.

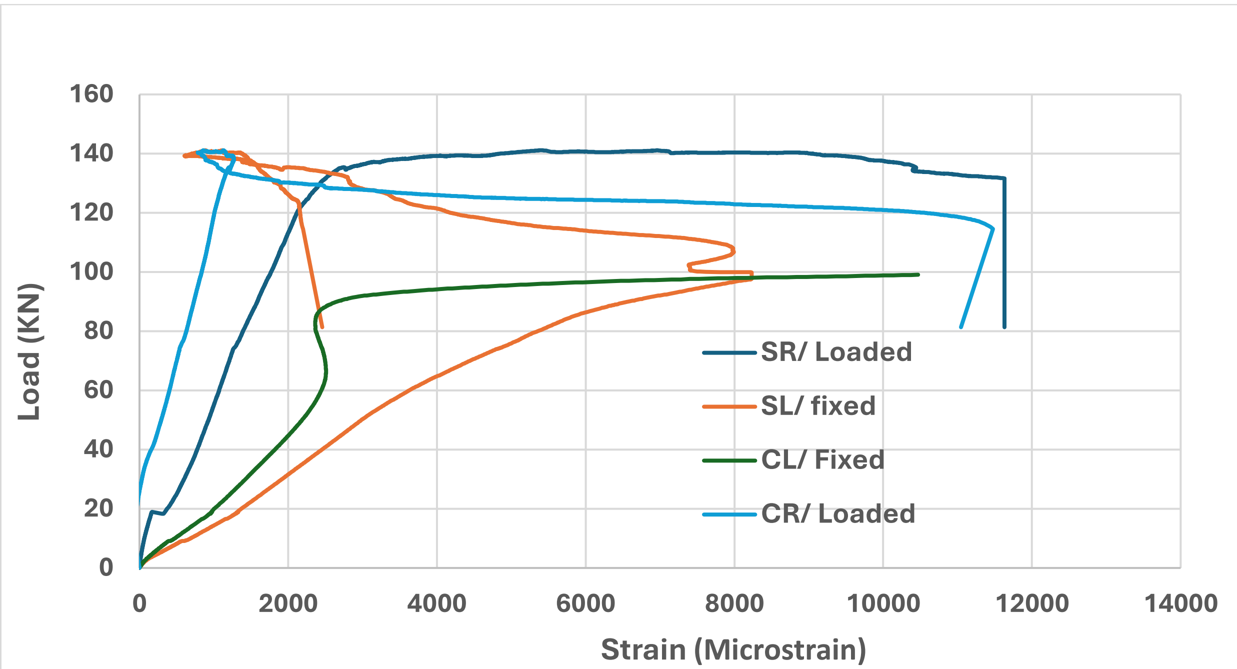

Figure 0.19: Transverse reinforcement strain response of the S-R specimen

Figure 4.18 shows the load-displacement response and corresponding DIC results for the roughened unrestrained specimen, R-NR. This specimen had a rough UHPC-HSC interface and no transverse reinforcement. Therefore, its response represents the effect of surface roughness without reinforcement restraint.

As shown in Figure 4.19(a), the load increased gradually until the first major cracking event occurred at approximately 200 kN and 0.42 mm displacement. At this stage (point A), the load dropped suddenly to about 100 kN, indicating crack initiation or localized damage development near the shear-key connection. The DIC result in figure 4.19 (b) shows the strain filed at this stage clearly indicating larger strain field on the right side of the specimen. After the first load drop, the specimen was able to regain load resistance and continued carrying additional load. This indicates that the rough interface provided mechanical interlock and allowed load transfer to continue after the initial crack. The load increased to approximately 285 kN at Point B, followed by another reduction in load. This response shows progressive damage development rather than immediate failure after the first crack. The specimen reached its maximum load of approximately 305 kN at

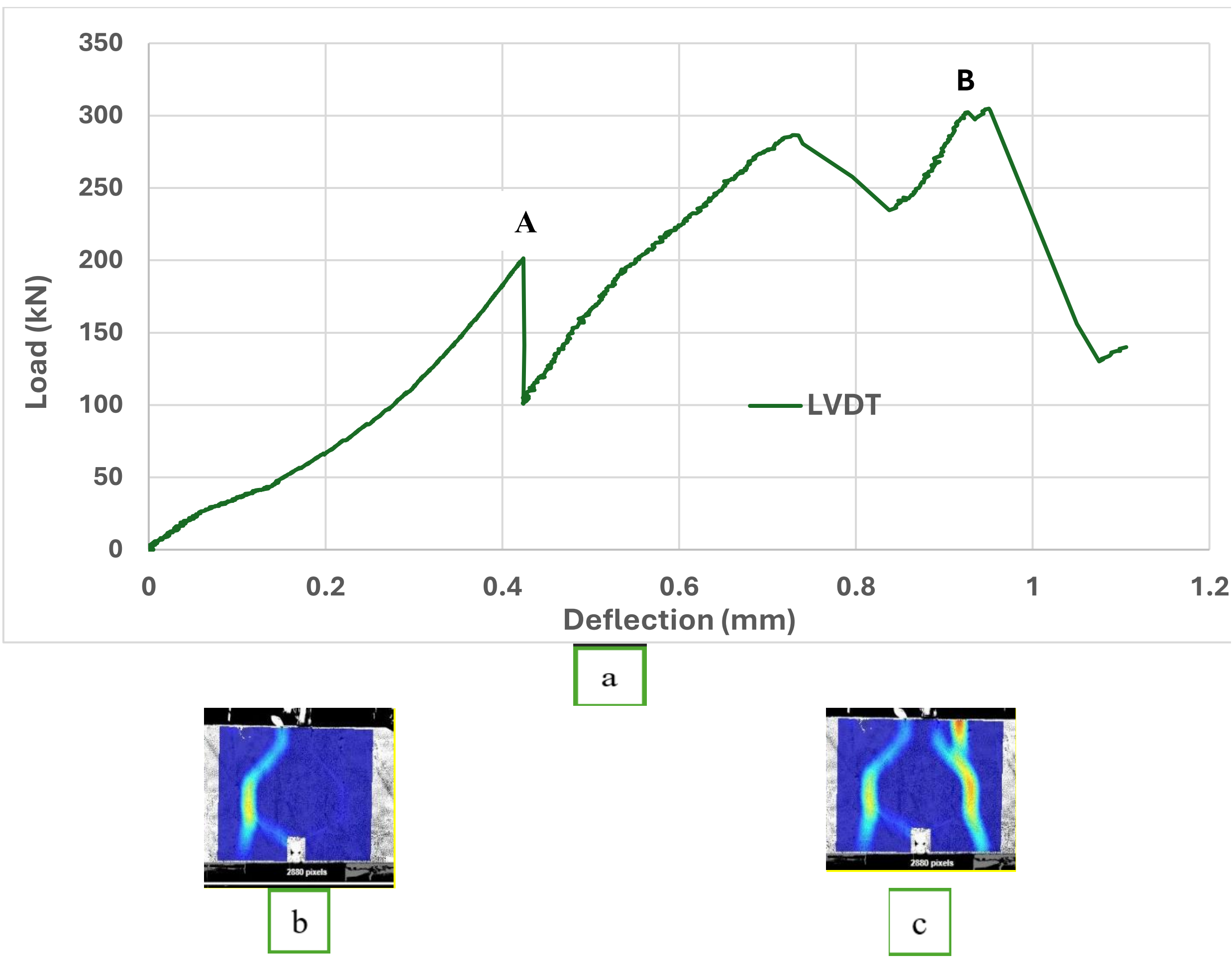

Figure 0.20: Effect of mechanical interlock in specimen R-NR: (a) load deflection curve, (b) DIC at Pont A, and (c) DIC at Point C

about 0.95 mm displacement, identified as Point C. Near this stage, the DIC strain field in Figure 4.19 (c) shows a more developed localized damage zone near the UHPC-HSC interface. After peak load, the specimen experienced a sharp reduction in resistance, indicating failure progression through the connection region.

Figure 4.20 shows the load-displacement response and corresponding DIC results for the rough restrained specimen, R-R. This specimen had a rough UHPC-HSC interface and transverse reinforcement. Therefore, its response represents the combined effect of mechanical interlock and reinforcement restraint.

As shown in Figure 4.20(a), the first crack occurred at approximately 174 kN. This stage is identified as Point A. The DIC strain field shown in Figure 4.20 (b) indicates the beginning of localized strain development near the shear-key connection region. The relatively high cracking load suggests that the rough interface preparation enhanced the mechanical interlock and contributed to delaying crack initiation. After first cracking, the specimen continued to carry additional load, indicating that the roughened interface and transverse reinforcement helped maintain load transfer. A second load drop occurred at approximately 380 kN, identified as Point B. This stage indicates additional damage and development in the connection region. However, the load did not drop suddenly to a very low level because the transverse reinforcement provided restraint and helped control crack opening. The specimen then continued to resist load until it reached a peak load of approximately 480 kN, identified as Point C. Near this stage, in Figure 4.20 (d) the DIC strain shows more strain localization near the UHPC-HSC interface and shear-key region. After peak load, the specimen showed a gradual reduction in resistance, indicating continued post-cracking load transfer rather than sudden brittle failure.

Figure 4.21 shows the load strain responses measured by the concrete strain gauges embedded in the HSC and UHPC shear-key regions of the R-R specimen. Both the HSC and UHPC shear-key gauges recorded tensile strain in the horizontal direction, indicating that the connection region experienced horizontal opening or stretching as the applied load increased. The horizontal tensile strain continued to develop through the first cracking stage, the second load-drop stage, and toward the peak load, indicating continued deformation of the connection while load resistance was maintained.

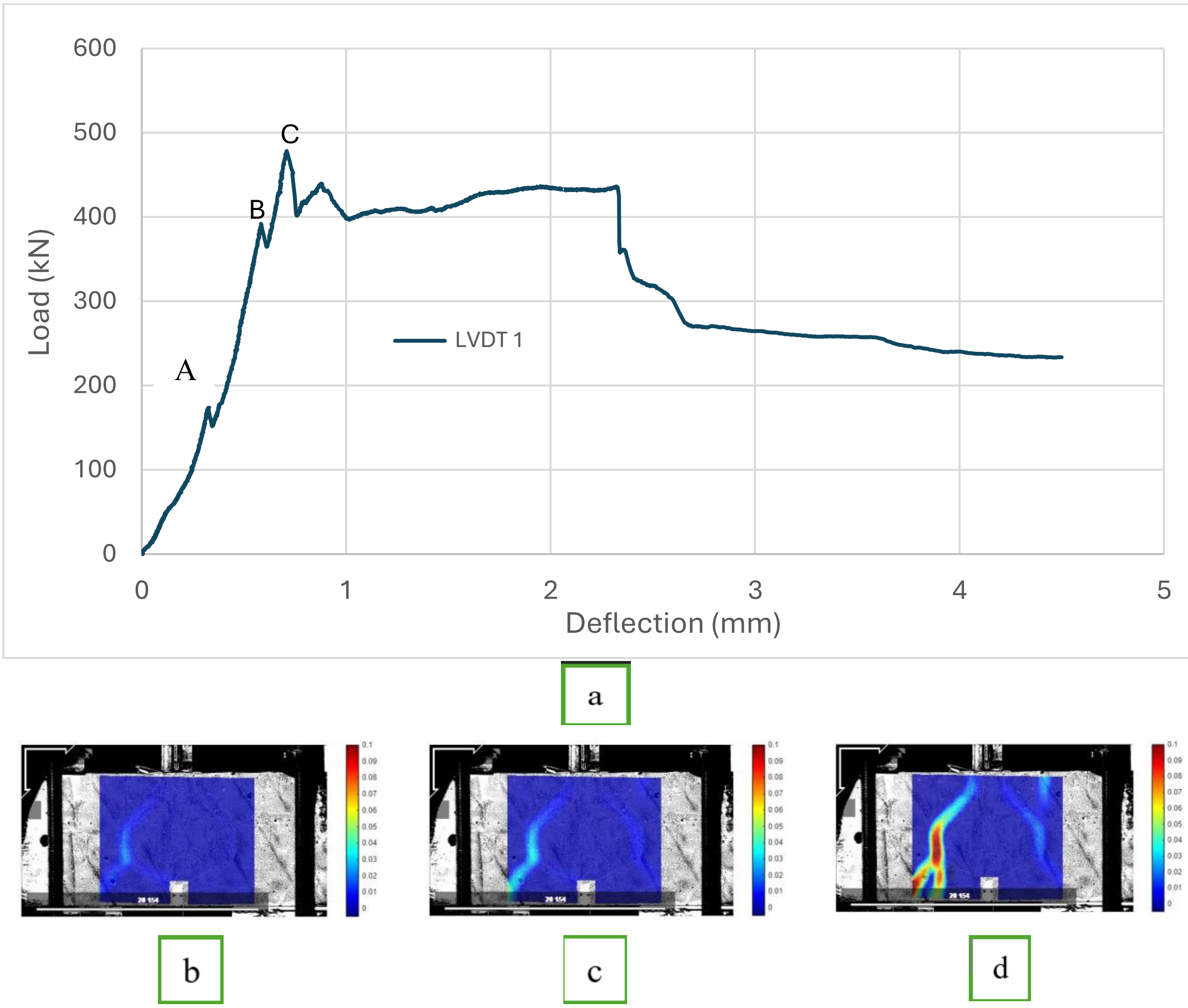

Figure 0.21: Effect of mechanical interlock and dowel action (a) Load-deflection curve, (b) strain field at point A, (c) strain field at point B, and (d) strain field at point C

In the vertical direction, the concrete vertical (CV) gauge recorded compressive strain in the HSC close to concrete crushing strain of 0.0035, whereas the shear key vertical (SV) gauge recorded tensile strain in the UHPC shear key. The values of the strains I UHPC were approximately 30% of those in HSC. This difference indicates that the HSC and UHPC regions did not deform uniformly during loading due to the way they were supported. The HSC was clamped while trying to resist the shear force applied to the UHPC shear key. The horizontal strain in the UHPC started to increase only after the load reached nearly 400 kN and the interface of the shear key was significantly cracked. The vertical strain in UHPC increased gradually throughout the loading and reached similar magnitudes of the horizontal strain gauge in HSC. While the gauges SV and SH were placed in vicinity of each other in UHPC, the gauges CV and CH were placed on the opposite side of the shear key.

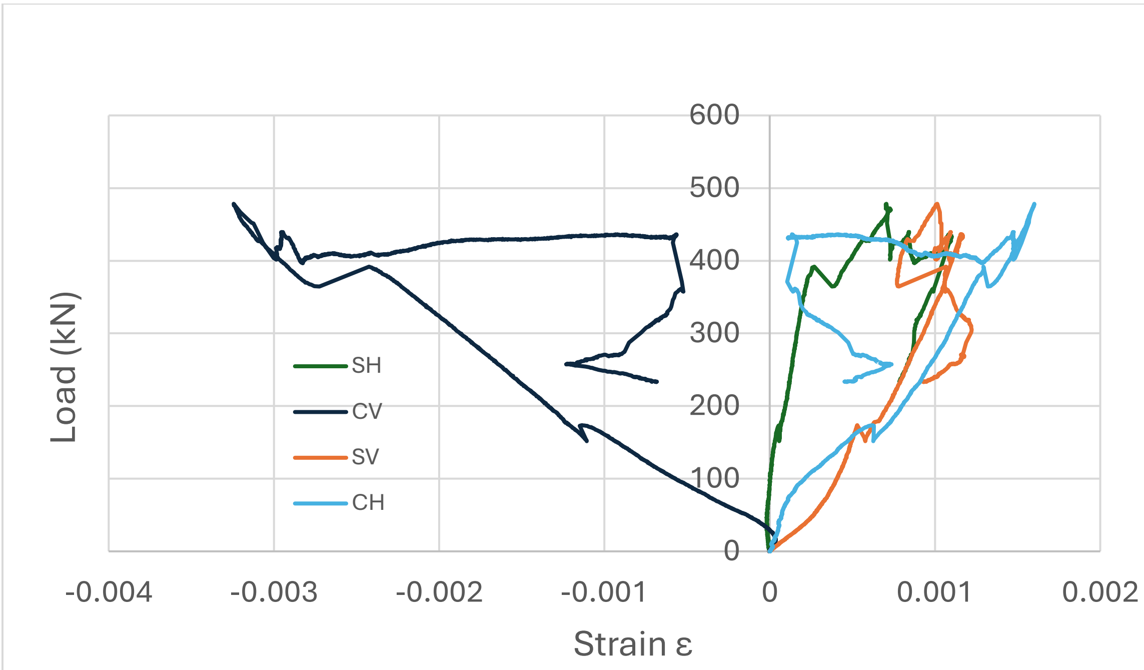

Figure 0.22: Internal concrete strain response of the R-R specimen

Figure 4.22 shows the load strain responses measured by the strain gauges attached to the transverse reinforcing bars of the R-R specimen. The reinforcing bars became progressively engaged as the applied load increased. On the left side, the concrete left (CL) gauge developed substantial tensile strain, indicating that the reinforcing bar carried tension and helped resist crack opening near the shear-key connection. The shear key left (SL) gauge also recorded tensile strain during part of the loading response but subsequently shifted in the opposite direction, indicating strain redistribution following cracking and the associated load drops.

On the right side, the shear key right (SR) gauge developed tensile strain as the applied load increased, indicating that the reinforcing bar on this side was also engaged in resisting connection deformation. In contrast, the concrete right (CR) gauge shifted predominantly toward compression during the later stages of loading. The differences among the left- and right-side gauge responses demonstrate that strain was distributed nonuniformly along the reinforcing bars as cracking progressed and the load-transfer mechanism changed within the shear-key connection.

Overall, the reinforcing-bar strain results indicate that the transverse reinforcement contributed to the response of the R-R specimen by controlling crack opening and maintaining load transfer after the first crack at approximately 174 kN and the second load drop at approximately 380 kN. The continued engagement of the reinforcing bars contributed to the specimen reaching a peak load of approximately 480 kN and exhibiting greater deformation capacity than the unrestrained specimens.

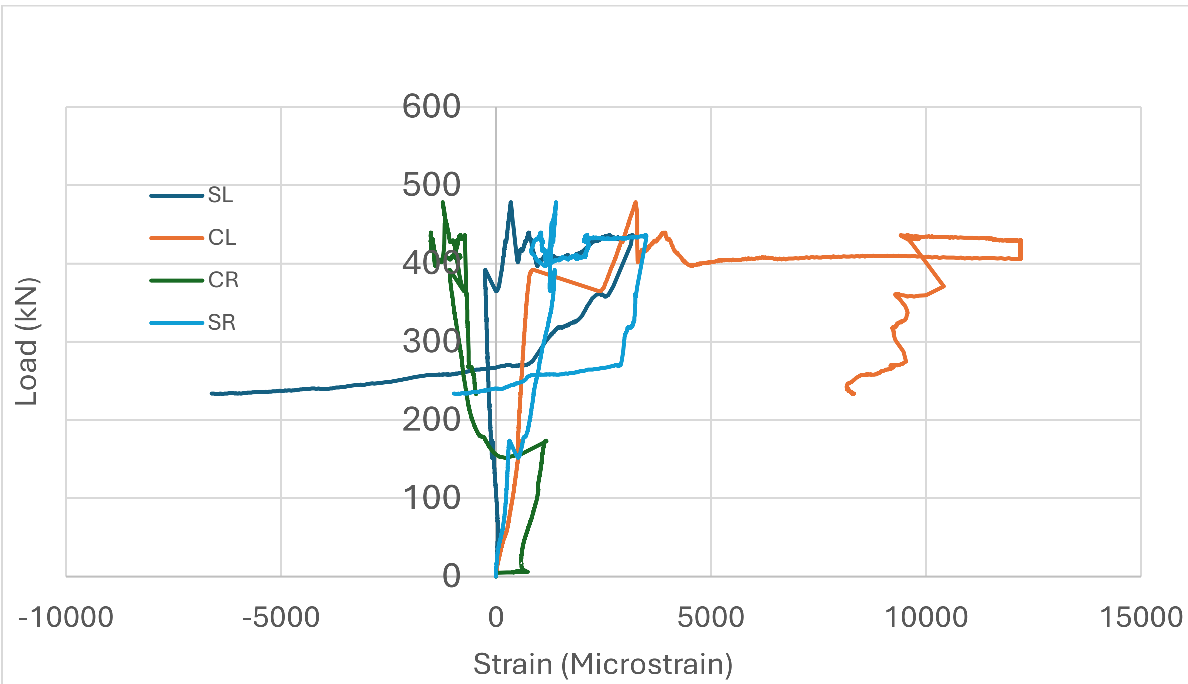

Figure 0.23: Transverse reinforcement strain response of the R-R specimen

The load displacement and DIC results show that crack initiation and propagation were strongly influenced by the interface surface condition and the presence of transverse reinforcement. In general, cracking initiated near the lower portion of the shear-key connection, where the DIC strain fields first identified localized strain concentrations. As the applied load increased, these concentrations intensified and developed into distinct crack paths along the UHPC–HSC connection region. The DIC results also detected localized damage that was not clearly visible during testing, demonstrating the value of DIC for identifying the onset and progression of cracking.

Table 4.13 shows DIC results for approximately the same loads in the specimens S-NR, R-NR and R-R. The DIC shows that while specimen S-NR cracked at 82 kN, the DIC in the other two specimens did not indicate increased strain field. It was after the S-NR specimen failed that the DIC in R-NR indicated cracking, while the strains remained very small in specimen R-R. Column 3 in Table 4.13 shows the DIC results at failure of R-NR, and at peak load for R-R. Finally, the last column shows the progression of strain field development for specimen R-R at failure.

Table 0.13: Summary of strains corresponding with load

Specimen ID	DIC with Load [kN]	DIC with Load [kN]	DIC with Load [kN]	DIC with Load [kN]
S-NR	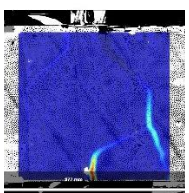 (82 kN)	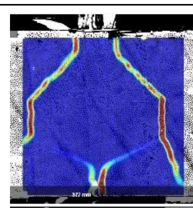 (220 kN-Failure)	N/A	N/A
R-NR	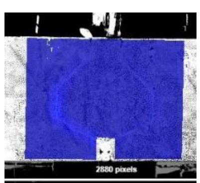 (82 kN)	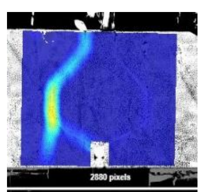 (200 kN)	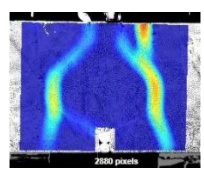 (300 kN-Failure)	N/A
R-R	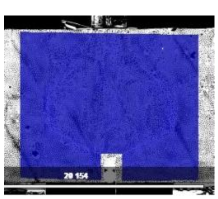 (82 kN)	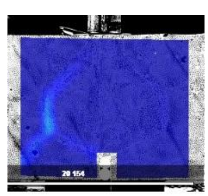 (174 kN)	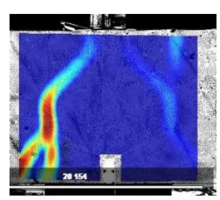 (480 kN)	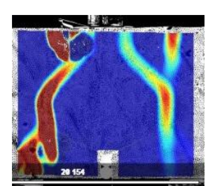 (430 kN-Failure)

The photographs of failure modes of the shear key specimens are shown in Figure 4.23.

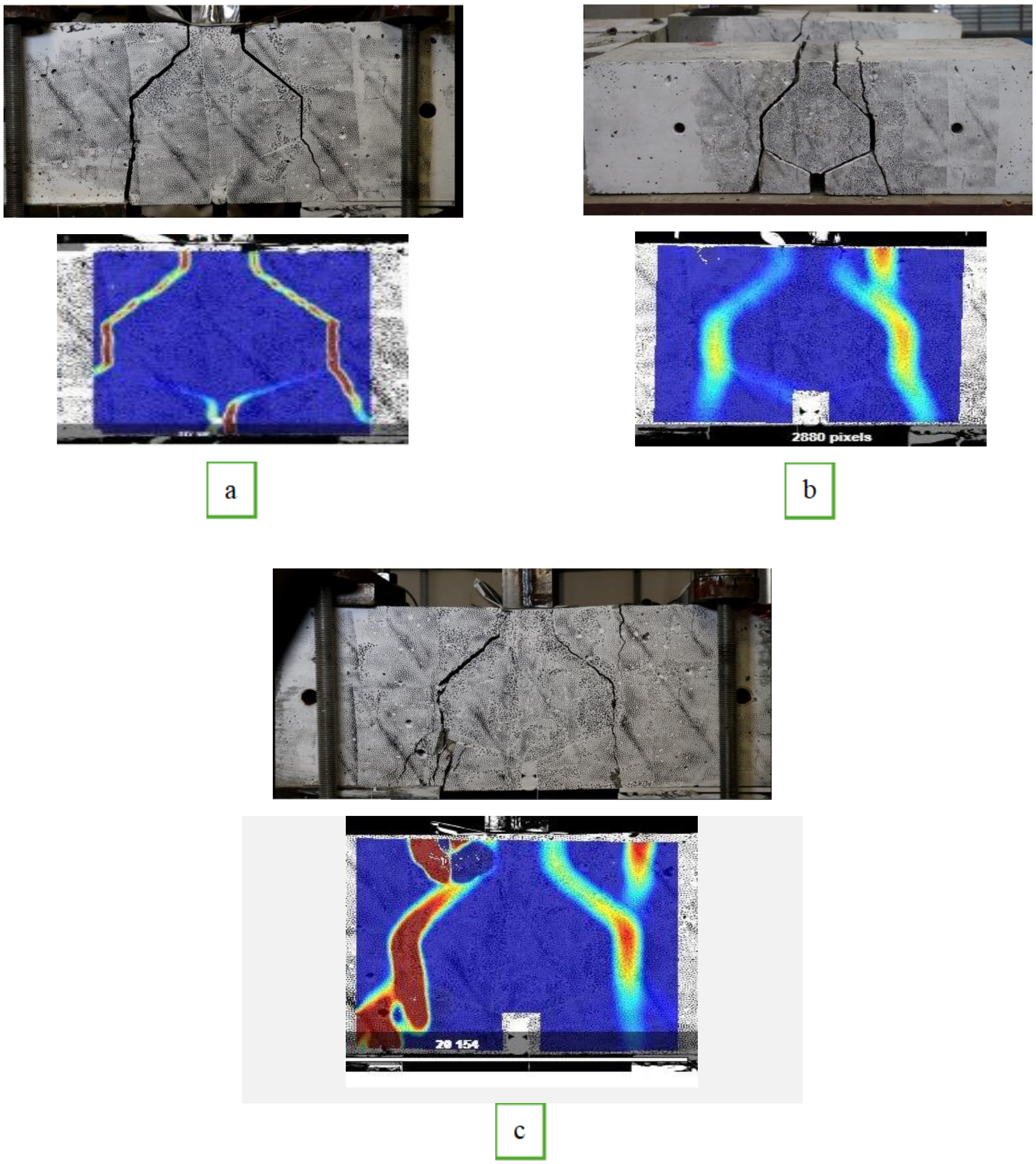

Figure 0.24: Crack propagation with DIC strain localization; (a) S-NR specimen; (b) R-NR specimen; (c) R-R specimen

5. CONCLUSIONS AND RECOMMENDATIONS

5.1 Summary

This thesis evaluated the shear behaviour of UHPC–HSC shear-key specimens' representative of connection regions between adjacent box beam bridge girders. The study formed part of the broader Little Morris Bridge UHPC shear-key research program and extended the earlier work by focusing on the direct-shear response of structural UHPC–HSC shear-key specimens.

The experimental work consisted of two independent components. The first component provided a durability assessment of retained material and interface performance following long-term storage and environmental exposure. The specimens were exposed to the outdoor environment for approximately seven years, during which temperatures ranged from approximately -40°C to +37.0°C. Compressive strength and indirect tensile tests were used to evaluate changes in material strength and tensile cracking resistance, while pull-off, slant shear, and bi-shear tests assessed the retained response of the UHPC–HSC system under different interface loading conditions. Where previous results were available, they were compared with the present measurements to examine changes in mechanical performance over time. This component was evaluated separately from the structural shear-key testing because the specimens had different material and exposure histories.

The second component consisted of structural shear-key testing. The principal variables were interface surface condition and transverse reinforcement. Smooth/as-cast and roughened interfaces were evaluated, while the restraint condition was varied by testing specimens with and without transverse reinforcement crossing the UHPC–HSC interface. The directly comparable group consisted of S-NR, R-NR, R-R-1, and R-R-2, which were tested using the revised direct-shear setup. The S-R specimen was evaluated separately because it was tested using the combined shear-bending setup.

The structural shear-key responses were evaluated using peak load, load–displacement behaviour, nominal shear stress, crack initiation and propagation, DIC strain fields where available, concrete and reinforcing-bar strains, and observed failure modes. This approach was adopted because peak load alone does not describe the complete structural response of a shear-key connection. The measured behaviour reflected the interaction of interface surface condition, mechanical interlock, friction, localized slip, crack opening, transverse-reinforcement action, and the resulting failure path.

5.2 Conclusions

Based on the experimental results, the following conclusions were drawn. The conclusions are organized into two parts: durability-related material and interface test conclusions, and structural shear-key test conclusions.

Durability-Related Material and Interface Test Conclusions

1. The remaining UHPC specimens cast during the Little Morris Bridge construction reached an average compressive strength of 218.8 MPa, while the UHPC specimens cast during Erfani's experimental program had an average strength of 161.3 MPa. These UHPC groups were evaluated separately because they had different materials, casting, curing, storage, and age histories. Both groups had experienced increase in compressive strength compared to original casting times and testing. Where the present specimen has 38% increment on compressive strength compared to Tan (2021) reported and the one retained from Erfani (2025) showed 15.2% increment when tested in the present program.
2. The HSC indirect tensile strength ranged from 4.70 to 7.20 MPa, with an average of 6.25 MPa and a standard deviation of 0.71 MPa. This average was approximately 17.3% higher than the value reported by Tan (2021). No reduction in indirect tensile strength was evident from this comparison; however, the individual effects of continued hydration, specimen age, and outdoor environmental exposure could not be isolated.
3. The 11 pull-off specimens had an average tensile resistance of 3.96 MPa and a standard deviation of 0.71 MPa. All specimens failed within the HSC substrate rather than along the UHPC-HSC interface and average pull off strength showed 4% increment when compared with Tan (2021). Therefore, the measured pull-off values represent the resistance of the bonded system up to HSC substrate failure and should not be reported as direct interface debonding strength.

4. The slant shear specimens failed within the HSC rather than by separation along the UHPC-HSC interface. This indicates that the bonded interface remained intact up to failure under the applied combination of compression and shear. The present test results showed 26.1% increment in average compressive stress, 35.9% increment in average normal shear stress, and 20.6% increment in average shear stress.
5. The bi-shear specimens developed an average shear strength of 9.42 MPa which Tan (2021) reported 6.63 MPa which is 42.1% increment in average shear strength. Their failure modes included interface-related failure, A-shaped cracking, and shear failure on both sides. These results show that the response of the bi-shear specimens involved both interface resistance and specimen-level cracking.

Structural Shear-Key Test Conclusions

6. Within the shear-key group tested in pure shear, surface roughness increased the measured peak load from 219.8 kN for S-NR to 304.8 kN for R-NR, corresponding to an increase of approximately 38.7%. Because both specimens were unrestrained and tested using the same revised direct-shear setup, this increase was attributed primarily to the difference in interface surface condition.
7. The rough restrained specimens, R-R-1 and R-R-2, reached peak loads of 506.1 kN and 478.4 kN, respectively, with an average peak load of 492.3 kN. This average was approximately 61.5% greater than the R-NR peak load. Within the tested roughened configuration, transverse reinforcement substantially increased the measured shear resistance.
8. The nominal shear stress results show the separate and combined influence of surface roughness and transverse reinforcement on the shear-key response. Comparing S-NR with S-R indicates the effect of transverse reinforcement under the smooth/as-cast interface condition. The nominal shear stress increased from 4.34 MPa for S-NR to 5.60 MPa for S-R, representing an increase of approximately 29.0%. Comparing S-NR with R-NR isolates the contribution of surface roughness, since both specimens were unrestrained and tested without transverse reinforcement. The nominal shear stress increased from 4.34 MPa to 6.02 MPa, representing an increase of approximately 38.7%. The added effect of

reinforcement under the rough interface condition was evaluated by comparing R-NR with the R-R specimens. The average nominal shear increased from 6.02 MPa for R-NR to 9.72 MPa for R-R, representing an increase of approximately 61.5%. Overall, the combined use of surface roughness and transverse reinforcement increased the nominal shear stress from 4.34 MPa for S-NR to 9.72 MPa for R-R, corresponding to an increase of approximately 124.0%. These results indicate that reinforcement alone improved the nominal shear response, roughness alone produced a larger increase, and the combination of roughness and transverse reinforcement produced the greatest improvement in the shear-key connection.

9. Surface condition and transverse reinforcement affected crack development and post-cracking response. S-NR specimen exhibited early strain localization followed by abrupt loss of resistance. R-NR showed greater resistance than S-NR and more developed damage progression, but ultimately still developed localized failure near the connection because no transverse reinforcement crossed the interface. The R-R specimens exhibited progressive cracking, crack branching, and greater residual load-carrying capacity after cracking.
10. DIC identified localized strain concentrations before some cracks became clearly visible and allowed crack development to be correlated with the load-displacement response. The DIC results showed that the rough restrained configuration produced the most progressive and stable damage-development response among the directly comparable shear-key specimens.
11. No cracking was observed within the interior of the UHPC key during the structural shear-key tests. Observed damage was concentrated near the UHPC-HSC connection and within the adjacent HSC. This indicates that the measured structural response was governed mainly by localized connection damage, HSC cracking, interface slip, and reinforcement action rather than by cracking through the UHPC key.

5.3 Recommendations

Based on the findings and limitations of this study, the following recommendations are proposed for future research.

1. Additional replicate shear-key specimens should be tested for each surface condition and reinforcement condition to improve statistical reliability and quantify variability.
2. Future shear-key programs should include companion material and interface specimens cast from the same HSC and UHPC batches as the shear-key specimens and subjected to the same curing, storage, and exposure conditions. This would allow material, interface, and shear-key results to be compared directly without differences caused by casting history, age, or storage condition.
3. Load test for Little Morris Bridge would be important to carry out together with the materials testing of the specimens that were left at the bridge site since 2019. This would provide the load-sharing effectiveness of the UHPC shear key system,
4. DIC should be applied consistently to all shear-key specimens in future testing. Separate DIC procedures may be developed for the independent bi-shear specimens because their geometry and loading conditions differ from those of the structural shear-key specimens.
5. Cyclic and fatigue testing should be conducted to evaluate stiffness degradation, progressive crack growth, residual resistance, and reinforcement response under repeated loading.
6. Additional transverse-reinforcement details should be investigated, including bar size, reinforcement ratio, spacing, embedment length, and layout. These variables may affect crack control, dowel action, residual capacity, and ductility after cracking.
7. Larger-scale connection specimens and field monitoring should be considered to evaluate member stiffness, field restraint, temperature effects, load distribution, and long-term bridge performance.

5.4 Closing Statement

This thesis contributes to the understanding of UHPC–HSC systems through two independent experimental components. The material and interface tests provided a durability-related assessment of retained mechanical and bond performance following long-term storage or outdoor exposure, including approximately seven years of exposure to temperatures ranging from -40°C to +37.0°C. The structural shear-key tests evaluated the direct-shear response of representative UHPC–HSC connections. Within the tested shear-key configurations, surface roughening and transverse reinforcement increased shear resistance and promoted a more progressive damage-development response.

Overall, the structural results demonstrate the potential of UHPC for use as a shear-key material in adjacent box beam bridge girders. However, satisfactory connection performance depends on more than the strength of the UHPC alone. Interface preparation, transverse reinforcement, shear-key geometry, boundary conditions, crack development, and load-transfer mechanisms all influence the structural response. Long-term environmental exposure must also be considered separately when evaluating the retained material and interface performance of UHPC–HSC systems.

6. Reference

[1] AASHTO. 2020. *LRFD Bridge Design Specifications*. 9th ed. Washington, DC: American Association of State Highway and Transportation Officials.

[2] Ahmed, Ghafur H., and Omar Q. Aziz. 2019a. "Shear Strength of Joints in Precast Posttensioned Segmental Bridges during 1959–2019, Review and Analysis." *Structures* 20 (August): 527–42. https://doi.org/10.1016/j.istruc.2019.06.007.

[3] Ahmed, Ghafur H., and Omar Q. Aziz. 2019b. "Shear Strength of Joints in Precast Posttensioned Segmental Bridges during 1959–2019, Review and Analysis." *Structures* 20 (August): 527–42. https://doi.org/10.1016/j.istruc.2019.06.007.

[4] Al Rikabi, Fouad T., Husam H. Hussein, and Shad M. Sargand. 2019. "Effects of Interface Roughness on Shear Key Performance of Ultra-High-Performance Concrete in Adjacent Box Girder Bridges." Paper presented at Second International Interactive Symposium on UHPC. *Second International Interactive Symposium on UHPC*, June 2. https://doi.org/10.21838/uhpc.9530.

[5] Alhassan, Mohammad A., and Mohsen A. Issa. 2010. "Long-Term Protection of Bridge-Deck Systems with Structural Latex-Modified Concrete Overlays." *PCI Journal* 55 (3): 122.

[6] Annamalai, Gangatharan, Alan Clarke, and Kurt H. Gerstle. 1990. "Shear Strength of Post-Tensioned Grouted Keyed Connections." *PCI Journal* 35 (3): 64–73. https://doi.org/10.15554/pcij.05011990.64.73.

[7] ASTM International. 2017a. *ASTM C496/C496M-17: Standard Test Method for Splitting Tensile Strength of Cylindrical Concrete Specimens*. West Conshohocken, PA: ASTM International.

[8] ASTM International. 2017b. *ASTM C1856/C1856M-17: Standard Practice for Fabricating and Testing Specimens of Ultra-High-Performance Concrete*. West Conshohocken, PA: ASTM International.

[9] ASTM International. 2020. *ASTM C1583/C1583M-20: Standard Test Method for Tensile Strength of Concrete Surfaces and the Bond Strength or Tensile Strength of Concrete Repair and Overlay Materials by Direct Tension (Pull-off Method)*. West Conshohocken, PA: ASTM International.

[10] ASTM International. 2021. *ASTM C39/C39M-21: Standard Test Method for Compressive Strength of Cylindrical Concrete Specimens*. West Conshohocken, PA: ASTM International.

[11] ASTM International. 2023. *ASTM C882/C882M-23: Standard Test Method for Bond Strength of Bonding Systems Used with Concrete by Slant Shear*. West Conshohocken, PA: ASTM International.

[12] Buyukozturk, Oral, Mourad M. Bakhoum, and S. Michael Beattie. 1990. "Shear Behavior of Joints in Precast Concrete Segmental Bridges." *Journal of Structural Engineering* 116 (12): 3380–401. https://doi.org/10.1061/(ASCE)0733-9445(1990)116:12(3380).

[13] Cheng, Fake, Tong-Ning Wang, Dong-Xu Liu, and Wei-Hong Yan. 2016. "Strengthen Method of the Shear Keys in Adjacent Concrete Box-Beam Bridges Using High-Performance Grouting Material." Paper presented at 4th 2016 International Conference on Material Science and Engineering (ICMSE 2016). *Proceedings of the 4th 2016 International Conference on Material Science and Engineering (ICMSE 2016)*. https://doi.org/10.2991/icmse-16.2016.40.

[14] CSA Group. 2019a. *A23.2-19: Test Methods and Standard Practices for Concrete*. Toronto, ON: CSA Group.

[15] CSA Group. 2019b. *CSA S6:19: Canadian Highway Bridge Design Code*. Toronto, ON: CSA Group.

[16] Di Bella, Carmelo, and B. A. Graybeal. 2014. "Volume Stability and Cracking Potential of Prebagged, Cement-Based Nonshrink Grouts for Field-Cast Connections." *Transportation Research Record: Journal of the Transportation Research Board* 2441 (1): 6–12. https://doi.org/10.3141/2441-02.

[17] Erfani, Mana. 2025. *Early Age Shrinkage and Bond Performance of UHPC in Shear Keys*. https://mspace.lib.umanitoba.ca/items/1160a38a-498e-4175-a442-3a4ea9d4fd5d.

[18] Fasching, Stephan Johann, Tobias Huber, Michael Rath, and Johann Kollegger. 2021. "Semi-Precast Segmental Bridge Construction Method: Experimental Investigation on the Shear Transfer in Longitudinal and Transverse Direction." *Applied Sciences* 11 (12): 5502. https://doi.org/10.3390/app11125502.

[19] Flores, Elsy Y., Jordan Varbel, William K. Toledo, Craig M. Newtson, and Brad D. Weldon. 2021. "Ultra-High-Performance Concrete Shear Keys in Concrete Bridge Superstructures." *Transportation Research Record: Journal of the Transportation Research Board* 2675 (2): 108–20. https://doi.org/10.1177/0361198120964725.

[20] Frosch, Robert J., Christopher S. Williams, Ryan T. Molley, and Ryan T. Whelchel. 2020. *Concrete Box Beam Risk Assessment and Mitigation: Volume 1—Evolution and Performance*. https://rosap.ntl.bts.gov/view/dot/54603.

[21] Graybeal, Ben. 2014. *Design and Construction of Field-Cast UHPC Connections.* https://rosap.ntl.bts.gov/view/dot/28283.

[22] Graybeal, Benjamin A. 2006. *Material Property Characterization of Ultra-High-Performance Concrete*. United States. Federal Highway Administration. Office of Infrastructure …. https://rosap.ntl.bts.gov/view/dot/38714.

[23] Gulyas, Robert J., Gregory J. Wirthlin, and Jeffrey T. Champa. 1995. “Evaluation of Keyway Grout Test Methods for Precast Concrete Bridges.” *PCI Journal* 40 (1): 44–57. https://doi.org/10.15554/pcij.01011995.44.57.

[24] Haber, Zachary B., Igor De la Varga, Benjamin A. Graybeal, Brian Nakashoji, and Rafic El-Helou. 2018. *Properties and Behavior of UHPC-Class Materials*. https://rosap.ntl.bts.gov/view/dot/37528.

[25] Halbe, Kedar, Patrick Joyce, Carin L. Roberts-Wollmann, and Thomas E. Cousins. 2017. *Development of Improved Connection Details for Adjacent Prestressed Member Bridges.* https://rosap.ntl.bts.gov/view/dot/32436.

[26] Halbe, Kedar Ram. 2014. “New Approach to Connections between Members of Adjacent Box Beam Bridges.” PhD Thesis, Virginia Polytechnic Institute and State University. https://search.proquest.com/openview/d48bde1d2e80961d0a4c91f035c425fc/1?pq-origsite=gscholar&cbl=18750.

[27] Hanna, Kromel E., George Morcous, and Maher K. Tadros. 2009. “Transverse Post-Tensioning Design and Detailing of Precast, Prestressed Concrete Adjacentbox-Girder Bridges.” *PCI Journal* 54 (4): 160.

[28] Huckelbridge Jr, A. A., and Hassan Hussein El-Esnawi. 1997. *Evaluation of Improved Shear Key Designs for Multi-Beam Box Girder Bridges*. https://trid.trb.org/View/496164.

[29] Hussein, Husam H., Shad M. Sargand, Fouad T. Al Rikabi, and Eric P. Steinberg. 2017a. “Laboratory Evaluation of Ultrahigh-Performance Concrete Shear Key for Prestressed Adjacent Precast Concrete Box Girder Bridges.” *Journal of Bridge Engineering* 22 (2): 04016113. https://doi.org/10.1061/(ASCE)BE.1943-5592.0000987.

[30] Hussein, Husam H., Shad M. Sargand, Fouad T. Al Rikabi, and Eric P. Steinberg. 2017b. “Laboratory Evaluation of Ultrahigh-Performance Concrete Shear Key for Prestressed Adjacent Precast Concrete Box Girder Bridges.” *Journal of Bridge Engineering* 22 (2): 04016113. https://doi.org/10.1061/(ASCE)BE.1943-5592.0000987.

[31] Hussein, Husam H., Shad M. Sargand, and Eric P. Steinberg. 2018. “Shape Optimization of UHPC Shear Keys for Precast, Prestressed, Adjacent Box-Girder Bridges.” *Journal of Bridge Engineering* 23 (4): 04018009. https://doi.org/10.1061/(ASCE)BE.1943-5592.0001220.

[32] Hussein, Husam H., Kenneth K. Walsh, Shad M. Sargand, and Eric P. Steinberg. 2016. “Interfacial Properties of Ultrahigh-Performance Concrete and High-Strength Concrete Bridge Connections.” *Journal of Materials in Civil Engineering* 28 (5): 04015208. https://doi.org/10.1061/(ASCE)MT.1943-5533.0001456.

[33] Issa, Mohsen A., and Hiba A. Abdalla. 2007. “Structural Behavior of Single Key Joints in Precast Concrete Segmental Bridges.” *Journal of Bridge Engineering* 12 (3): 315–24. https://doi.org/10.1061/(ASCE)1084-0702(2007)12:3(315).

[34] Issa, Mohsen A., Cyro L. Ribeiro Do Valle, Hiba A. Abdalla, Shahid Islam, and Mahmoud A. Issa. 2003. “Performance of Transverse Joint Grout Materials in Full-Depth Precast Concrete Bridge Deck Systems.” *PCI Journal* 48 (4): 92–103. https://doi.org/10.15554/pcij.07012003.92.103.

[35] Koseki, K., and John Edward Breen. 1983. *Exploratory Study of Shear Strength of Joints for Precast Segmental Bridges*. https://library.ctr.utexas.edu/digitized/texasarchive/phase1/248-1-ctr.pdf.

[36] Lall, Jyotirmay, Sreenivas Alampalli, and Eugene F. DiCocco. 1998. “Performance of Full-Depth Shear Keys in Adjacent Prestressed Box Beam Bridges.” *PCI Journal* 43 (2): 72–79. https://doi.org/10.15554/pcij.03011998.72.79.

[37] Lopez de Murphy, Maria, Jubum Kim, Zi Sang, and Chao Xiao. 2010. *Determining More Effective Approaches for Grouting Shear Keys of Adjacent Box Beams.* https://rosap.ntl.bts.gov/view/dot/18123.

[38] Miller, R. A., G. M. Hlavacs, T. Long, and A. Greuel. 1999. “FULL-SCALE TESTING OF SHEAR KEYS FOR ADJACENT BOX GIRDER BRIDGES.” *PCI Journal* 44 (6). https://trid.trb.org/View/639856.

[39] Neirinck, Timothy, Ali A. Semendary, Evangeline Murison, and Dagmar Svecova. 2023. “Performance of UHPC Shear Keys in Box Girder Bridges-Field and Finite Element Study.” *Engineering Structures* 296 (December): 116896. https://doi.org/10.1016/j.engstruct.2023.116896.

[40] Ni, Xiaojing, Ahehehinnou Ougbe Anselme, Guannan Wang, Yuan Xing, and Rongqiao Xu. 2022. “Experimental Investigation of Shear Keys for Adjacent Precast Concrete Box Beam Bridges.” *Materials* 15 (4): 1459. https://doi.org/10.3390/ma15041459.

[41] Ozyildirim, H. Celik, and Gail M. Moruza. 2016. “High-Performance Grouting Materials in Shear Keys Between Box Beams.” *Transportation Research Record: Journal of the Transportation Research Board* 2577 (1): 35–42. https://doi.org/10.3141/2577-05.

[42] Russell, H. G., National Research Council (U S.). Transportation Research Board, and National Cooperative Highway Research Program. 2009. *Adjacent Precast Concrete Box Beam Bridges: Connection Details*. Transportation Research Board.

[43] Russell, Henry G. 2011. “Adjacent Precast Concrete Box-Beam Bridges: State of the Practice.” *PCI Journal*, 75.

[44] Russell, Henry G., and Benjamin A. Graybeal. 2013. *Ultra-High-Performance Concrete: A State-of-the-Art Report for the Bridge Community.* https://rosap.ntl.bts.gov/view/dot/26387.

[45] Seibert, Peter J., Vic H. Perry, and Dominique Corvez. 2019. "Performance Evaluation of Field Cast UHPC Connections for Precast Bridge Elements." *International Interactive Symposium on Ultra-High-Performance Concrete Papers* 2 (1). https://www.iastatedigitalpress.com/uhpc/article/id/9634/.

[46] Semendary, Ali A., Eric P. Steinberg, Kenneth K. Walsh, and Elné Barnard. 2017. "Live-Load Moment-Distribution Factors for an Adjacent Precast Prestressed Concrete Box Beam Bridge with Reinforced UHPC Shear Key Connections." *Journal of Bridge Engineering* 22 (11): 04017088. https://doi.org/10.1061/(ASCE)BE.1943-5592.0001127.

[47] Semendary, Ali A., Eric P. Steinberg, Kenneth K. Walsh, and Elné Barnard. 2019. "Effects of Temperature Distributions on Thermally Induced Behavior of UHPC Shear Key Connections of an Adjacent Precast Prestressed Concrete Box Beam Bridge." *Journal of Bridge Engineering* 24 (2): 04018115. https://doi.org/10.1061/(ASCE)BE.1943-5592.0001346.

[48] Shokrgozar, Ali, Bipin Aryal, Arya Ebrahimpour, and Mustafa Mashal. 2024. "Bond-Slip Behavior of Steel Reinforcing Bars in Ultra-High-Performance Concrete for Field-Cast Connection of Precast Bridge Decks." *Frontiers in Built Environment* 10 (May): 1354657. https://doi.org/10.3389/fbuil.2024.1354657.

[49] Swenty, Matthew K., and Benjamin A. Graybeal. 2017. "Characterization of Materials Used in Field-Cast Precast Concrete Connections." *PCI Journal* 62 (6): 33–44.

[50] Tan, Li Xin. 2021. *Early Age and Durability Study of the Bond Strength on the Interface between UHPC – HSC*. October 29. http://hdl.handle.net/1993/36094.

[51] Yoo, Doo-Yeol, Wonsik Shin, and Booki Chun. 2020. "Corrosion Effect on Tensile Behavior of Ultra-High-Performance Concrete Reinforced with Straight Steel Fibers." *Cement and Concrete Composites* 109 (May): 103566. https://doi.org/10.1016/j.cemconcomp.2020.103566.

[52] Yuan, Aimin, Chen Yang, Jiwei Wang, Leike Chen, and Rongwei Lu. 2019a. "Shear Behavior of Epoxy Resin Joints in Precast Concrete Segmental Bridges." *Journal of Bridge Engineering* 24 (4): 04019009. https://doi.org/10.1061/(ASCE)BE.1943-5592.0001362.

[53] Yuan, Aimin, Chen Yang, Jiwei Wang, Leike Chen, and Rongwei Lu. 2019b. "Shear Behavior of Epoxy Resin Joints in Precast Concrete Segmental Bridges." *Journal of Bridge Engineering* 24 (4): 04019009. https://doi.org/10.1061/(ASCE)BE.1943-5592.0001362.

[54] Yuan, Jiqiu, and Benjamin Graybeal. 2016. "Full-Scale Testing of Shear Key Details for Precast Concrete Box-Beam Bridges." *Journal of Bridge Engineering* 21 (9): 04016043. https://doi.org/10.1061/(ASCE)BE.1943-5592.0000906.

[55] Zhou, Xiangming, Neil Mickleborough, and Zongjin Li. 2005. “Shear Strength of Joints in Precast Concrete Segmental Bridges.” *ACI Structural Journal* 102 (1): 3.

[56] Zou, Yu, and Dong Xu. 2022. “Experimental Study on Shear Behavior of Joints in Precast Concrete Segmental Bridges.” *Structures* 39 (May): 323–36. https://doi.org/10.1016/j.istruc.2022.03.037.